A PHOTOELASTIC INVESTIGATION OF THE DISTRIBUTION OF SHEARING STRESSES IN A STIFFENED FLAT PANEL

Thesis by

W. N. Bell and J. K. Bussey

In Partial Fulfillment of the Requirements for the Degree of Master of Science in Aeronautical Engineering.

California Institute of Technology
Pasadena, California
1938

ACKNOWLEDGMENTS

The authors wish to express their appreciation to Dr. Th. von Karman, who suggested the research problem of this thesis, and to Dr. E. E. Sechler for his helpful criticisms and suggestions during the year. Grateful acknowledgment is also made to Arthur Gross, senior in mechanical engineering, for his work as assistant during the final term.

TABLE OF CONTENTS

NOTATION

X - Vertical coordinate, positive upward.

Y - Horizontal coordinate, positive to the right.

P - Total applied load.

M - Moment.

t - Thickness of model.

σ - Normal stress (tension or compression).

p, q - Principal normal stresses, mutually perpendicular; $p = \sigma_{max}$, $q = \sigma_{min}$, or vice-versa.

τ - Tangential stress (shear).
$\tau_{max} = \frac{1}{2} (p - q)$

θ - Isoclinic angle, the inclination of one principal stress (p, say) as measured clockwise from the X-axis.

β - Angle of inclination of a principal stress trajectory to an isoclinic line.

r, ϕ - Polar coordinates;

$$r = \sqrt{x^2 + y^2}, \qquad \tan^{-1} = \frac{Y}{X}$$

PART I.

INTRODUCTION

a. Design considerations.

In the construction of modern metal airplanes it is common practice to employ panels of thin sheet reinforced by longitudinal stiffeners; and, since it is necessary to design to close strength limits in order to obtain an efficient structure, it is important to know the allowable load which the individual stiffened panel may carry. Compression loads are transferred in shear through the sheet, and it has been found that difficulties in the prediction of strength characteristics arise because of the non-uniform stress distribution between stiffeners in such an assembly. This is the so-called "shear lag" phenomenon.

b. Statement of thesis problem.

The final attainment of a completely valid design criterion in the case of the stiffened thin sheet panel should be facilitated, it seems reasonable to believe, by an investigation of the shear properties of the sheet in this type of structure. With this idea in mind, the research problem of this thesis has been undertaken. It was proposed to examine by photoelastic means a model typifying the very simplest case of a stiffened panel, namely, a flat rectangular panel with

one centrally located stiffener. By loading this model in compression through the stiffener and recording photographically the resulting stress patterns, a study has been made of the distribution of shearing stresses through the sheet. The photoelastic method, it may be remarked, appears to be of considerable advantage in the investigation of this particular problem, since its most direct result is the determination of the maximum shearing stresses in magnitude and direction.

c. Previous investigations.

Numerous tests have been made in various laboratories to determine the compressive strengths of flat and curved panels, both stiffened and unstiffened. In the Guggenheim Aeronautical Laboratory of the California Institute of Technology, in specific, investigations have been made by Sechler[1], White and Antz[2], Lovett and Rodee[3], and others, into the particular problems of stiffened panel construction, including the effects of various stiffener-sheet combinations, the transfer of stress from stiffener to stiffener, and the calculation of "effective widths" of sheet for use in design. Aside from a photoelastic test with celluloid sheets, supported at the edges by V-blocks (to simulate stiffeners) and subjected to compression, proposed by August Zinnser, Jr.[4], of Massachusetts Institute of Technology, however, the

authors have knowledge of no other photoelastic investigations of stiffened panel construction.

---

[1] E. E. Sechler, Stress Distribution in Stiffened Panels under Compression. Journal of the Aeronautical Sciences, June, 1937.

[2] White and Antz, Tests on the Stress Distribution in Reinforced Panels. Journal of the Aeronautical Sciences, April, 1936.

[3] Lovett and Rodee, Transfer of Stress from Main Beams to Intermediate Stiffeners in Metal Sheet - covered Box Beams. Journal of the Aeronautical Sciences, October, 1936.

[4] August Zinnser, Jr., Letter to the Journal of the Aeronautical Sciences, May 15, 1934.

PART II.

METHODS OF INVESTIGATION.

a. Theory of elasticity.

1. The problem of this research project is fundamentally of an experimental nature. In general, such a laboratory test in the field of structural design and analysis is intended to aid in the determination of an analytical expression for stress distribution. Besides the experimental method, however, analysis is also possible by the mathematical theory of elasticity. In order to avoid too great mathematical complexities in this latter method, either fairly specialized cases must usually be considered or assumptions must be made which will simplify the analytical solution of the problems. Because of the physical limitations upon engineering materials, therefore, these approximate theories of elasticity do not always give an exact picture of the distribution of stresses throughout a structure. These methods, nevertheless, give a valuable clue to the stress field in any loaded structure, and in the simpler cases may be considered to give, within practical limits, the exact solution.

For the problem under consideration, the simplest type of analytical solution will be obtained if the sheet-stiffener combination is assumed to comprise

a completely two-dimensional stress field. This simplification points to the consideration of an unstiffened panel of thickness t, loaded by means of a uniform pressure w exerted over a distance 2a along the edge of the panel. If it is assumed further that the dimensions of the panel are large in comparison with the distance 2a, then the solution obtained for a semi-infinite panel will be valid in the region near the point of application of the load. For this case, the following results may be obtained[1]:

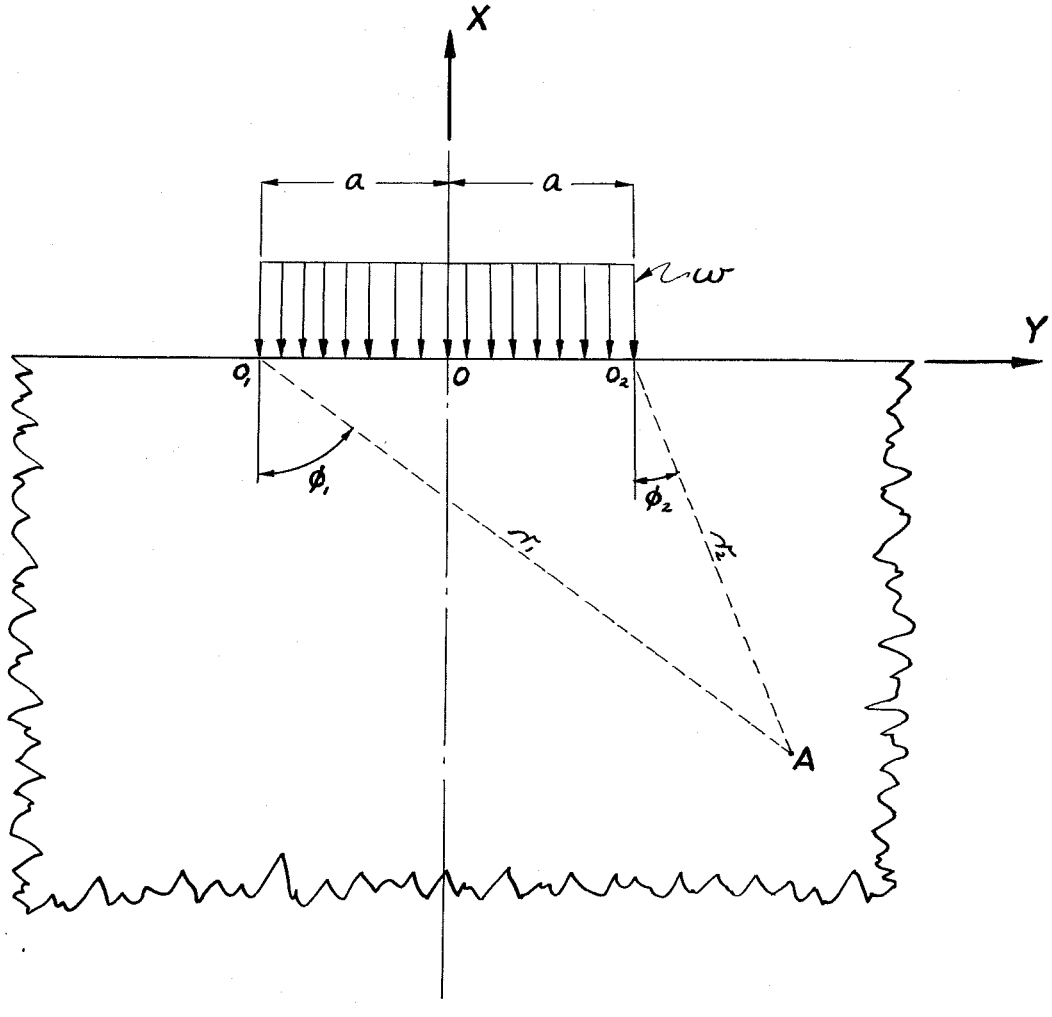

[1] References (2), (4), & (6).

(a) Airy's stress function:

$$F = \frac{w}{2\pi}\left(r_2^2\,\phi_2 - r_1^2\,\phi_1\right)$$

(b) Stresses at any point A, in directions parallel to the axes $\overline{OX}$ and $\overline{OY}$:

$$\sigma_x = \frac{w}{2\pi}\left[2(\phi_2 - \phi_1) - \sin 2\phi_2 + \sin 2\phi_1\right]$$

$$\sigma_y = \frac{w}{2\pi}\left[2(\phi_2 - \phi_1) + \sin 2\phi_2 - \sin 2\phi_1\right]$$

$$\tau_{xy} = \frac{w}{2\pi}\left(\cos 2\phi_1 - \cos 2\phi_2\right)$$

(c) Maximum shear at any point A:

$$\tau_{max} = \frac{w}{\pi}\sin\left(\phi_1 - \phi_2\right)$$

Hence, the lines of constant maximum shear (isochromatics) are circles with centers on $\overline{OX}$ and passing through O_1 and O_2. The greatest value of the maximum shear is $\tau_{max} = w/\pi$ which occurs when $(\phi_1 - \phi_2) = \pi/2$ (i.e., on a semicircle with center at O and radius equal to a).

(d) The isoclinic lines (see Part II,b(2) for definition) are a set of rectangular hyperbolas passing through O_1 and O_2, and whose asymptotes make an angle $(\phi_1 + \phi_2)/2$ with $\overline{OX}$ and $\overline{OY}$ respectively.

(e) The trajectories of the principal normal stresses are systems of confocal ellipses and hyperbolas with foci at O_1 and O_2.

(f) The trajectories of the maximum shearing stresses (the so-called Luders', or

slip, lines) form a second set of orthogonal systems of curves, which everywhere cross the principal stress trajectories at an angle of $\pi/2$.

Two factors prevent an exact experimental reproduction of this case. The first is the presence of the boundaries of the finite panel which causes the stress conditions todeviate from those of the ideal case. Secondly, a uniformly distributed load is difficult to obtain since the intensity of the pressure becomes infinite at the edges of a rigid contact. As shown by Timoshenko (reference 5), the distribution of pressure under a rigid contact is given by the expression:

$$q = \frac{P}{\pi \sqrt{a^2 - y^2}}$$

where q is the intensity of pressure, P is the total applied load, and the coordinates are the same as above.

Notwithstanding these practical limitations, the theoretical s olution is approximately true at a sufficient distance from the sides and bottom of the panel, as has been shown by Coker and Filon (reference 2).

2. If now we consider the case of a stiffened panel, assuming for our purposes that the stiffener is integral with the panel and of the form shown b elow, we see immediately that the exact stress function solution will be considerably more complex than for the

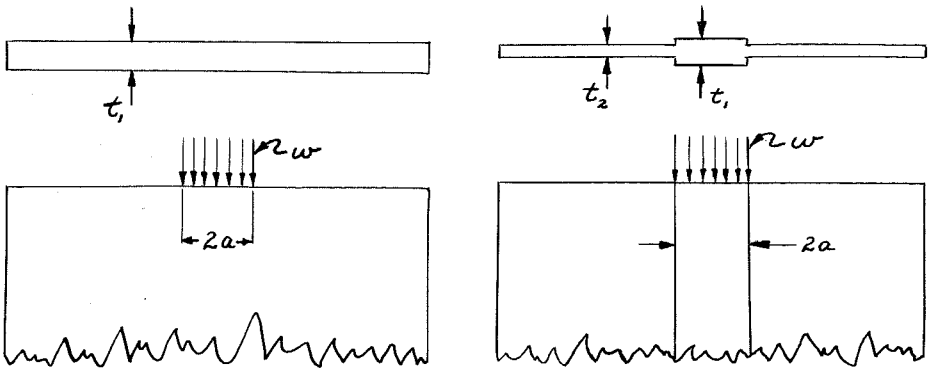

Unstiffened Panel Stiffened Panel

case above. Hence, let us attempt to obtain a less involved, though approximate, solution by making such simplifying assumptions as will permit us to deduce the stress field in the stiffened panel from that in the unstiffened panel.

In the first place, since we define unit stress as the stress per unit area, we may say that having given two unstiffened panels of thicknesses t_1 and t_2 respectively ($t_1 > t_2$), but with other dimensions identical and having equal loads applied in the manner of the first case, the distribution of stresses through the panels will be the same, but the intensity of stress at corresponding points in the two panels will be in the ratio of t_1/t_2. Now, if we assume, for a stiffened panel having a thickness t_1 at the stiffener, and a panel thickness t_2, that the stress field remains essentially two-dimensional throughout (i.e., neglect the effects of the discontinuity in thickness due to the presence of the stiffener, as well as the method of transfer of stress from the stiffener into the panel), we may conclude that,(1) the stress distribution in the stiffened

panel will be fundamentally the same as that in the unstiffened panel; (2) the stress intensities at the stiffener will be the same as for the unstiffened panel of thickness t_1, and (3) the intensities in the panel will be greater and in the ratio of t_1/t_2 to those in the unstiffened panel.

Hence, for a uniformly distributed load w over a stiffener of width 2a and thickness t_1, the maximum shearing stress at any point A in the panel of thickness t_2 becomes, according to our deduction:

$$\tau_{max} = \frac{t_1}{t_2} \frac{w}{\pi} \sin(\phi_1 - \phi_2)$$

In practice, the stiffened sheet must necessarily deviate considerably from the case of the semi-infinite panel; as would be expected, the stress patterns in a finite panel of relatively small dimensions are greatly altered from those of the more ideal case. It is this case of a small panel with a comparatively large stiffener which has been investigated in this project by photoelastic means, to a discussion of which method we now proceed. The assumptions made above, being of a general nature, would indicate that although the stress distribution corresponding to a given applied load will vary for panels of different dimensions, the only variation for panels of equal dimensions throughout (except for different sheet thicknesses) will, to a first approximation, be in the intensity of the stresses. The tests

made will perhaps help to substantiate this assumption.

b. The photoelastic method.

1. General remarks.

Photoelasticity is an experimental method which uses polarized light for determining the stresses in transparent models of structural parts loaded either statically or dynamically. It provides a convenient tool for checking the results obtained by means of the mathematical theory of elasticity and for obtaining independent solutions to problems too complex for a reasonably simple mathematical treatment. The great advantage of the photoelastic method is the possibility of observing directly the formation, growth, and intensity of internal stresses. Any problem of two-dimensional stress analysis may be investigated solely by the optical method to completely determine the distribution, magnitude, and direction of the internal forces.

The usefulness of the photoelastic method lies in its adaptability to practical investigation, i.e., in the validity of transfering the results obtained from the model to the actual structure. According to Alexander (reference 1), an accuracy of within 2 per cent is possible, for the stresses at corresponding points are rigorously proportional, provided that, (1) the elastic limit is exceeded in neither the structure nor its model; (2) the external forces are everywhere in strict

proportion, and (3) the ratio of elastic constants is the same in both materials if the plate contains any holes. Since the mechanism of polarization is actuated by stress alone (i.e., the polarizing effect of the model is independent of strain), the results are fully independent of the stress-strain relations of the materials.

2. Working Fundamentals.

The optical theory of photoelasticity may be found in a number of texts, among which are references (1), (2), and (3). In undertaking such an investigation as this, one is primarily interested in the results applicable for direct use; the working fundamentals of the method will, therefore, be briefly summarized here.

A list of the necessary laboratory apparatus is given in Part III. If an understanding of the polarization phenomenon may be assumed, we will proceed directly to list the data obtained from the image of the loaded model and the use which is made of that data.

Isochromatic lines. Referring to Appendix A, photographs 9A - 13A, it is seen that there appears on the loaded model a series of alternating bright and dark lines. These so-called "isochromatics" are shear contour lines; i.e., lines along which the maximum shearing stress is a constant. The increment of stress value between lines is constant for a given thickness of the model; and by means of a proper calibration

method these lines may be readily evaluated and τ_{max} determined at every point.

Isoclinic lines. The isochromatics have no bearing on the directions of the stresses in the material. By a suitable manipulation of the apparatus (described under Procedure), a second series of dark lines, called isoclinics, is obtained. Along each of these the directions of the principal stresses (and, hence, also that of τ_{max}) are constant.

Isotropic points. A point at which the value of (p - q) is zero is called an isotropic point. This means that at such a point there is radial tension, radial compression, or zero stress. A locus of such points is termed a neutral line. Since at an isotropic point the directions of the stresses are indeterminate, an infinite number of isoclinics pass through the point. An example of this appears on the model investigated.

Principal stress trajectories. The directional distribution of each of the principal stresses may be plotted graphically after the isoclinic lines have been determined; the two systems form a network of orthogonal curves. It should be noted that p and q are not necessarily constant along these curves, but vary according to the relations:

$$\frac{dp}{d\theta} = (p-q)\cot\beta$$

$$\frac{dp}{d\theta} = (p-q)\tan\beta$$

Maximum shearing stress trajectories. Since

the maximum shearing stress at any point acts at an angle $\pi/4$ to the directions of p and q, the directional distribution of τ_{max} may be similarly plotted. This determines a second network of orthogonal curves which coincide approximately with the lines of slip (the so-called Luders' lines) which appear in a test piece of mild-steel, or other ductile material, when the limit of plasticity is reached.

Separation of the principal stresses. The isolation of the individual values of p and q are not so simple, nor so accurate as the (p - q) determination. There are available such analytical methods as separation by graphical integration processes and by plotting the so-called isopachics, lines along which the value of (p + q) is constant. There are also such mechanical means for determining (p + q) as the membrane method and the lateral strain measurement method.

In view of the necessity for placing limits upon the scope of this investigation, no attempt has been made to isolate the values of the principal stresses. From a practical standpoint, in fact, the main value of the photoelastic method lies not in the possibility of obtaining the exact values of the principal stresses, but in giving directly a physical picture of the stress distributions and concentrations. For purposes of reference, however, an analytical method of separating p and q is outlined in Appendix C.

PART III

LABORATORY PROCEDURE

a. Apparatus.

A complete diagram of the photoelasticity equipment is shown in Fig. 1. Ingeneral, it is the usual polariscope employing: a light source, a polarizer, and an analyser, with their respective quarter - wave plates, a projection screen, and a loading frame.

However, the polariscope shown has advantages over the usual type. Two spherical mirrors and condensing lenses are employed to give a large beam of polarized light through the model. The polarizer and analyser are placed at the focal points of their respective mirrors as shown, with the result that a beam of 20 centimeters in diameter is obtained from polaroids 5 centimeters in diameter. Since the light beam is broken by the use of these mirrors, the light path can be long in actual length yet fit into a small room. A polariscope of this type will operate without distortion to the image if the angle, α, is less than 8 degrees.

The light source is a monochromatic 60-watt Sodium Lab-Arc manufactured by the Vapor Lamp Company of the General Electric Company. The monochromatic light together with the quarter - wave plates for the light, produces circularly polarized light and allows the isochromatic lines of the model to be observed

without the presence of the isoclinic lines. This light also produces definite light and dark fringes on the screen which are necessary for a clear picture.

A set of 5.0 centimeter polaroids are used as polarizer and analyser instead of the usual nicol prisms. The polaroid is a transparent material that produces plane polarized light by simple transmission. The degree of polarization of light produced by commercial .0026 inch polaroid is 99.8% effective throughout the visible spectrum.

The two polaroids are mounted in individual stands and are free to rotate 180 degrees as required in determining the isoclinic lines. Attached directly to each polaroid is the quarter - wave plate inclined at 45 degrees to the axis of the polaroid. These quarter - wave plates are quickly detachable as the procedure demands.

The loading frames are shown in Fig. 2, and Fig. 3. The first is used to apply pure moment to a simple calibration beam, and hence, the stress per fringe order is determined. The second is the frame in which the model is loaded to 2000 pounds. It consists of a machined flat as a base, a method of applying the load, and a means of determining the load. The loading beam shown is calibrated, giving dial reading against load, and the calibration is shown in Fig. 7.

The screen of the polariscope is a five by seven inch camera. This gives a ground-glass screen for focusing, as well as a plate holder for pictures. As the optical system of the polariscope is complete within itself, the lens of the camera must be removed, but the iris may be used to good advantage in obtaining a clear image.

b. Models.

A summary of the desired requirements for a material to be used in making the model is given as follows:[1]

1. High stress-optical coefficient.
2. Facility of machining into intricate shapes.
3. Linear relation of stress to strain within limit of working stress.
4. High elastic constant.
5. Perfect homogeneity (physical and optical).
6. Absence of initial stresses.
7. Absence of creep while under constant stress.
8. No permanent set or residual double refraction upon removal of the applied force.
9. Dependence of double refraction on stress rather than on strain.
10. No development of edge stress aging of finished model.

---

[1] A. G. Solakian, A New Photoelastic Material, Mechanical Engineering, December 1935.

11. High transparancy.

12. Adaptability to built-up and reinforced models.

13. Low cost.

Bakelite BT61893, manufactured by the Bakelite Corporation, 247 Park Avenue, New York City, has been found to most nearly fit the above requirements, and it is used for all models in this paper. This bakelite is a clear, white material and lends to machining very readily. It usually is sufficiently free from initial stresses to be used without annealing, and no stresses will be produced during the machining process if the material is properly supported and if small cuts are made with a very sharp, well shaped tool.

Actually an 1/8 inch cut was made around the six by twelve inch stock as received from the Bakelite Corporation. This area did contain initial stress, but removing it left the remainder of the sheet free so that no annealing was necessary. Had annealing been necessary, a large hot water bath with circulation provided, was constructed with a gas thermostat control to keep the temperature at 80 degrees C. for four hours and then allow gradual cooling at a rate of not more than 4 degrees per hour. Experiments were carried out on old 3/8 inch stock, and initial stresses were removed satisfactorily.

The models used for study are shown in Fig. 5. They are the actual stiffened panel for study and the calibration beam. It should be noted that the comparison strip must be machined from the same sheet as the model in order to eliminate the two factors in the photo-elastic formula; namely, the optical constant and the thickness.

Machining was accomplished with a fly cutter. The specimens were mounted on flat boards by cementing, and, hence, ample support was obtained without clamping loads being introduced on the specimen. Machining left the surface covered with circular arcs, the height of the ridges being comparable to a surface prepared with 400 Alundum finishing paper.

The machined models allowed a very faint picture to be observed on the screen when loaded. This called for finishing of the surfaces through which the light was projected. Polishing of surfaces with a ridge down the middle would be a lengthy job, and rather than do this, a simple means to prepare the surface was sought.

Experiment showed that the machined surfaces could be built up with oil or lacquer to a smooth surface, and a high polish and transparency obtained. To verify this statement, a collection of pictures, Fig. 6, is exhibited. These pictures are of the same

beam under a constant load, but finished in four different ways. The four pictures in order are: 1) machined surface, 2) machined surface covered with a light oil film, 3) machined surface coated with clear lacquer, and 4) polished surface. The order of thickness of the lacquer film is .001 inch per side, as compared with the specimen thickness of .350 inches. The polishing of the surface in 4) was accomplished in four steps: grinding with 400 Alundum paper, wet, grinding with 500 and 600 Alundum powder respectively on canvas laps, and finishing with Levigated Alumina on a felt lap.

The optical constant of the material is not in any way changed, as the distance between fringes, the number of fringes, and the fringe location is the same for each type of finish. The pictures also illustrate the transparency of the different finishes, since the photographic negatives were exposed the same length of time for all four pictures. Finishing may be accomplished by coating the model with oil or lacquer, and hours of grinding and polishing time may be saved. The transparency in either case is as good as that of the polished specimen, but oil may prove a little inconvenient to work with. All of the results given in this paper are based upon machined models polished with clear lacquer.

c. Procedure.

Calibration beam. The fringe order of the photoelastic material is determined by applying a pure moment to a calibration of comparison beam. This is accomplished through the use of the loading frame, Fig. 3. By using the flexure formula, the stress at any distance from the neutral axis is calculated, and hence the stress determination per fringe is known. It is best to also observe the beam in white (polychromatic) light to determine the position of the neutral axis. Tests show that it is not necessarily in the center of the beam (see calculation, calibration beam). A recommended procedure for this calibration is to increase the moment in about five steps to the neighborhood of the elastic limit of the material, as a check in determining the stress per fringe.

Model loading. The model, Fig. 5, is loaded in three different ways. They are as follows:

Type I. Load is applied to the stiffener at the top and absorbed as a distributed load across the bottom. (See Fig. 13.)

Type II. Load is applied to the stiffener at the top and absorbed as a distributed load across the webs only. (See Fig. 18).

Type III. Load is applied at the top of the stiffener and absorbed at the bottom of the stiffener only. (See Fig. 21).

Determination of isochromatic lines. The quarter wave plates are inserted, and isochromatic lines are recorded in all three types of loading. A progressive load is shown for Type I in five steps from zero to 2000 pounds. See pictures 7A to 13A and 2C. Pictures 7A and 8A are included to show the model in the unstressed condition before and after loading. For Type II and III, one load of 2000 pounds is applied to each.

Determination of isoclinic lines. Removing the quarter-wave plates will give isoclinic lines superimposed on the isochromatic lines. For plotting isoclinics of a model, it is a good plan to record pictures from zero through 90 degrees in 10 degree steps, and make necessary additional pictures where the lines change rapidly. If difficulty is encountered in the interpretation of the isoclinic pictures, it is advised to view the model in white light, as the dark lines stand out more clearly than they do in monochromatic light.

The isoclinic pictures are differentiated from the isochromatic pictures by the notation of the angle θ through which the polaroids have been rotated in each case. Complete series of isoclinic photographs are given in Appendix A for Type I and Type II loadings. It was found advisable to take additional pictures in the range from $\theta = 70^{\circ}$ to $\theta = 80^{\circ}$, since here the isoclinic lines were changing rapidly

in the lower portion of the model; elsewhere, the isoclinic pictures are given for steps of 10° rotation of the polaroids.

PART IV. RESULTS.

a. Data.

1. Calibration of loading frame spring.

P = applied load in lbs.
D = dial gage reading in $\frac{1}{100}$ mm.

Run No.	1.		2.		3.		4.	
Reading	P	D	P	D	P	D	P	D
No. 1.	11	39	11	39	196	51	201	49
2.	199	85	203	87	425	99	399	95
3.	397	126	401	127	611	138	601	129
4.	590	165	598	166	787	176	796	169
5.	791	204	794	204	998	213	997	206
6.	1000	243	998	240	1199	247	1197	243
7.	1196	280	1211	281	1402	288	1401	278
8.	1394	316	1397	314	1606	325	1599	316
9.	1590	352	1590	349	1802	361	1794	353
10.	1793	387	1800	385	2002	401	1996	390
11.	2000	421	2000	420	2197	436	2190	419

Calibration runs made on "tension machine",
Galcit Structures Laboratory.
See Fig. 7. for calibration curve.

2. Photographs (see Appendix A).

Series A - Calibration beam loaded in pure bending.
(see pp. ii - iii)

Picture No.	Load, lbs.	Moment, in.-lbs.
3A	0	0
4A	11.16	16.9
5A	21.45	32.2
6A	28.81	43.2
7-	37.61	56.4
8-	48.10	72.1

2. Photographs (continued).

Series C - Model under Type I loading (pp. iv - xiv).

Picture No.	Dial rdg.	Load, lbs.	Isoclinic angle, θ
7A	0	0	(isochromatic)
8A	0	0	"
9A	40	417	"
10A	175	873	"
11A	245	1200	"
12A	317	1600	"
13A	385	2020	"
1C	0	0	"
2C	390	2065	"
3C	"	"	10 degrees
4C	"	"	20 "
5C	"	"	30 "
6C	"	"	40 "
7C	"	"	50 "
8C	"	"	60 "
9C	"	"	70 "
10C	"	"	75 "
11C	"	"	80 "

Series B - Model under Type II loading (pp. xv - xxi).

Picture No.	Dial rdg.	Load, lbs.	Isoclinic angle, θ
1B	386	2020	(isochromatic)
2B	"	"	0 degrees
3B	"	"	10 "
4B	"	"	20 "
5B	"	"	30 "
6B	"	"	40 "
7B	"	"	50 "
8B	"	"	60 "
9B	"	"	70 "
10B	"	"	$72\frac{1}{2}$ "
11B	"	"	$77\frac{1}{2}$ "
12B	"	"	80 "
13B	"	"	90 "

Series E - Model under Type III loading (p. xxii).

Picture No.	Dial rdg.	Load, lbs.	
1E	384	2000	(isochromatic)

b. Calculations and graphical work.

1. The evaluation of $\Delta\tau_{max}$ from the calibration beam. It was found that the neutral axis of the calibration beam (i.e., the line along which $p - q = 0$) varied in location with changes in load and that it moved from the compression edge of the beam, as load was first applied, toward the center line of the beam as the load was increased. At the same time, the change in stress per fringe, $\Delta\tau_{max}$, increased. No explanation is advanced for these effects, since they occurred for every type of application of pure bending moment which was tried, irrespective of the position of the beam.

In order to evaluate the isochromatic lines on the model, a value for $\Delta\tau_{max}$ was determined by the following extropolation process. Taking e equal to the distance of the neutral axis from the center line of the beam, a curve of $\Delta\tau_{max}$ vs. e was plotted from the experimental data; five points were obtained to give the straight line variation shown in Fig. 8. It was assumed that, in order to determine the fringe scale for the model, this curve should be carried to the point where $e = 0$ and $\Delta\tau_{max}$ taken there. This is admittedly an arbitrary assumption; for the purposes of this particular investigation, it seems a satisfactory

solution. However, for the sake of a logical explanation of the effects noted, a more thorough study of this individual problem might well be made.

Since the beam is loaded with a pure moment, tension and compression are found on opposite sides of the neutral axis and may be calculated from the flexure formula:

$$\sigma = \frac{My}{I}$$

Since $\sigma_c = \sigma_t = p$, and $q = 0$, the expression for maximum shearing stress becomes:

$$\tau_{max} = \sigma/2$$

where $\sigma = \sigma_c = \sigma_t$ (See Appendix B for fundamental stress relations). Therefore, the increment of shearing stress per fringe is the shearing stress at a given point divided by the fringe order n at the same point. That is,

$$\Delta \tau_{max} = \frac{\tau_{max}}{n}$$

SAMPLE CALCULATIONS

PICTURE NO.	4A	5A	6A	7-	8-
M , in.-lb.	16.9	32.2	43.2	56.4	72.1
e , inches	0.1030	0.0577	0.0406	0.0366	0.0289
I , $(in.)^4$	0.0121	0.0104	0.0099	0.0098	0.0097
σ , $lb./in^2$	1397c	3110c	4345c	5725c	7405c
y_c , in./line	0.1326	0.0748	0.0546	0.0346	0.0340
y_t , in./line	0.1326	0.0748	0.0573	0.0448	0.0356
$\sigma_{ave.}$, lb./in./line	185.2	232.6	243.3	253.2	257.5
τ_{max} , lb./in./line	92.6	116.3	121.7	126.6	128.8

FROM FIG. 8 , $\tau_{max} = 143.5\ n$ $lb./in.^2$

2. Evaluation of isochromatics. (Figs. 9-13, 18, 21). Since the increment in maximum shearing stress per fringe has been determined by means of the bakelite calibration beam, the value of τ_{max} at any point in the loaded model may now be determined by the simple process of counting the isochromatics which have passed over that point during the loading. Thus, beginning with the fringe of order zero, which may b e readily located by observing under white light the growth of the stress pattern during application of the load, the parameter of the fringe of the nth order, say, is given by the relation:

$$(\tau_{MAX})_n = n\Delta\tau_{MAX.}$$

$$= 143.5\, n \quad \text{LBS PER IN}^2$$

3. Isoclinic lines. (Fig. 15, 20). For both Series C and Series B, isoclinic diagram I (see Figs. 14 and 19) were drawn by tracing directly from the corresponding sets of photographs the isoclinic areas shown. Then diagram II for each series was drawn by estimating the position of the center line of each area in diagram I.

4. Trajectories of the principal normal stresses. (Fig. 16). The first set of these two families of curves was obtained by drawing between successive

isoclinics of parameters θ_1, θ_2, θ_3, etc., the sides of a series of polygons, such that the sides of each polygon made angles of $\frac{1}{2}(\theta_1+\theta_2)$, $\frac{1}{2}(\theta_2+\theta_3)$, etc., respectively, with $\overline{OX}$, the successive vertices lying on the successive isoclinics. These vertices then were points on a principal stress trajectory which could be easily faired in. In a similar manner, the second system of curves was drawn in orthogonal to the first family of principal stress trajectories.

5. Trajectories of maximum shearing stress. (Fig. 17). In a manner similar to that described under (4), these curves were also drawn for Type I loading. In this case, however, the polygons for the first system of shearing stress trajectories drawn were constructed with sides at angles of $\left[\frac{1}{2}(\theta_i+\theta_{i+1})+\frac{\pi}{4}\right]$ with the axis $\overline{OX}$.

c. Conclusion.

The model used in this project has been investigated sufficiently to give a fairly complete picture of the shear characteristics of the sheet in the type of panel considered, namely an unbuckled sheet reinforced with a light stiffener. The tests made tend to confirm the fact that the stress conditions in the panel are influenced largely by the edge conditions (i.e., the dimensions of the panel, the nearness of the edge boundaries either free or loaded, etc.). In

addition it was noted that for a load applied in compression through the stiffener, the stress distribution in the panel was closely analogous to that in an unstiffened panel with a uniformly distributed edge load over a distance equal to the width of the stiffener.

Appendix D contains the data and photographs obtained with one additional model. Due to unavoidable conflicts in the schedule of the Institute shop, this model was not obtained early enough to include the data in the main body of the thesis. These later tests, however, provide an interesting comparison with the first experiments made and serve as confirmation for the above remarks.

The experiments conducted indicate that a further and much more complete investigation of stiffened sheet characteristics by the photoelastic method would be of considerable value. The inherent advantages of the optical method for two-dimensional stress analysis make it highly adaptable to a study of the stress distributions in thin sheet structures below buckling.

REFERENCES

1. Alexander, Nicholas. Photoelasticity. Rhode Island State College. Kingston, Rhode Island. 1936.

2. Coker, E. G., and Filon, L. N. G. A Treatise on Photo-Elasticity. Cambridge University Press. London. 1931.

3. Filon, L. N. G. A Manual of Photo-Elasticity for Engineers. Cambridge University Press. London. 1936.

4. Nadai, A. Plasticity. McGraw - Hill Book Company. New York. 1931.

5. Timoshenko, S. Theory of Elasticity. McGraw - Hill Book Company. New York. 1934.

A P P E N D I C E S

APPENDIX A

Photographs. Pertinent data is given on each picture. The following photoelastic photographs are shown:

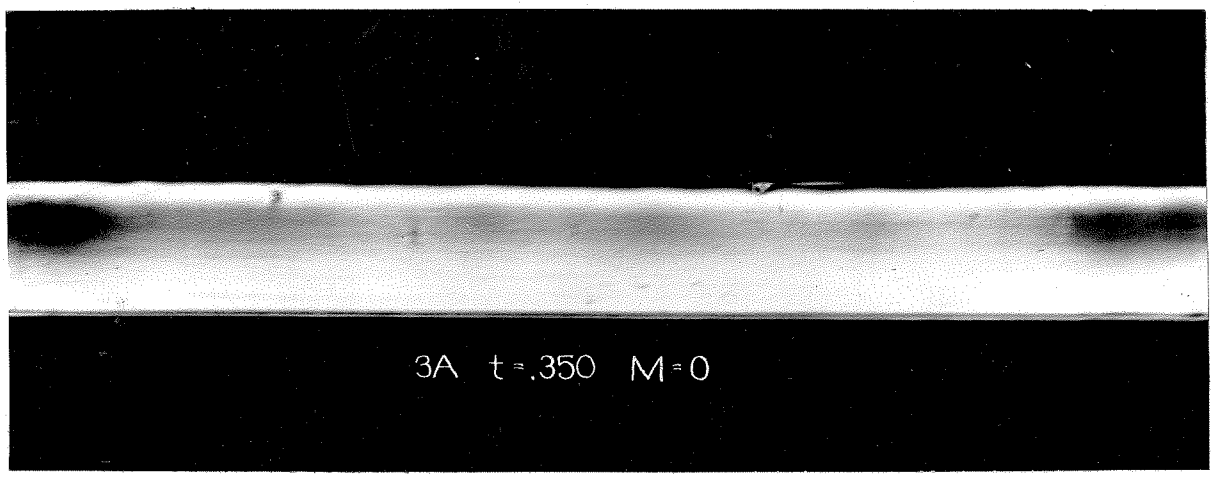

3A t=.350 M=0

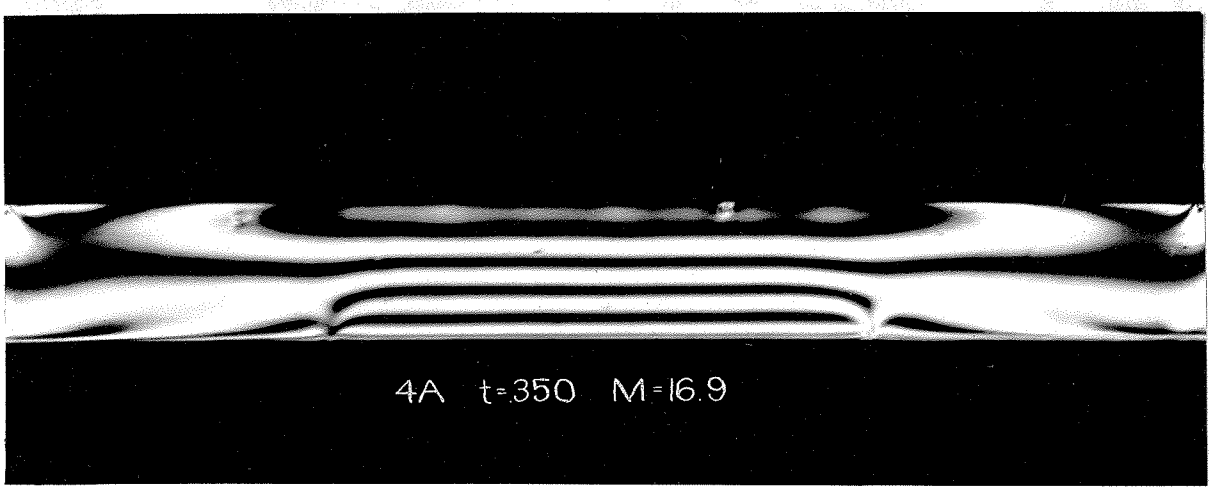

4A t=.350 M=16.9

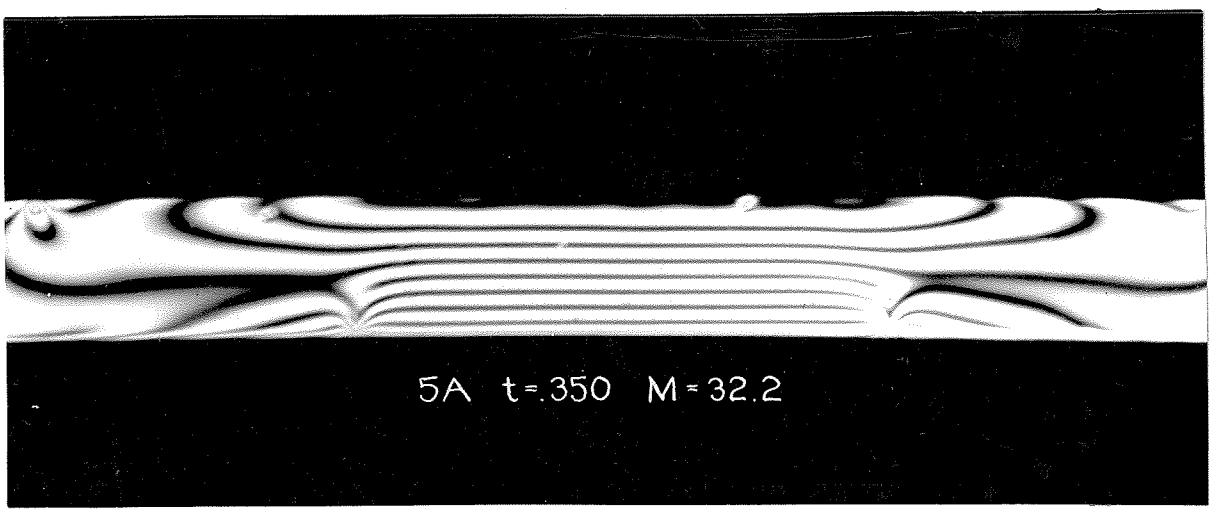

5A t=.350 M=32.2

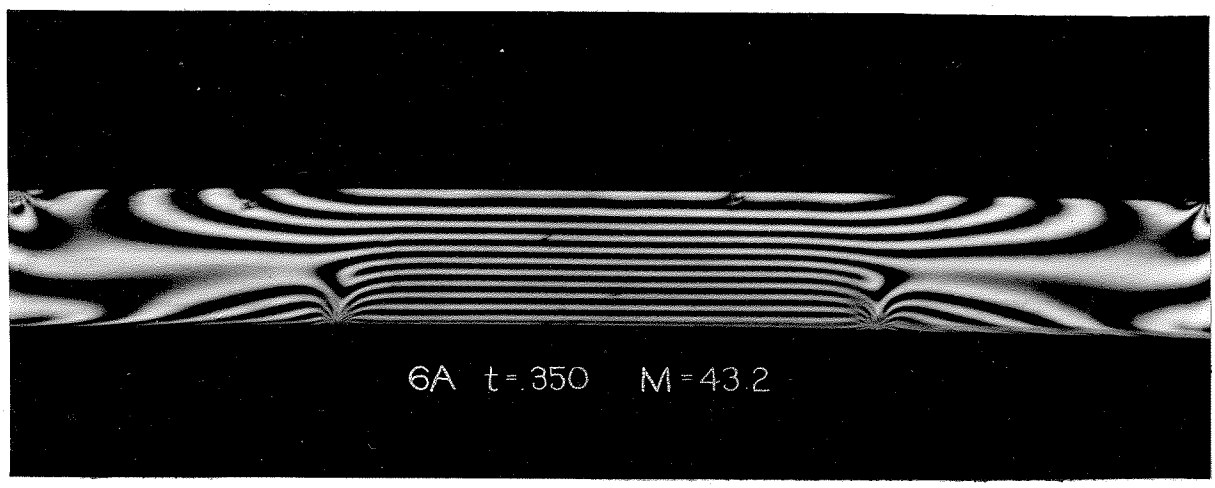

6A t=.350 M=43.2

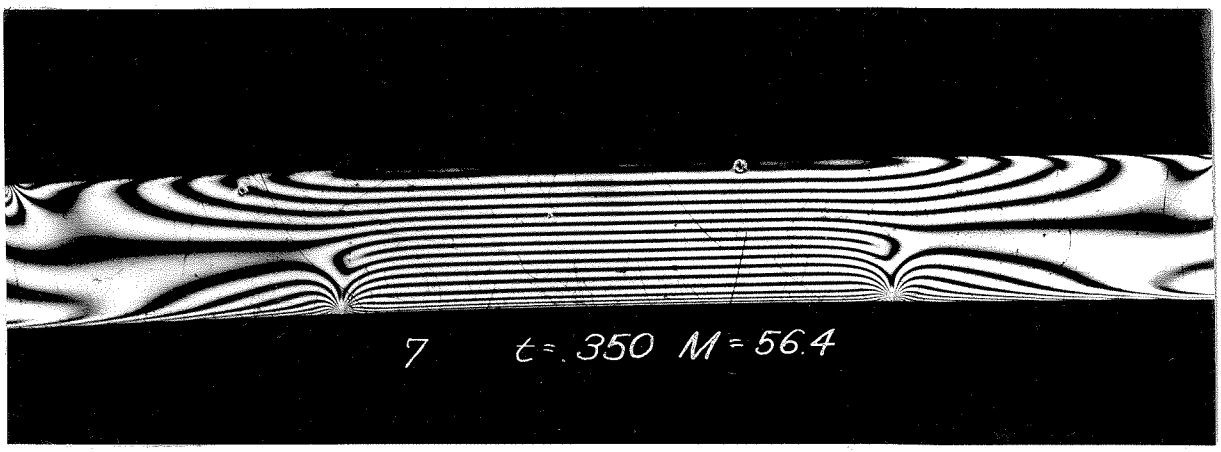

7 t=.350 M=56.4

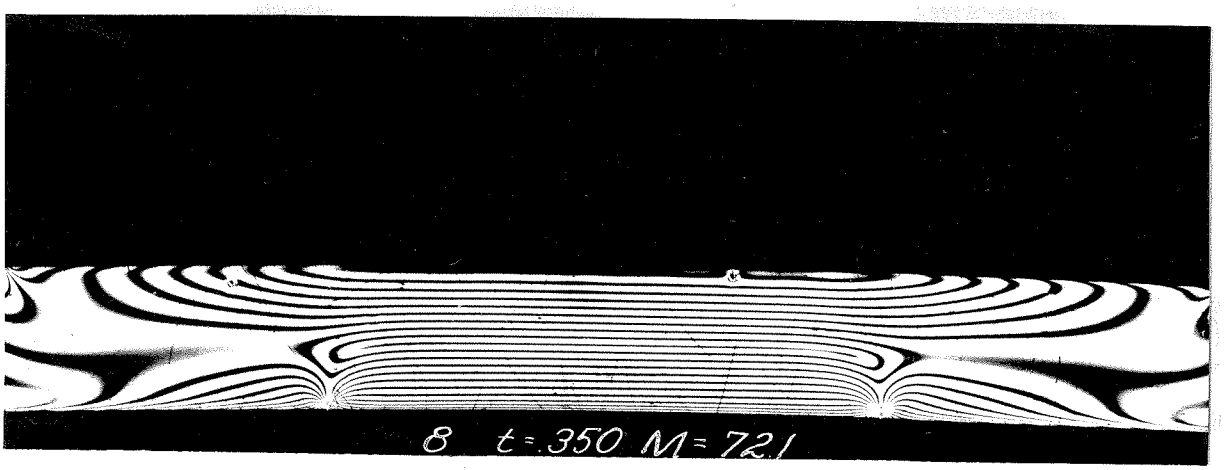

8 t=.350 M=72.1

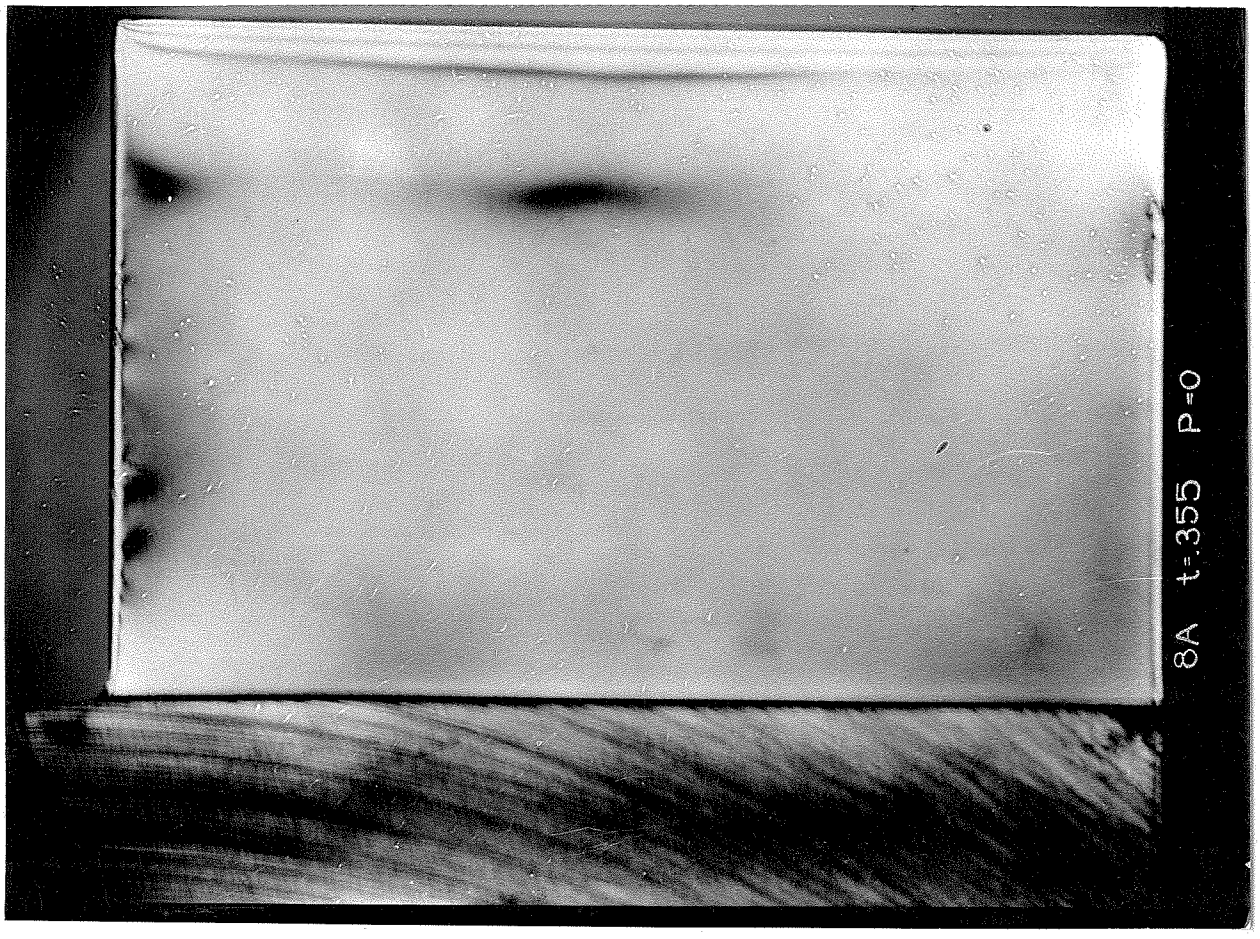
8A t=.355 P=0

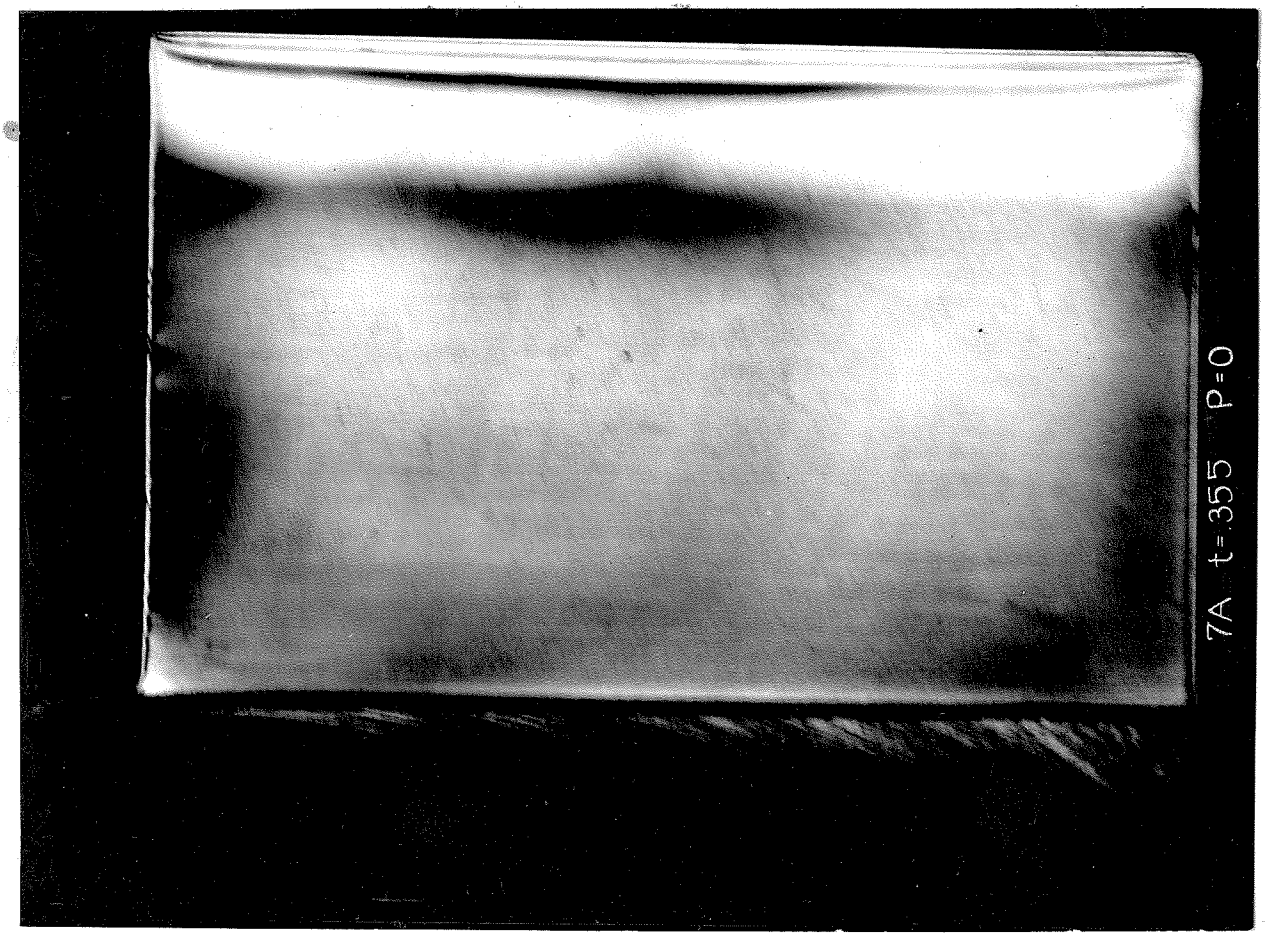
7A t=.355 P=0

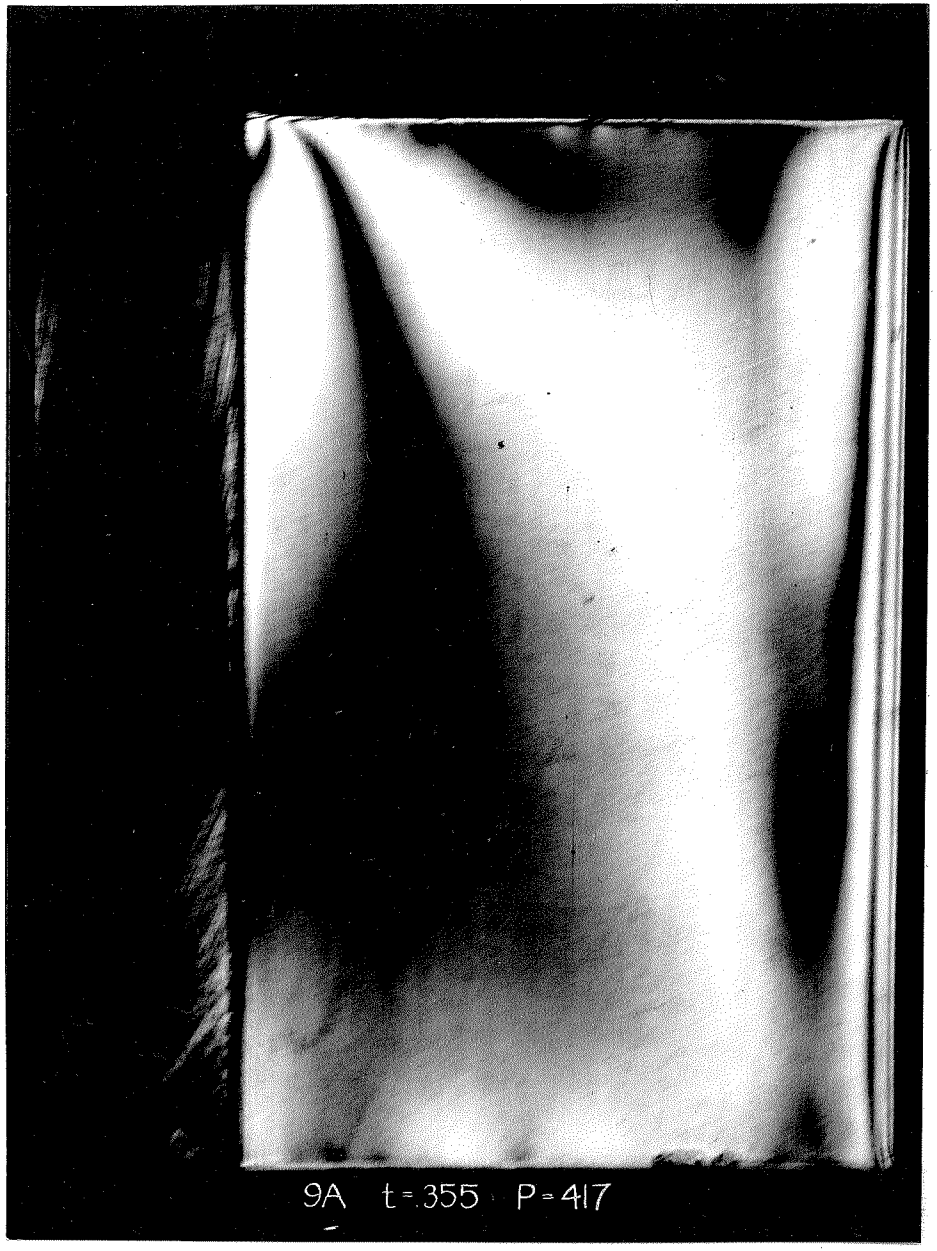
9A t=.355 P=417

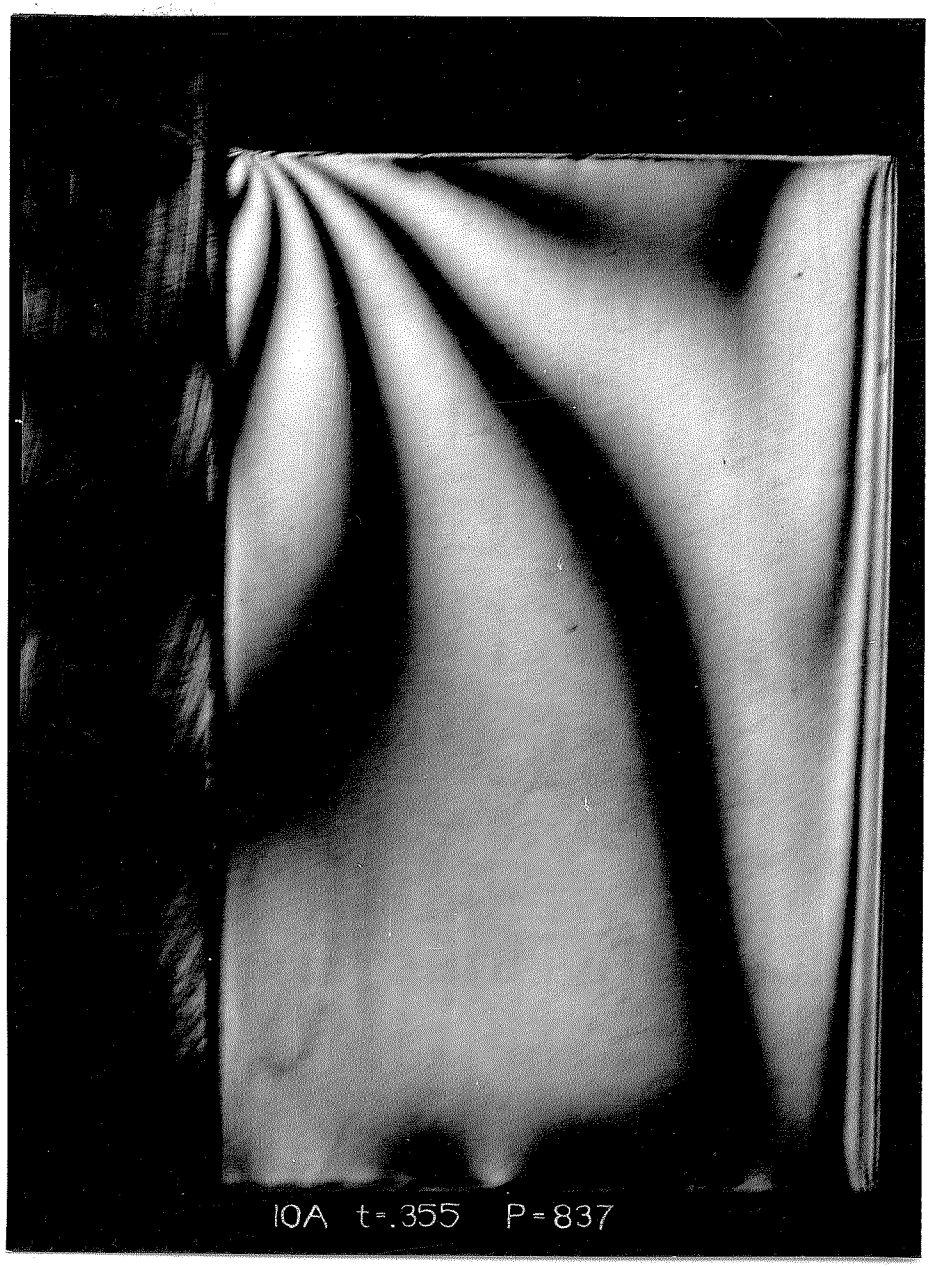
10A t=.355 P=837


11A t=.355 P=1200

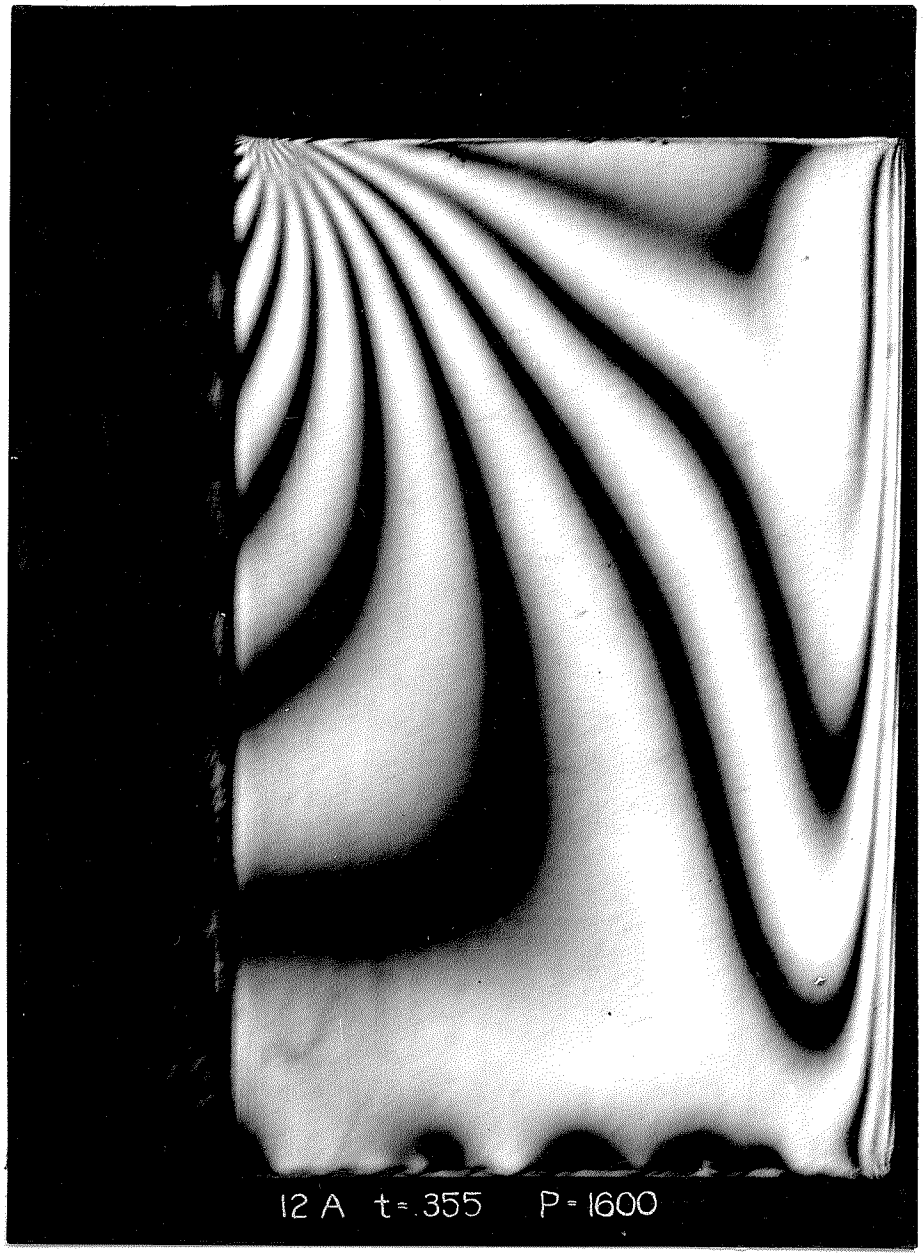
12 A t=.355 P=1600

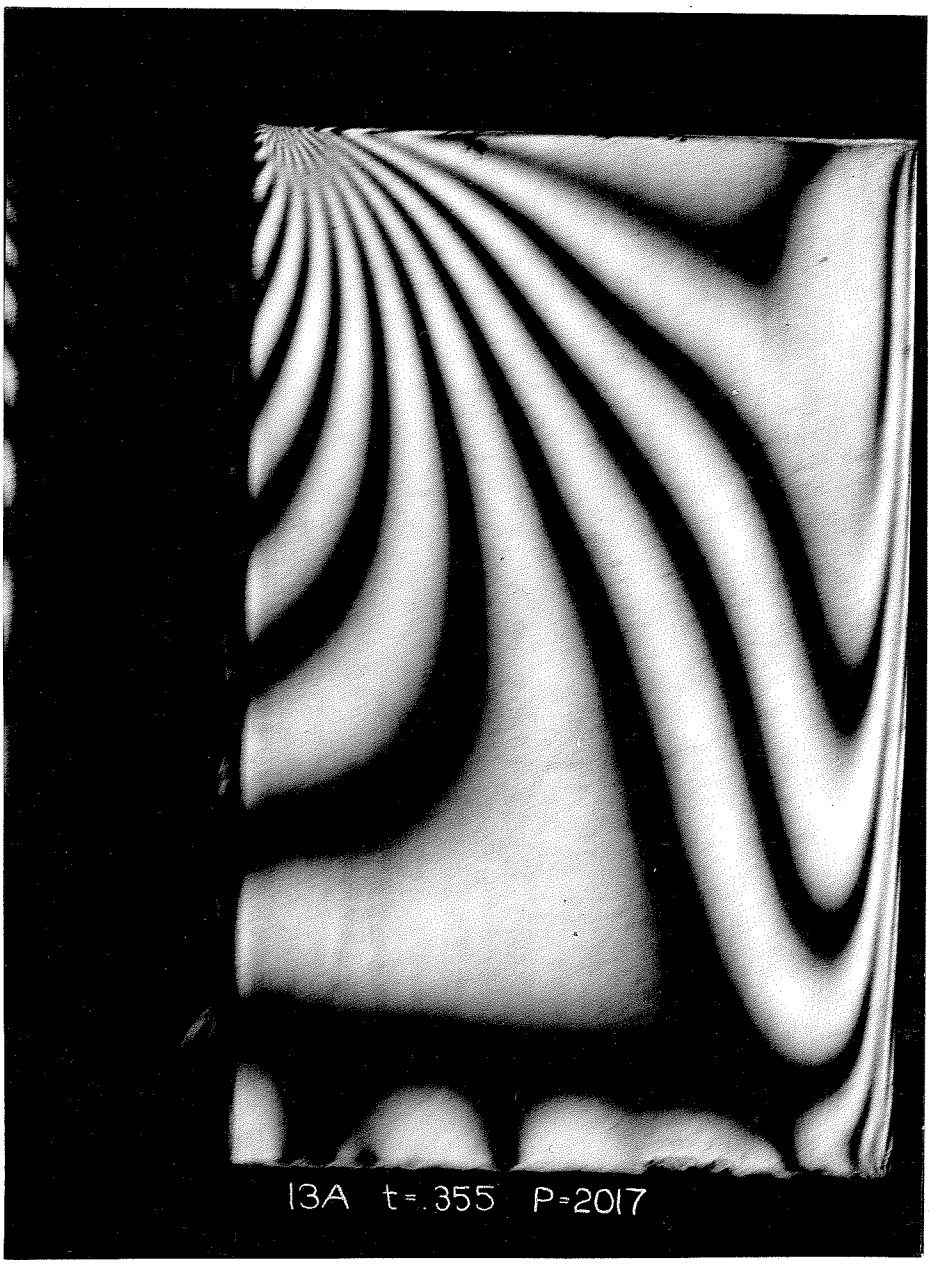
13A t=.355 P=2017

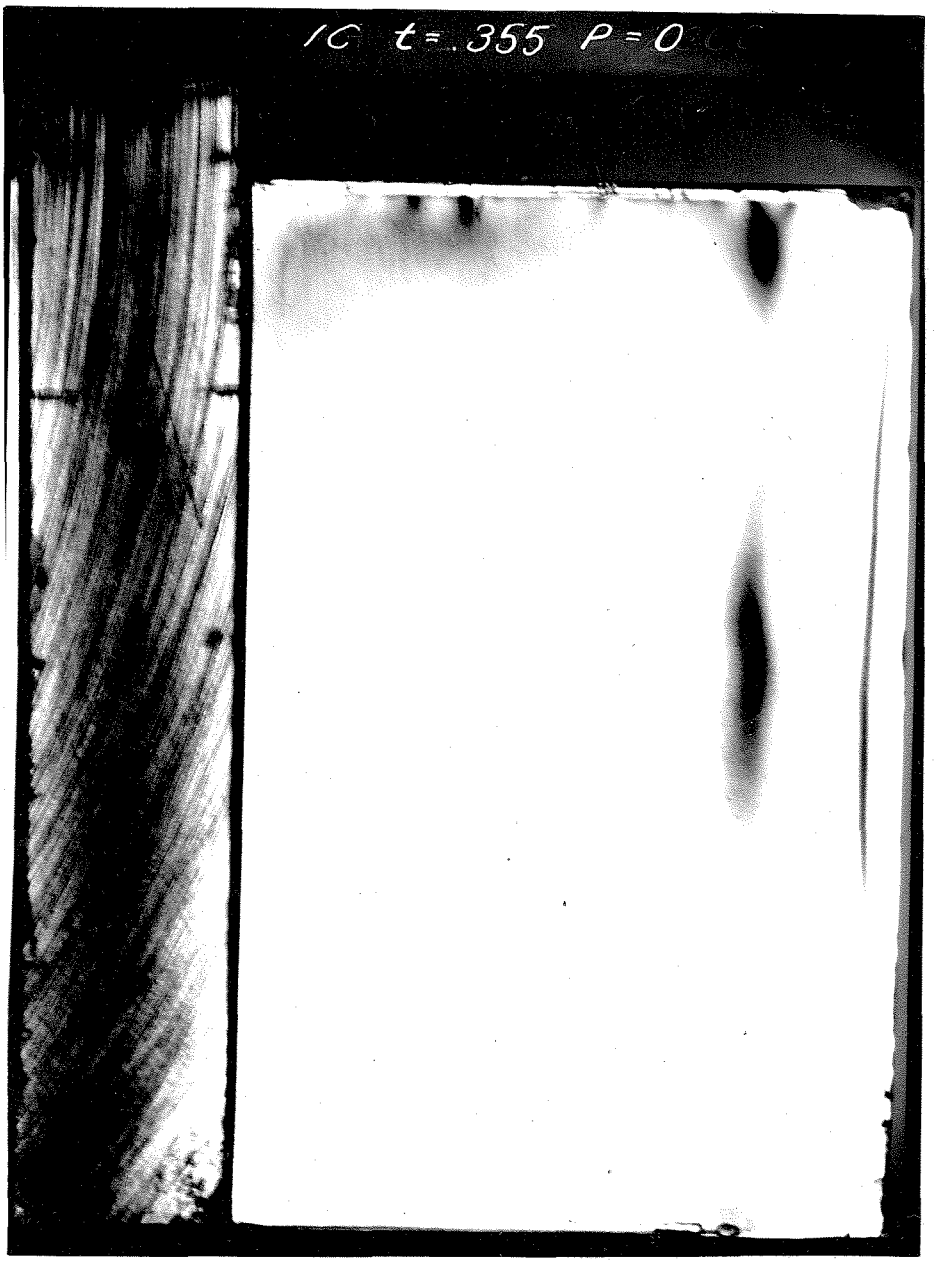
1C t=.355 P=0

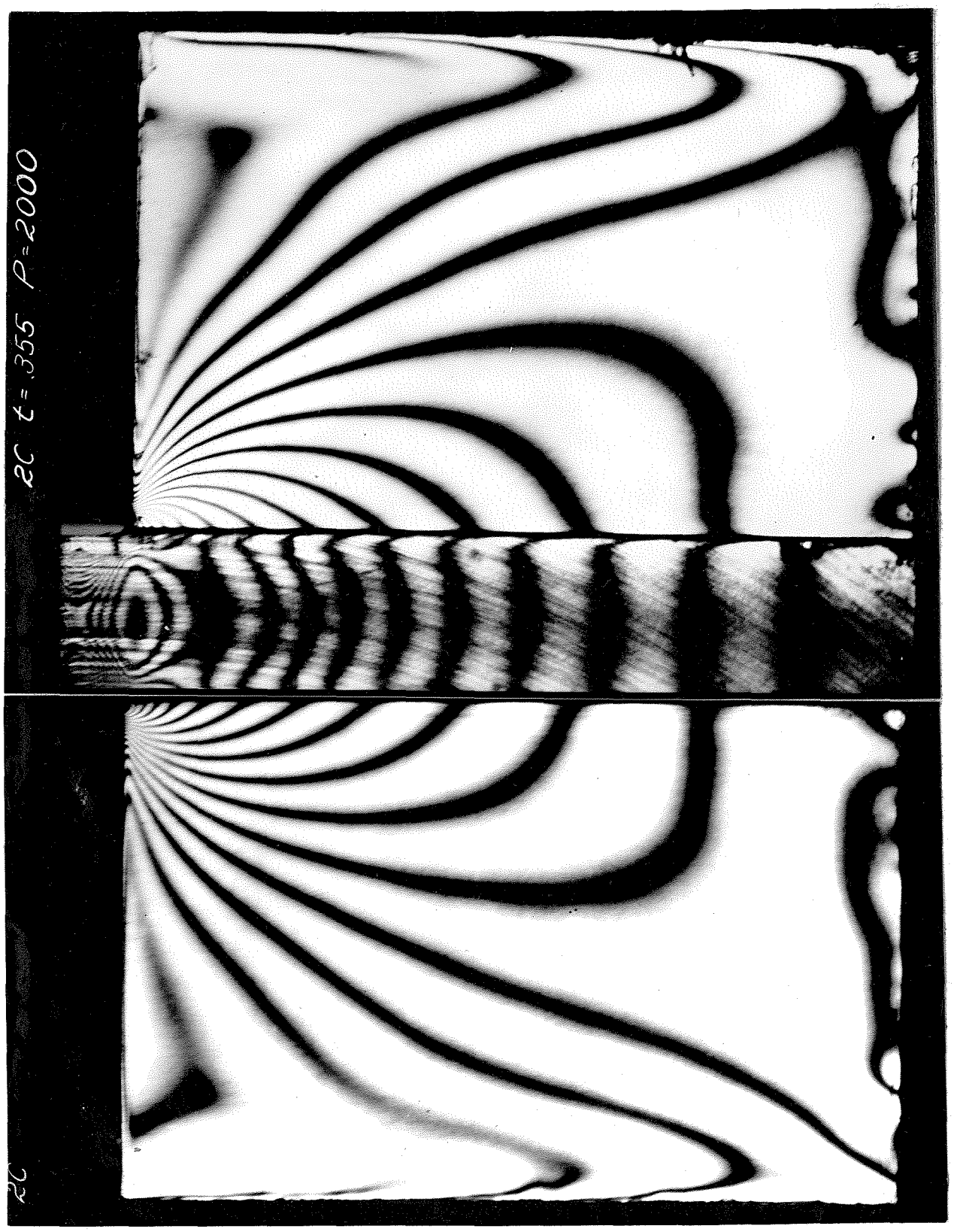
2C t=.355 P=2000
2C


3C t = 355 P = 2000 θ = 10°

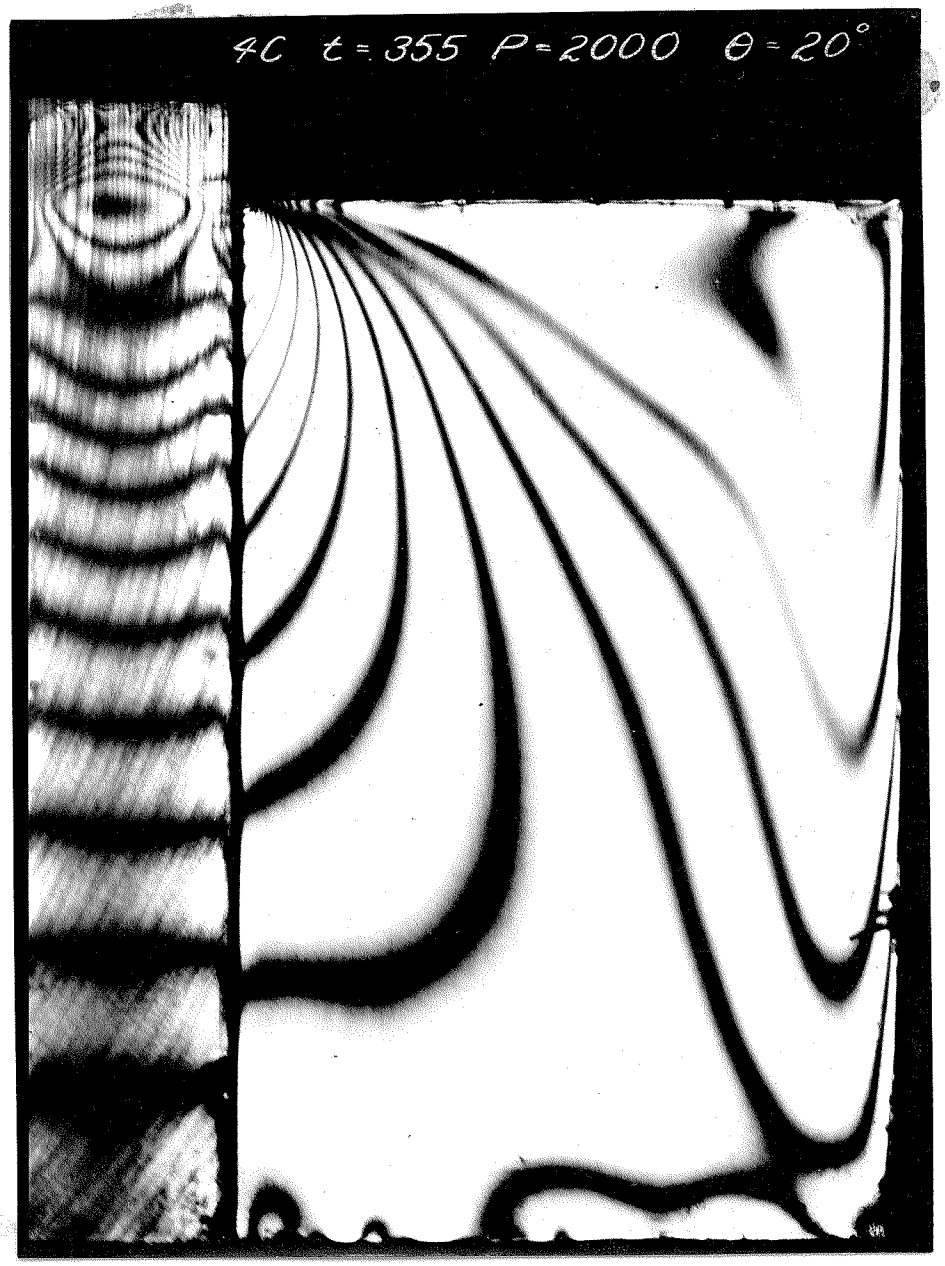
4C t = 355 P = 2000 θ = 20°

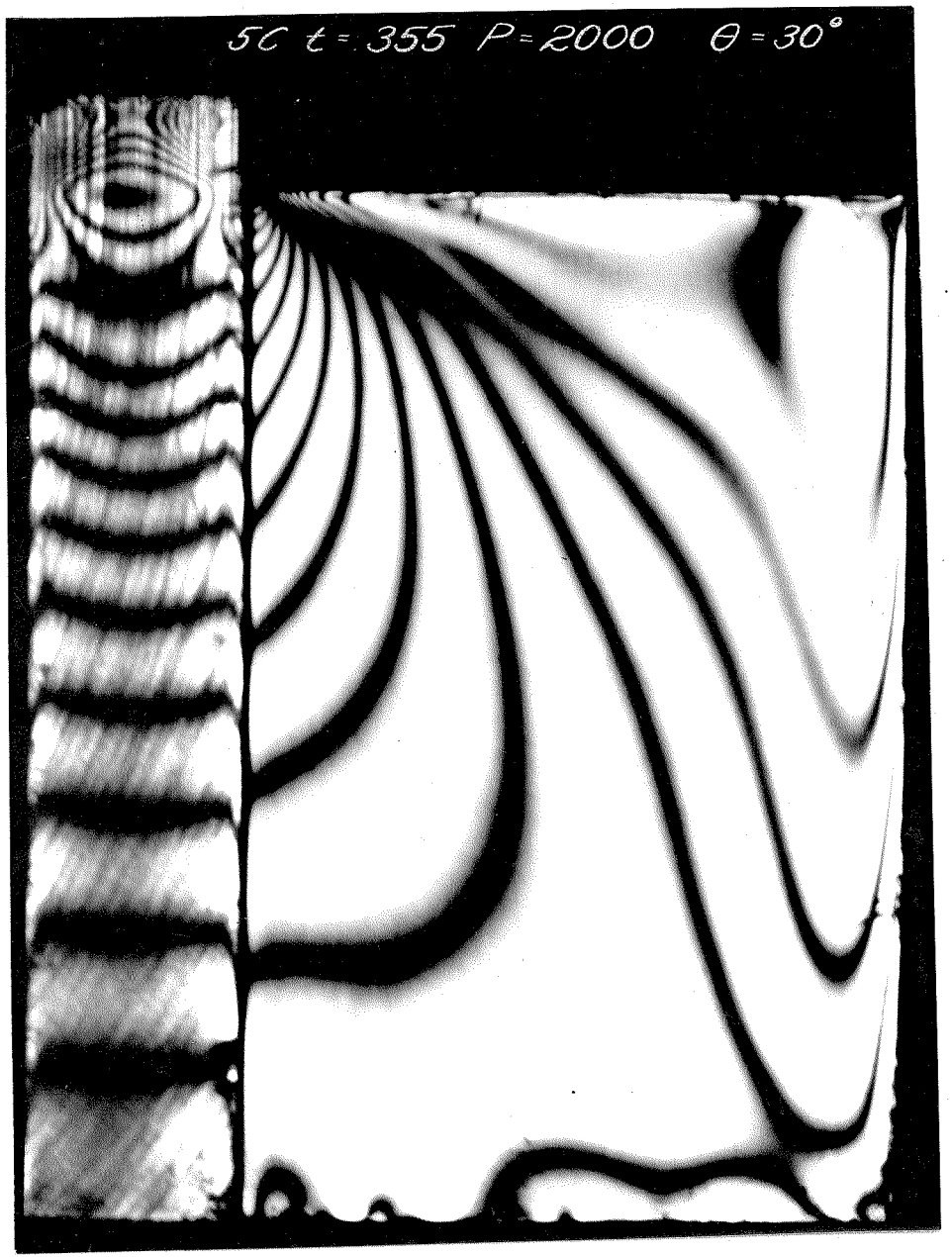
5C t = .355 P = 2000 θ = 30°

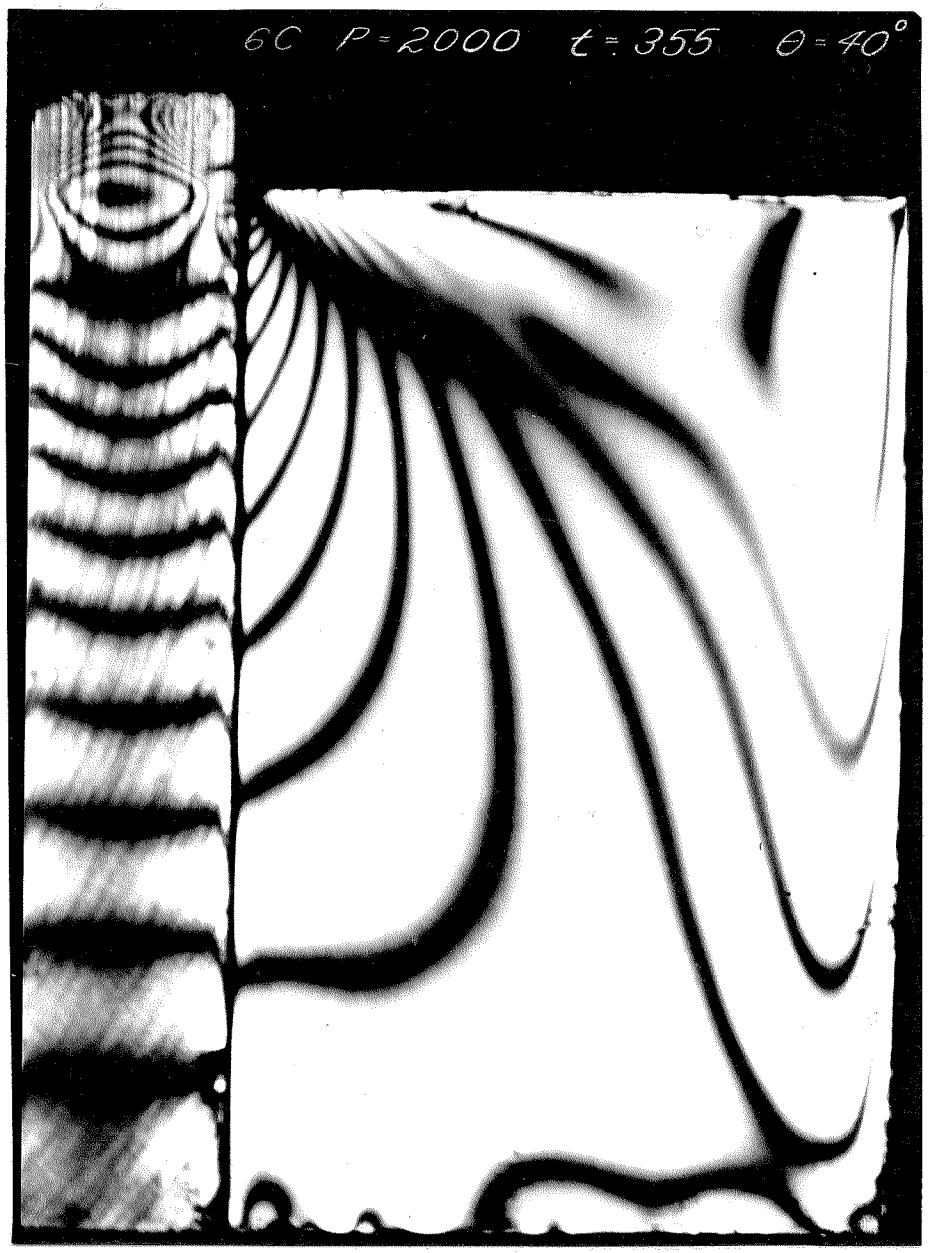
6C P = 2000 t = .355 θ = 40°


7C t=.355 P=2000 θ=50°

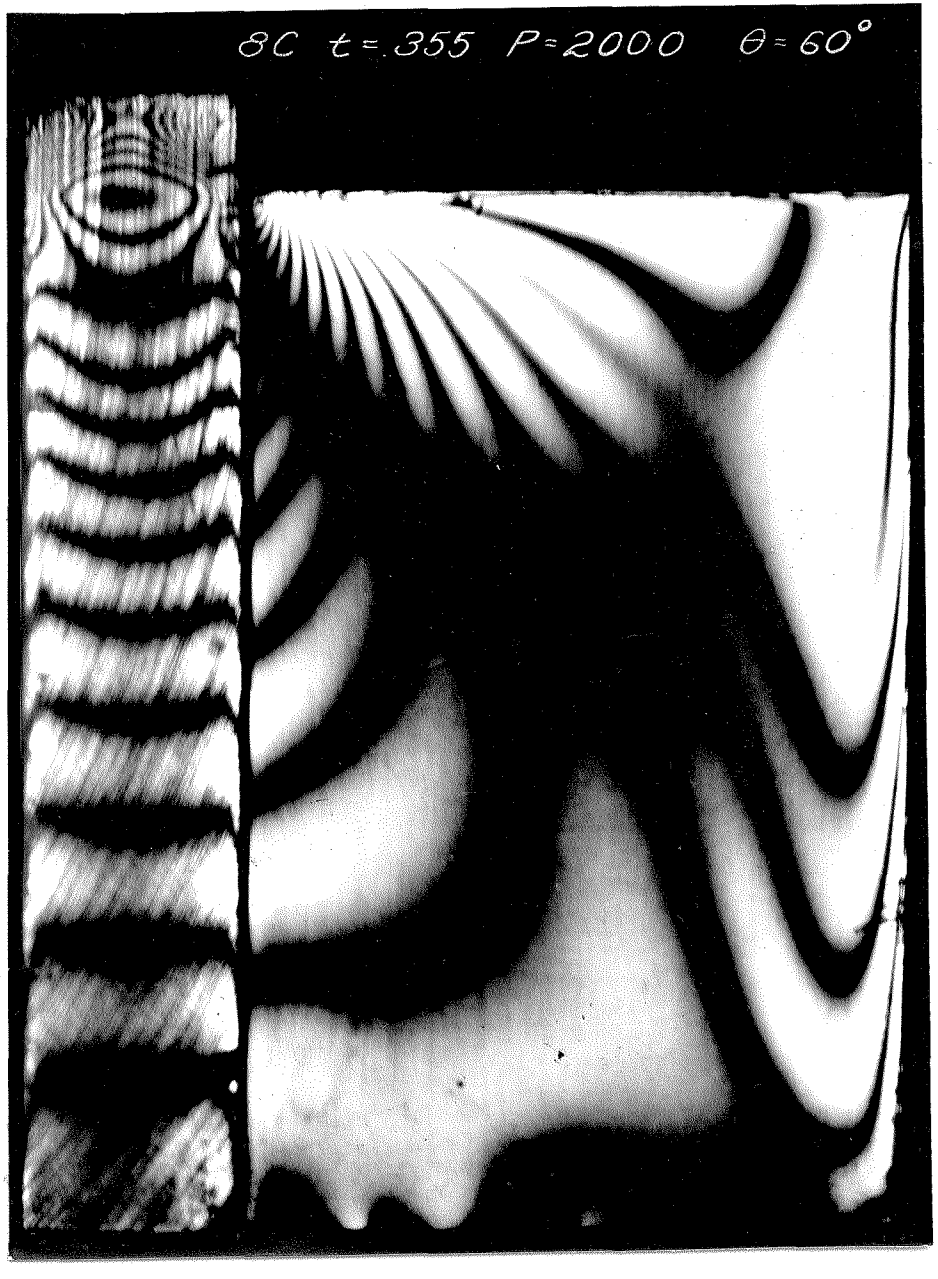
8C t=.355 P=2000 θ=60°

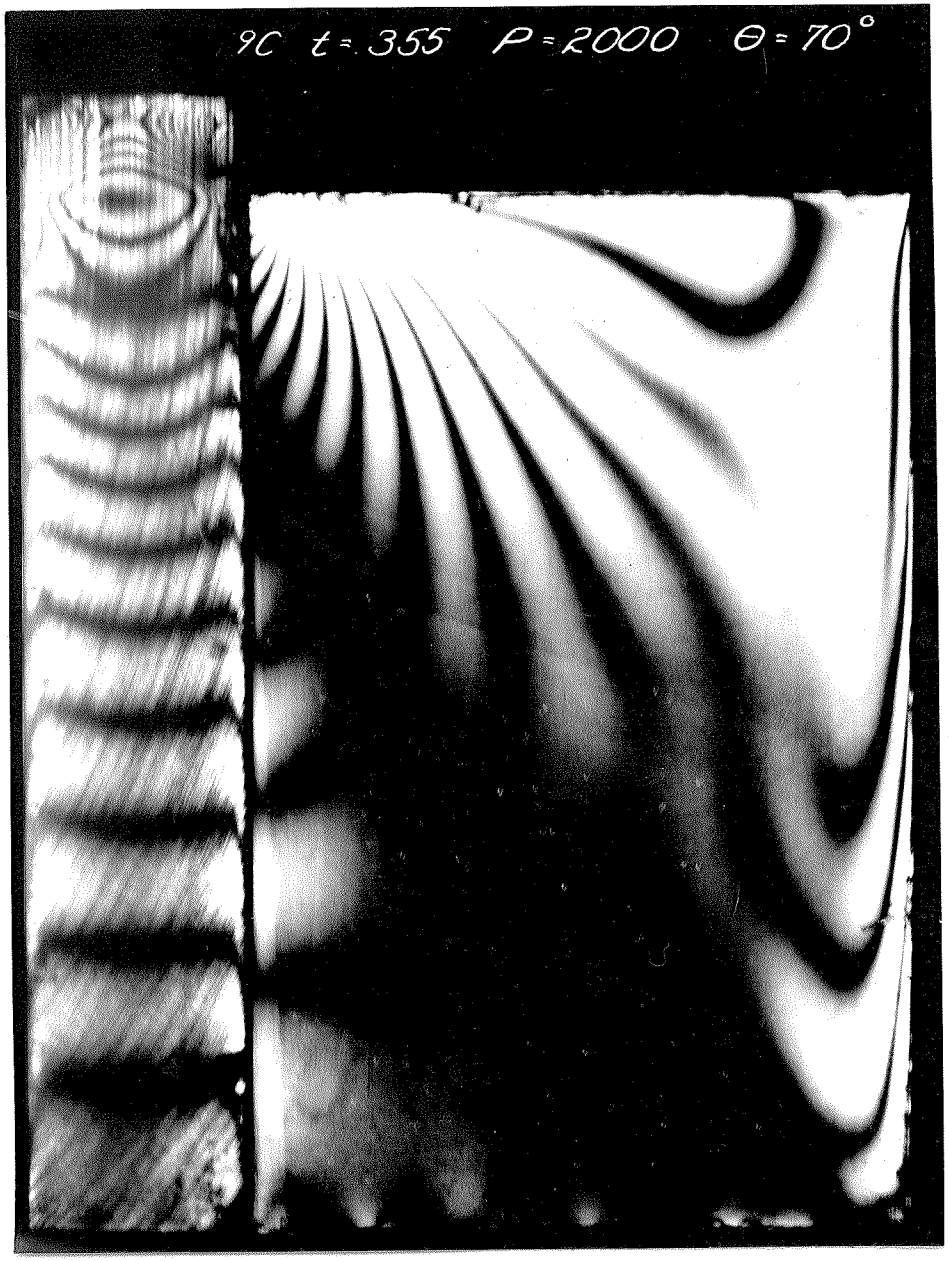
9C t = 355 P = 2000 θ = 70°


10C t = 355 P = 2000 θ = 75°


11C t=.355 P=2000 θ=80°

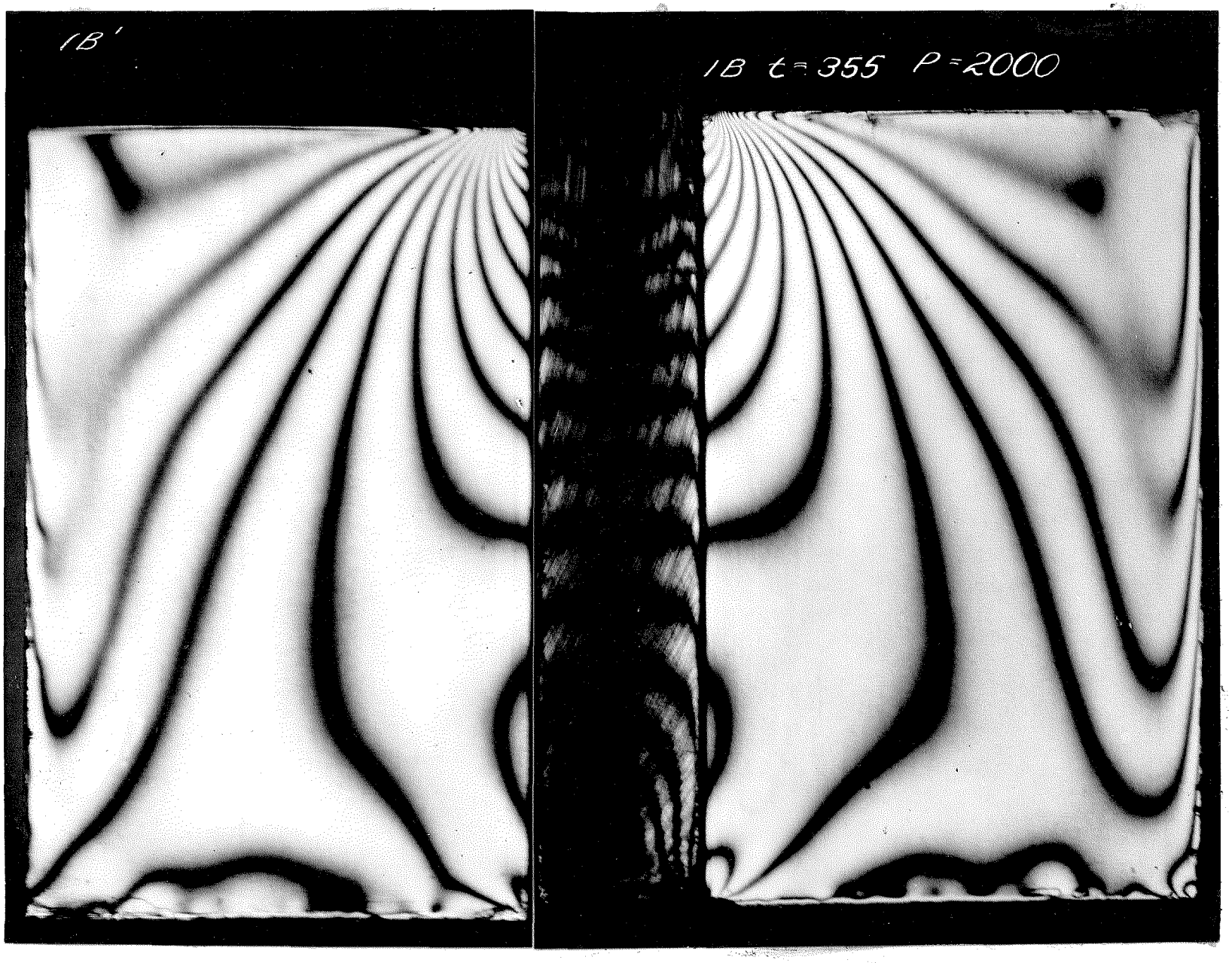
1B'
1B t=355 P=2000


2B t=.355 P=2000 θ=0°

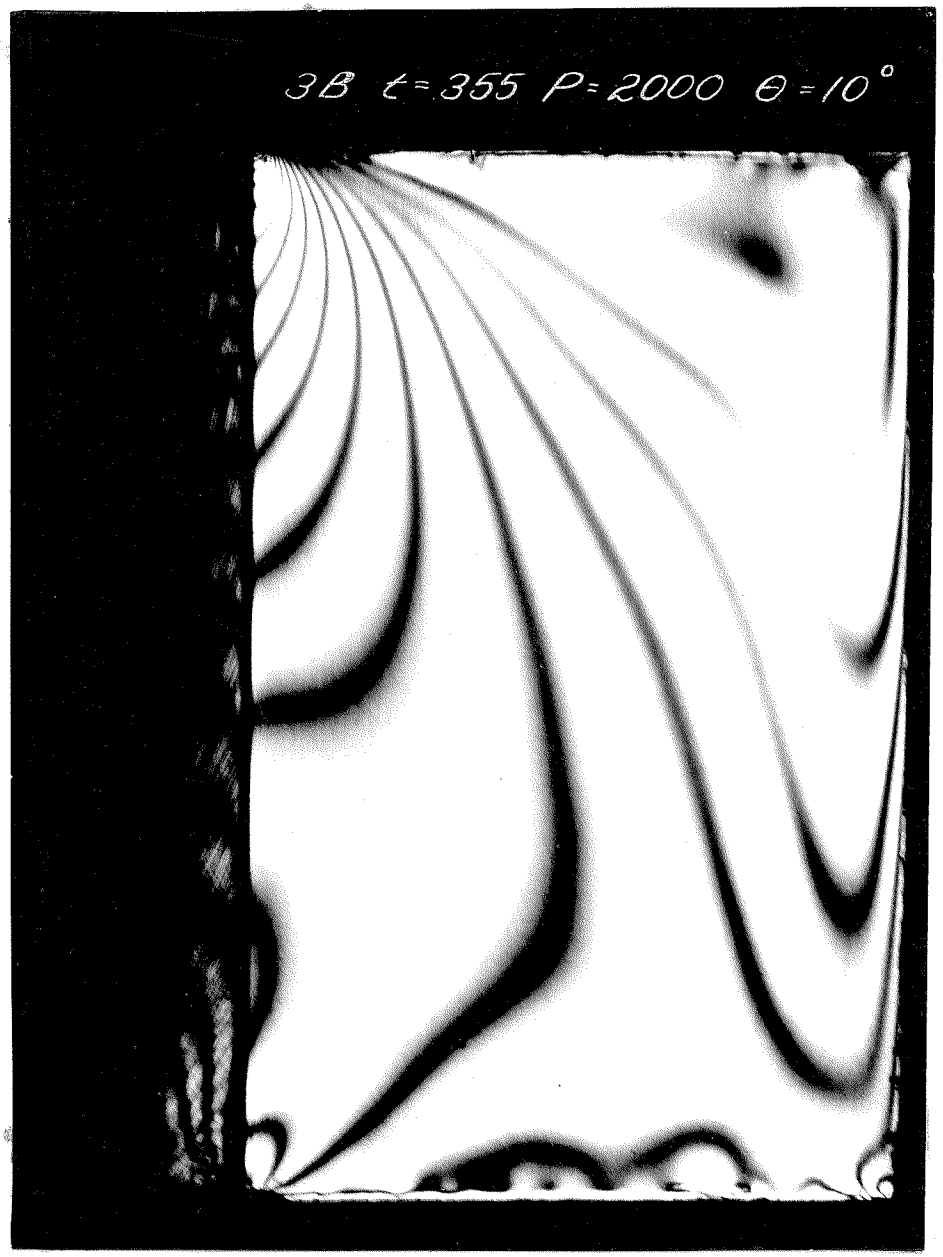
3B t=.355 P=2000 θ=10°

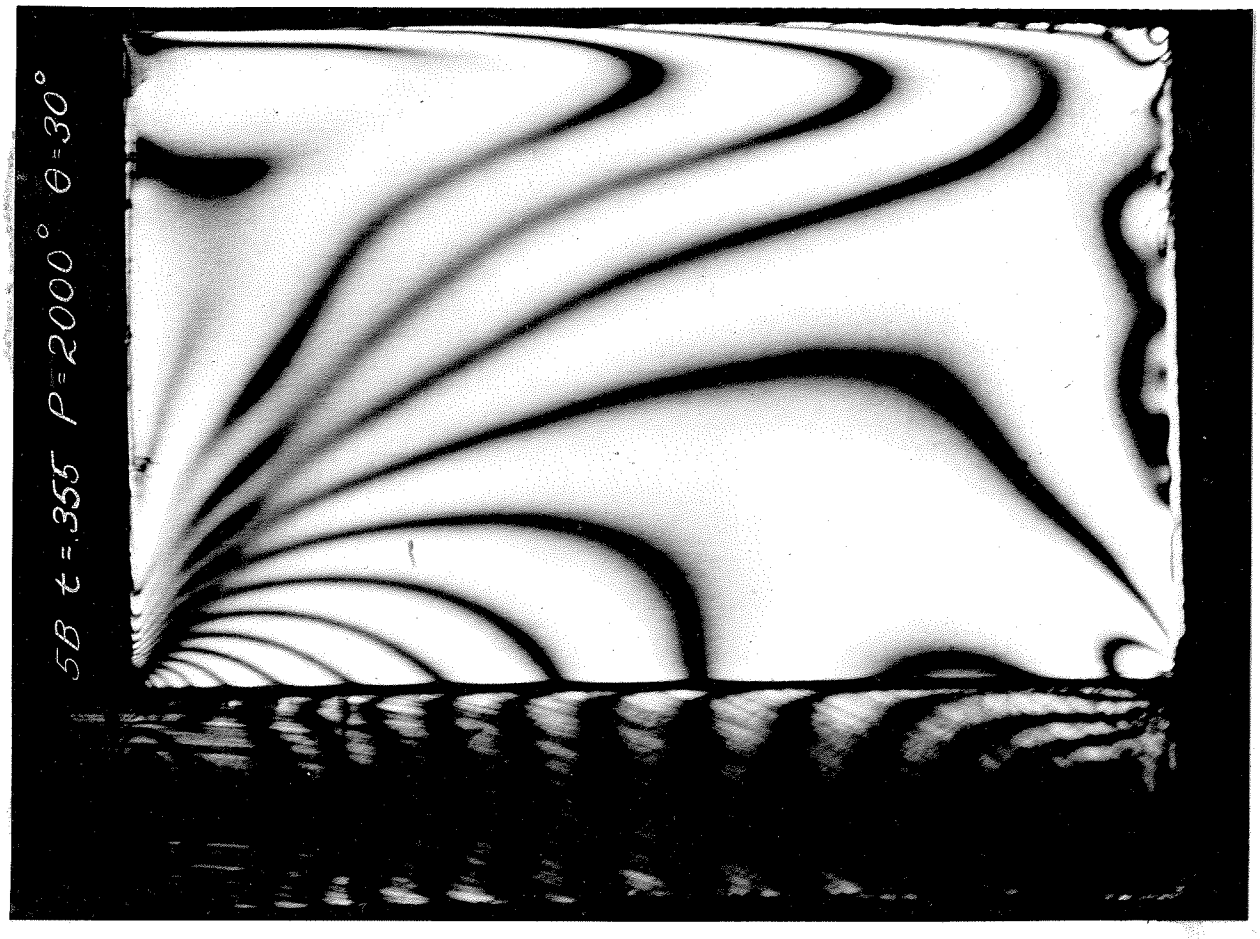
5B t=.355 P=2000° θ=30°

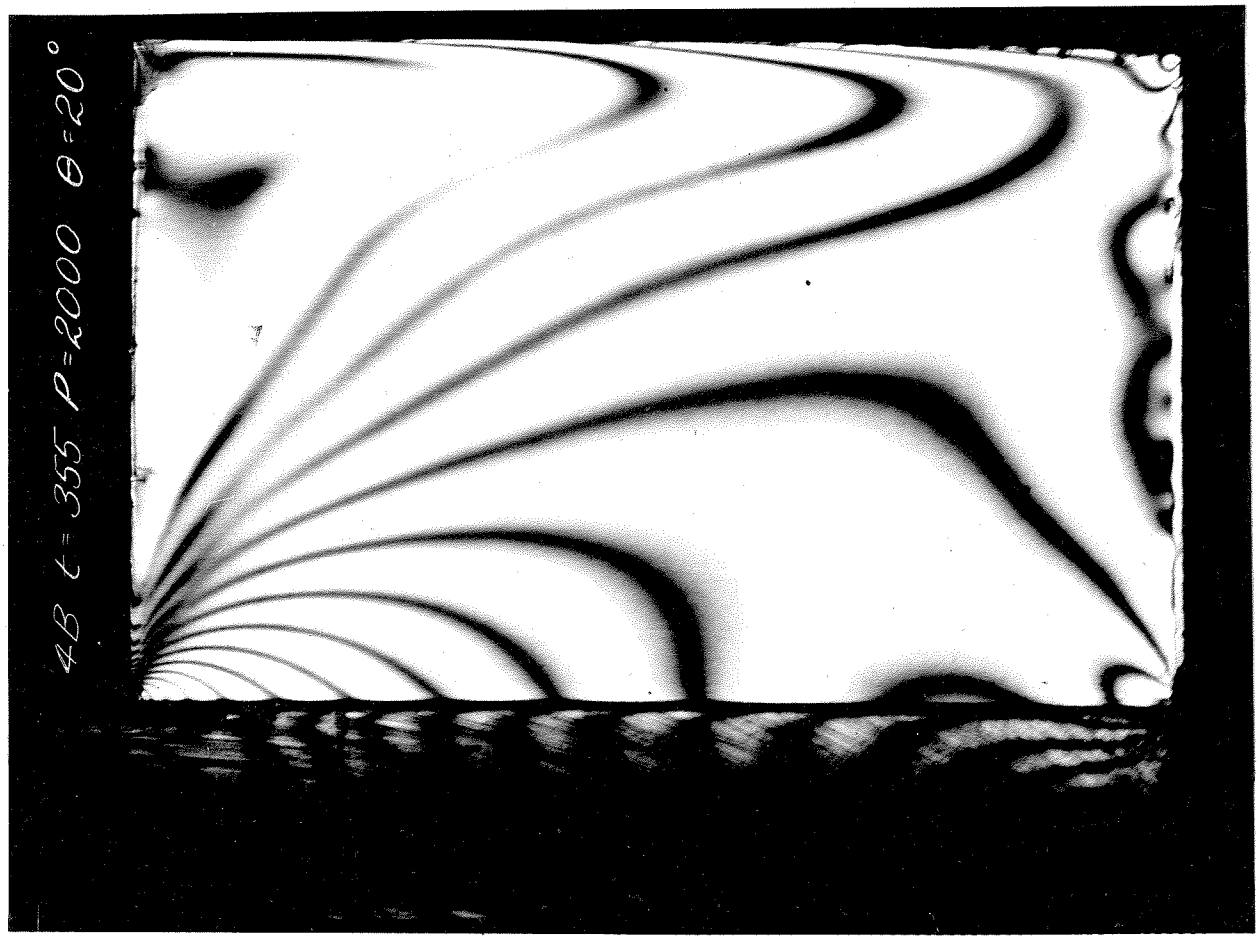
4B t=.355 P=2000 θ=20°

7B t=.355 P=2000 θ=50°

6B t=.355 P=2000 θ=40°

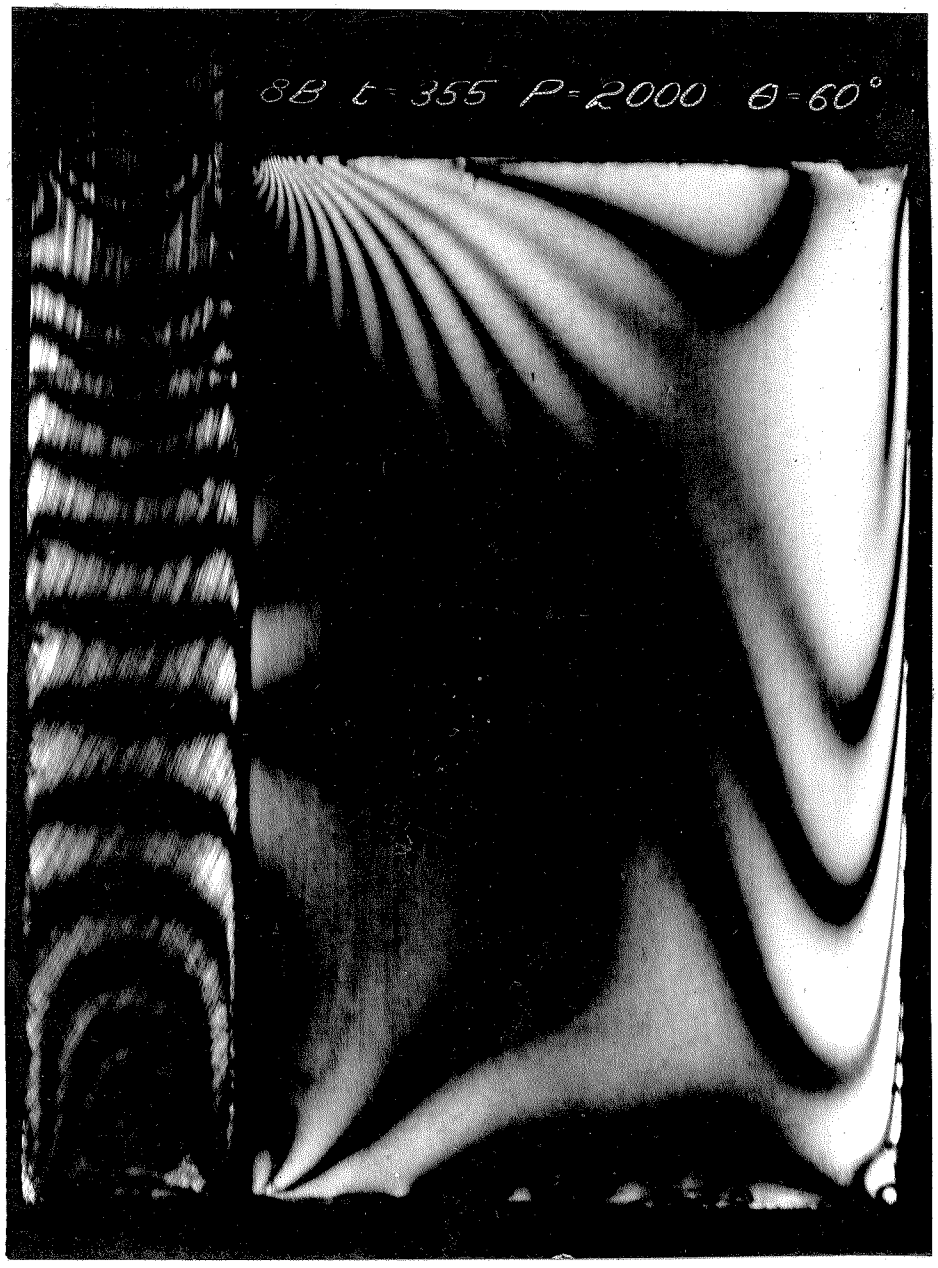

X / X


10.B t=.355 P=2000 θ=72½°

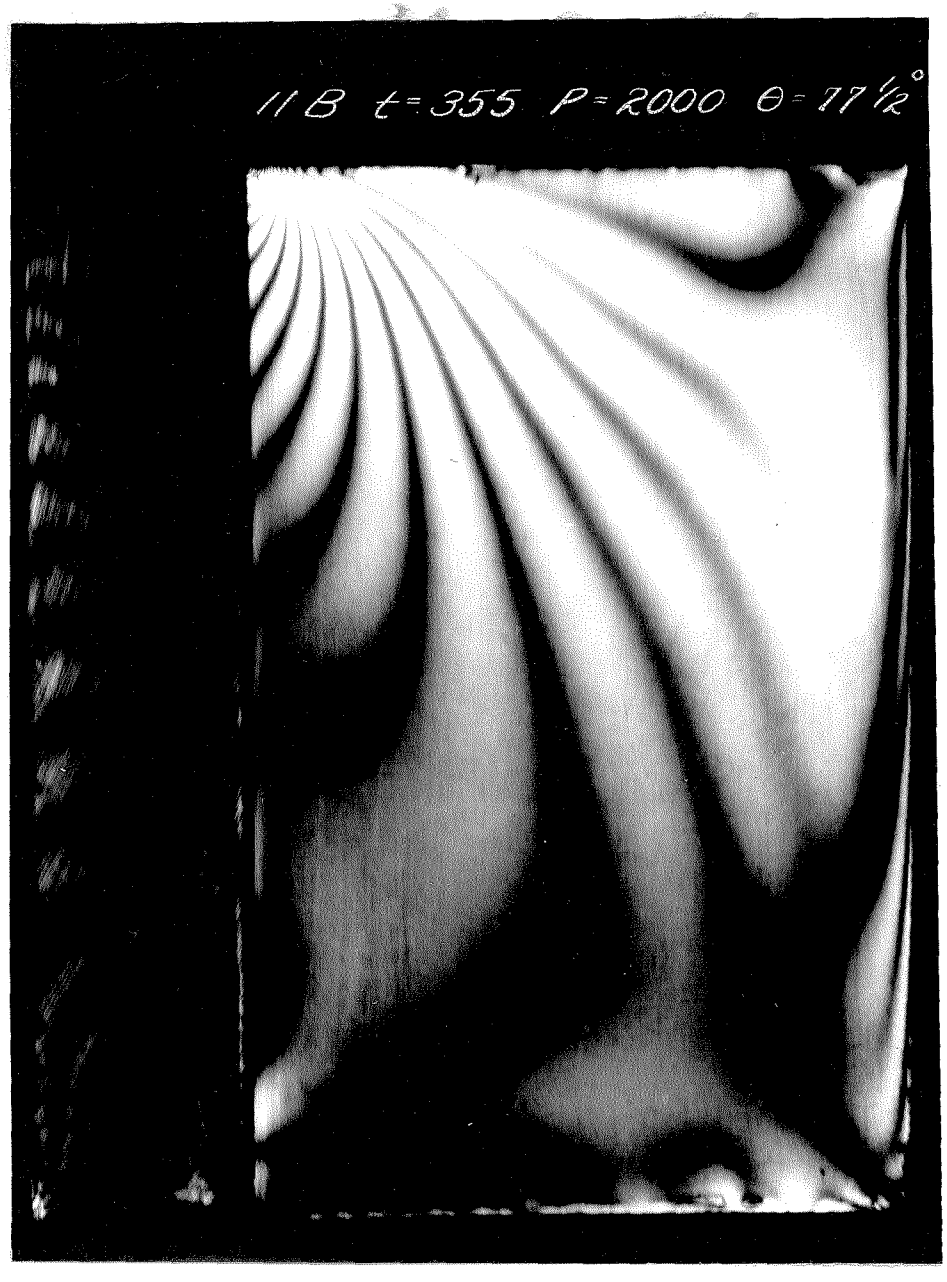
11 B t=.355 P=2000 θ=77½°


12B t=.355 P=2000 θ=80°


13B t=.355 P=2000 θ=90°

1E t=.355 P=2000
1E'

APPENDIX B

Fundamental stress relations. From the basic theory of elasticity, it is known that for a plane stress field the following relations are true:

(1) Consider a square element of small dimensions with sides respectively parallel to the reference axes .

$$\sigma_x + \sigma_y = \text{const.} = p + q$$

$$\tau_{xy} = \tau_{yx}$$

$$\sigma_x = p\cos^2\theta + q\sin^2\theta$$

$$\sigma_y = (p+q) - \sigma_x$$

$$\tau_{xy} = \tfrac{1}{2}(p-q)\sin 2\theta$$

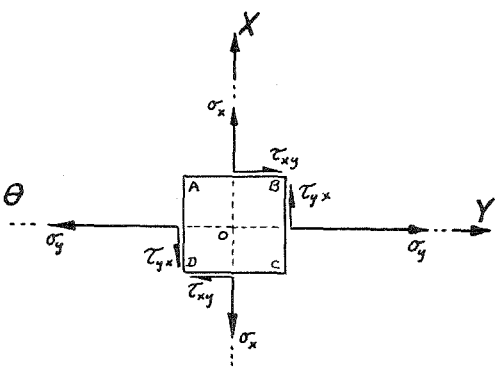

(2) Let the element be rotated clockwise through the angle θ, i.e.,until the sides are parallel to the directions of the principal stresses.

$$\tan 2\theta = \frac{2\tau_{xy}}{\sigma_x - \sigma_y}$$

$$p = \frac{\sigma_x + \sigma_y}{2} + \sqrt{\tau_{xy}^2 + \frac{(\sigma_x+\sigma_y)^2}{4}}$$

$$q = \frac{\sigma_x + \sigma_y}{2} - \sqrt{\tau_{xy}^2 + \frac{(\sigma_x+\sigma_y)^2}{4}}$$

$$\tau_{xy} = 0 \quad \text{(along all sides)}$$

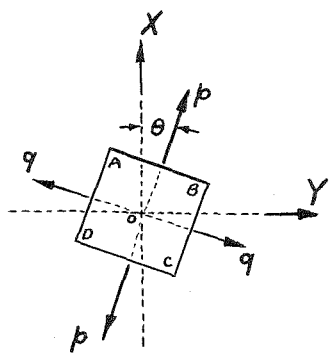

(3) Let the element be rotated through an additional angle of 45 degrees.

$$\tau_{max} = \frac{p-q}{2}$$

$$\tau' = \tau'' = \tau_{max}$$

$$\sigma' = \sigma''$$

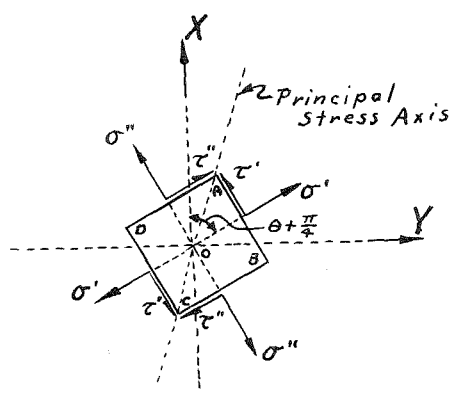

Appendix B (continued)

Since the photoelastic effect (i.e., the relative retardation of the light waves polarized in perpendicular planes while passing through a doubly refracting crystal) is proportional to the difference between the principal stresses, the above relation for τ_{max} explains the most direct result given by the optical method of stress analysis.

Analytically, the relative retardation is expressed by the following equation:

$$R = C(p - q)t$$

where C = a constant (the stress-optical coefficient of the material)

$$p - q = 2\tau_{max}$$

t = a constant (the thickness of the material)

Hence $R = C'\tau_{max}$

By a proper calibration method, therefore, the maximum shearing stresses throughout the model may be determined directly from the photoelastic pattern. This information, according to the Coulomb (or maximum shear) theory of failure, is sufficient for most design purposes, since in ductile materials such as steel, copper, aluminum, etc., failure occurs only when the maximum tangential stress reaches a critical value given by:

$$\tau_{max} = \sigma_y/2$$

where σ_y denotes the normal stress at the yield point of the material. In the case of thin sheet construction, of course, this principle alone is not strictly applicable since here failure generally occurs due to buckling.

APPENDIX C

A graphical method for the analytical separation of the principal stresses. Alexander (reference 5) suggests the following method of separating p and q . In company with the other analytical methods available, it involves a rather laborious process and is subject to the errors inseparable from a step-by-step integration.

Step 1. Select an an adequate coordinate system. Having given the axes OX and OY , say, divide each into unit increments dx, dy of the order of 0.1 inch or 0.2 inch.

Step 2. Draw the isochromatics to scale.

Step 3. From the isoclinics, obtain the angle θ for a selected network of points over the stress field.

Step 4. Calculate the tangential stress in the directions of the axes for each point by the relation:

$$\tau_{xy} = \frac{p - q}{2} \sin 2\theta$$

Step 5. From the results of (4), plot the curves of constant tangential stress; i.e., τ_{xy} = constant.

Step 6. Determine the derivatives $\left(\frac{\partial \tau_{xy}}{\partial x} , \frac{\partial \tau_{xy}}{\partial y}\right)$ graphically from the curves of (5).

Step 7. Integrate graphically along the X and Y axes, and calculate σ_x and σ_y at each point by the relations:

$$\sigma_x = (\sigma_x)_o - \int_o^x \frac{\partial \tau_{xy}}{\partial y} \, dx$$

$$\sigma_y = (\sigma_y)_o - \int_o^y \frac{\partial \tau_{xy}}{\partial x} \, dy$$

where $(\sigma_x)_o$ and $(\sigma_y)_o$ are known normal stresses such as may be determined at free boundary points from the isochromatic diagram.

Step 8. Calculate p and q for each of the selected points on the model from the relations:

$$p = \frac{\sigma_x + \sigma_y}{2} + \sqrt{\tau_{xy}^2 + \frac{(\sigma_x + \sigma_y)^2}{4}}$$

$$q = \frac{\sigma_x + \sigma_y}{2} - \sqrt{\tau_{xy}^2 + \frac{(\sigma_x + \sigma_y)^2}{4}}$$

Step 9. Check the results by means of Mohr diagrams.

APPENDIX D

Comparison Tests on an Additional Model.

This set of pictures, series F, consists of isochromatic photographs of the second model under each of the three types of loadings previously considered and of calibration beam photographs for the corresponding panel thickness. This model has dimensions identical to those of the original model with the exception that the panel thickness has been reduced from 0.35 inch to 0.25 inch. The stiffener is unchanged.

The value of $\Delta\tau_{max}$ was determined in the same manner as before. The observed and calculated data are as follows:

Picture No.	2F	3F	4F	5F	6F
M, in.-lb.	16.3	31.8	41.0	56.5	72.2
e, inches	.0684	.0274	.0209	.0149	.0115
I, $(in.)^4$	.0070	.0064	.0063	.0063.	.0062
c, inches	.1370	.0739	.0607	.0455	.0339
σ, lb/in^2	2328c	4980c	6480c	8970c	11500c
τ, lb/in^2 /line	159.3	184.2	196.2	204.0	195.0

From the resulting curve plotted in Fig. 22, the shearing stress increment is taken to be:

$$\Delta\tau_{max} = 206.6 \quad lbs./in.^2/line$$

The compressive load on the model in each case was 2000 lbs. The fringe order of each isochromatic is given on the photographs; and the value of τ_{max} along any fringe may therefore be found from the expression:

$$\tau_{max} = 206.6\ n \quad lbs./in.^2$$

Appendix D (continued)

The types of loading, in order, are given as follows:

Picture No.	7F	:	Type I
" "	8F	:	" II
" "	9F	:	" III

Since the type of calibration employed for evaluating the stress patterns in the models is unsatisfactory for accurate quantitative analysis, a valid comparison of stress intensities at corresponding points of the two models is not readily possible. Nevertheless a study of the results obtained from the two thicknesses investigated affords an interesting comparison by which to evaluate qualitatively at least the effect of varying the gage of the panel. Although the stress pattern along the lower edge of the panel shows minor variations because the nature of the local stress concentrations was unavoidably altered from loading to loading, it was observed that in general the following are true:

For a given type of loading, the stress pattern(i.e., the shape of the isochromatic lines) does not vary in the two models. Avery simple method of comparison, namely superposition of the negatives for similar loadings, shows that the contours are identical. This fact indicates that the distribution of stress, insofar as position and direction are concerned, is independent of the thickness of the panel. This, it will be remembered, was assumed in the discussion of Part II.

From the values of the shearing stresses calculated, it is

Appendix D (continued)

found(as was also assumed) that the intensity of stress for a given applied load increases for a decrease in the thickness of the panel. Because of the inaccuracy of the stress evaluation due to the necessity for approximating the value of $\Delta\tau_{max}$, it is impossible unfortunately to determine the exact relation for this variation.

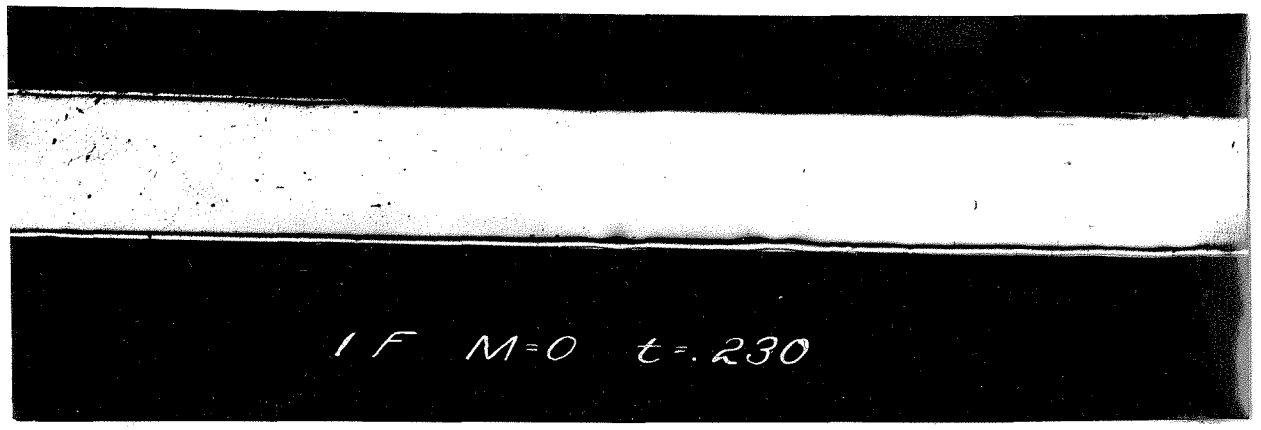
1F M=0 t=.230


2F M=16.3 t=.230

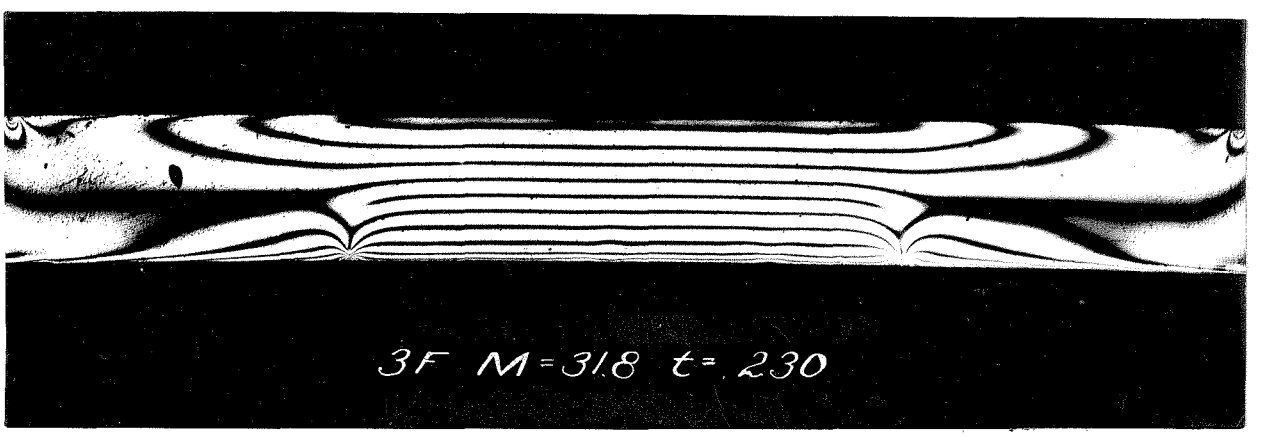
3F M=31.8 t=.230

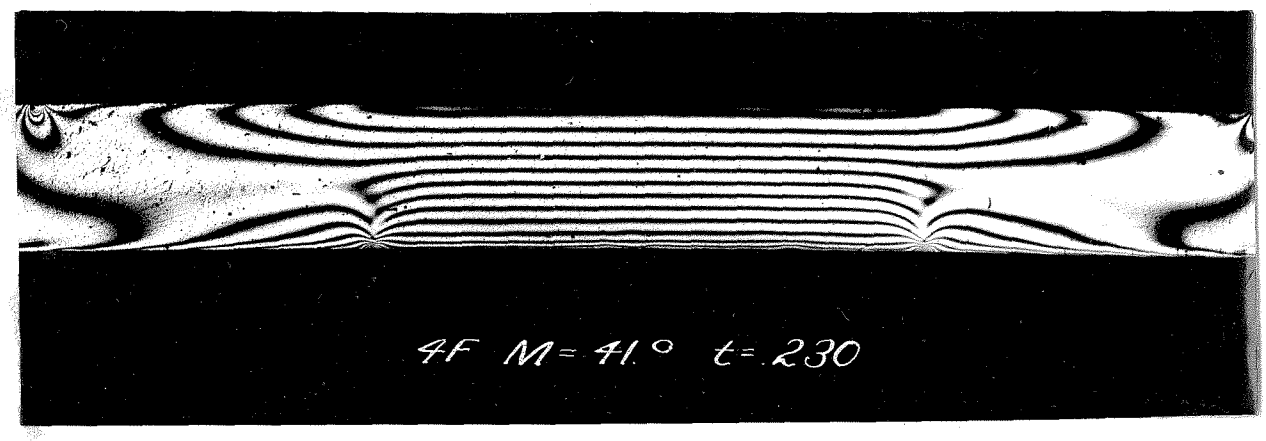
4F M=41.0 t=.230

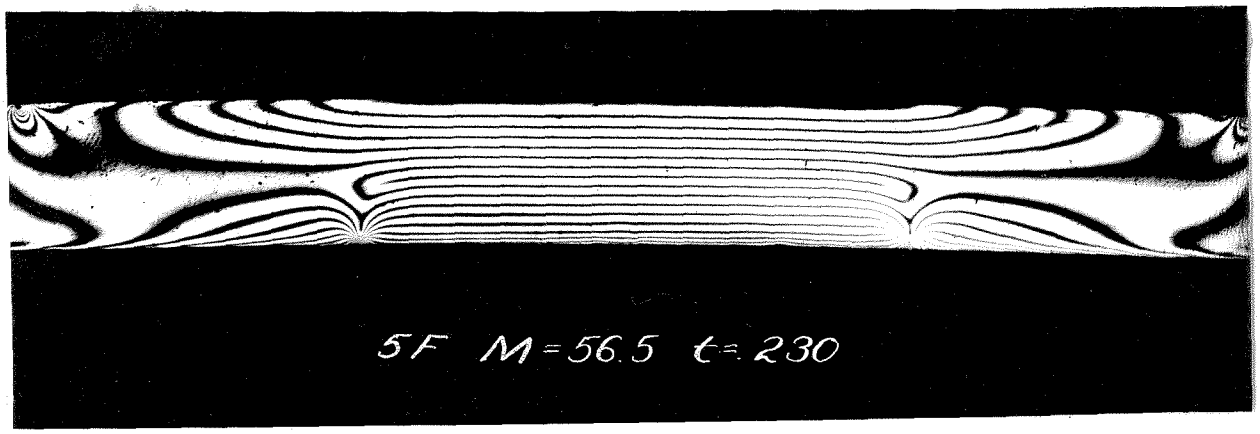
5F M=56.5 t=.230

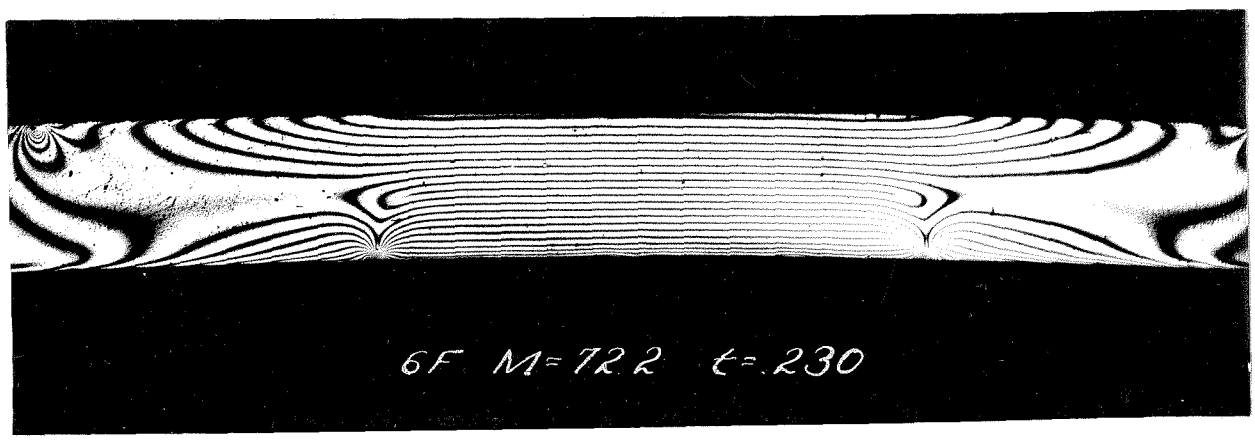
6F M=72.2 t=.230

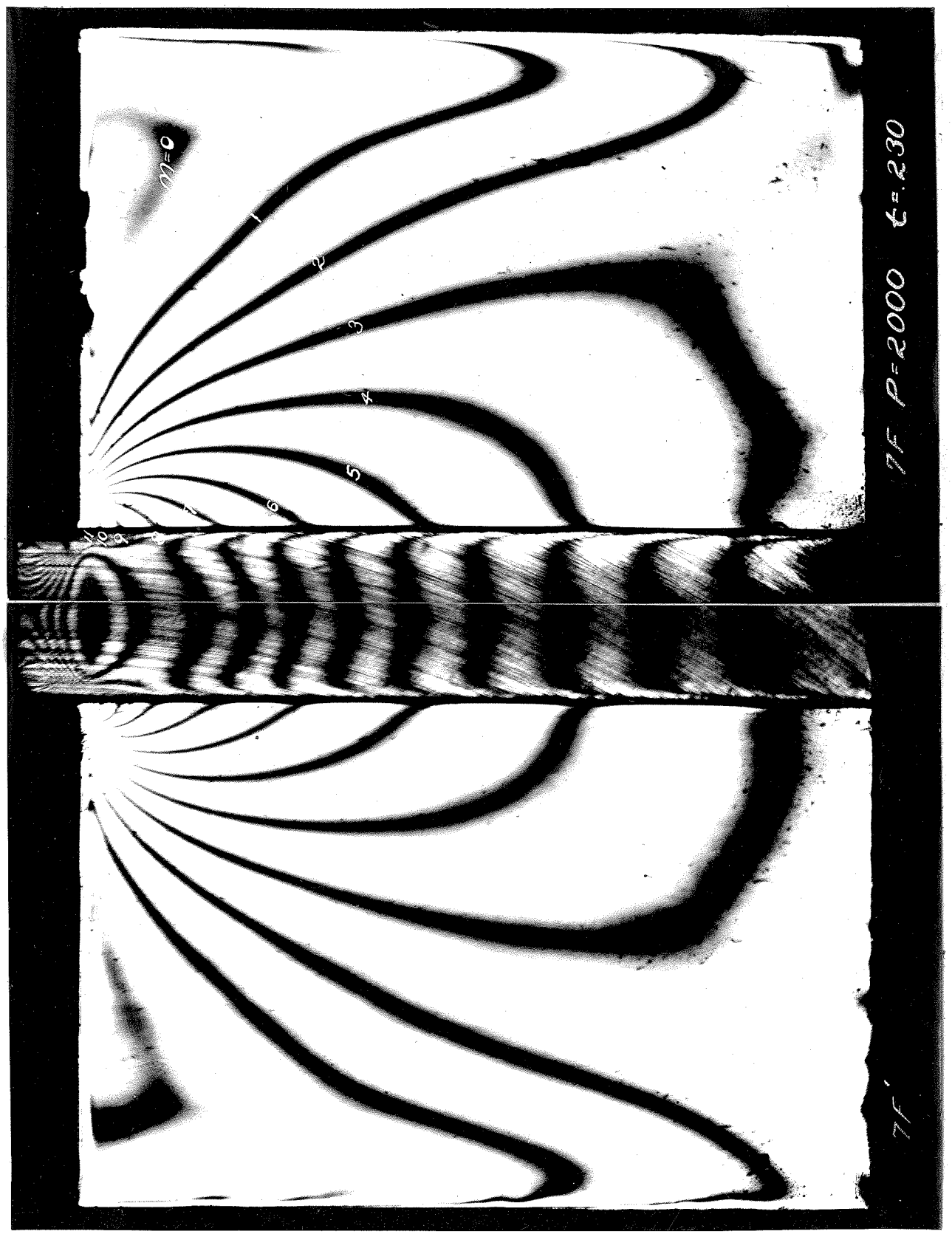
TF P=2000 t=.230
TF
1
2
3
4
5
6

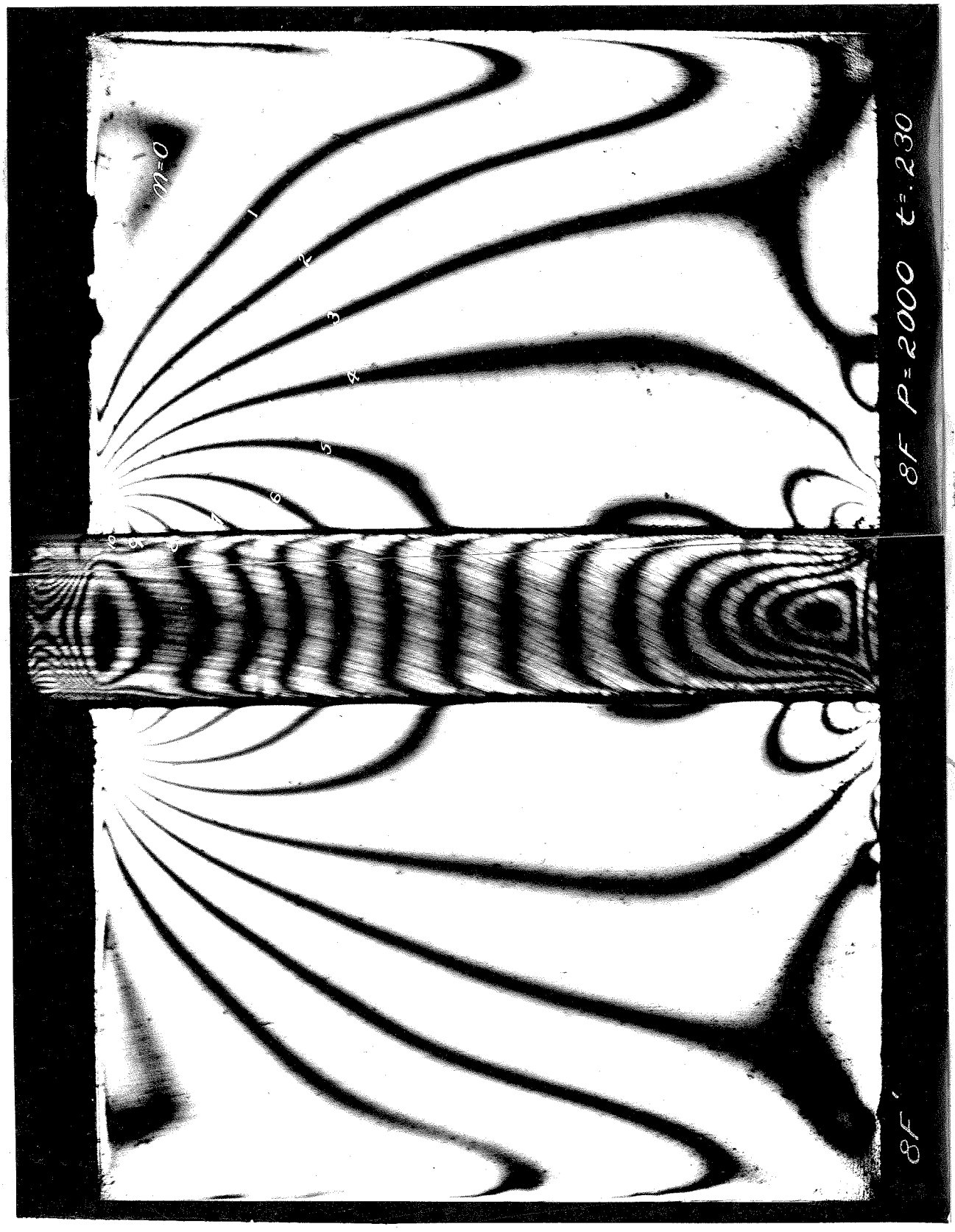
θ=0
1
2
3
4
5
6
7
8
9
8F P=2000 t=.230
8F'

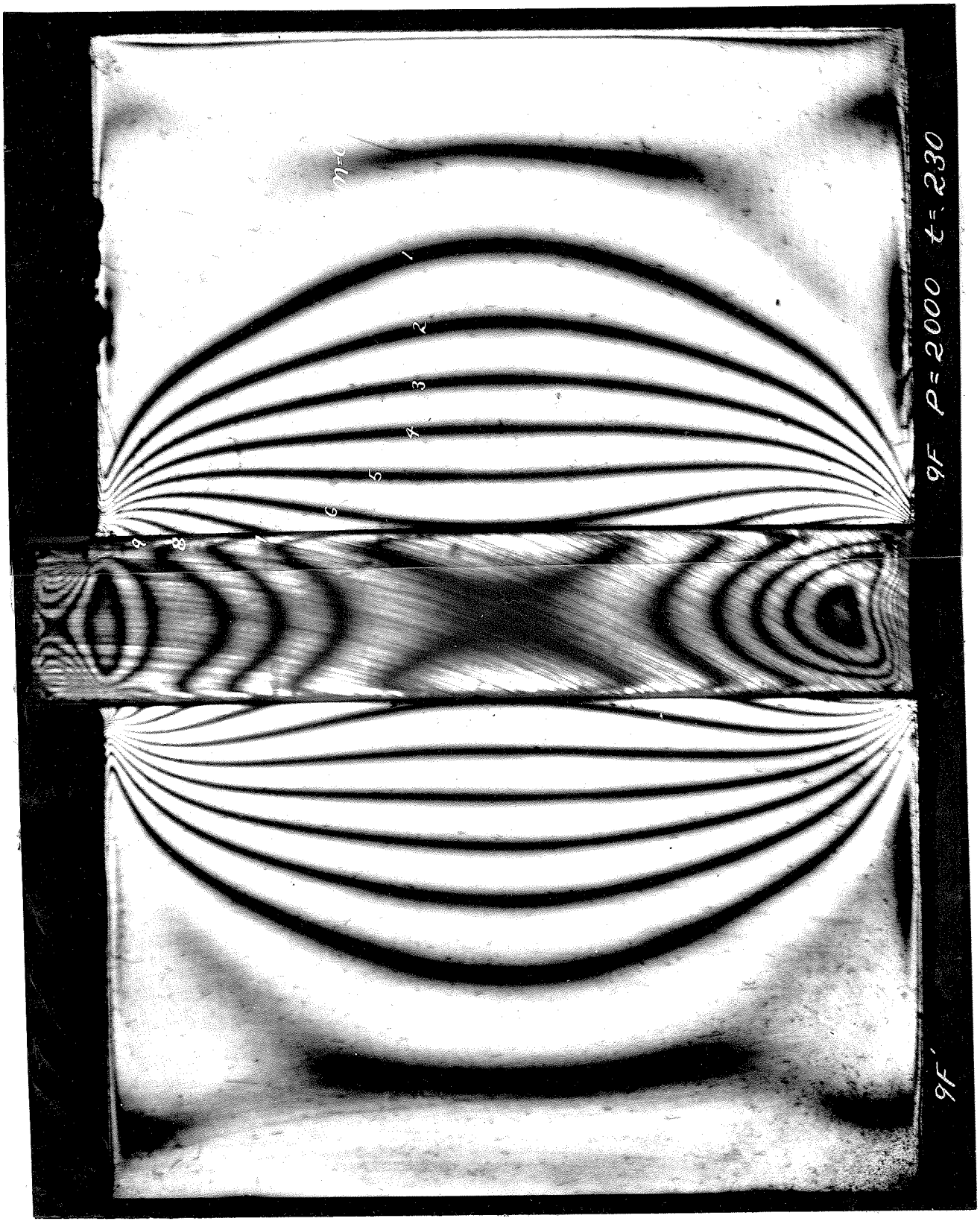
9F P=2000 t=.230
9F'
1
2
3
4
5
6
7
8
9
m=0

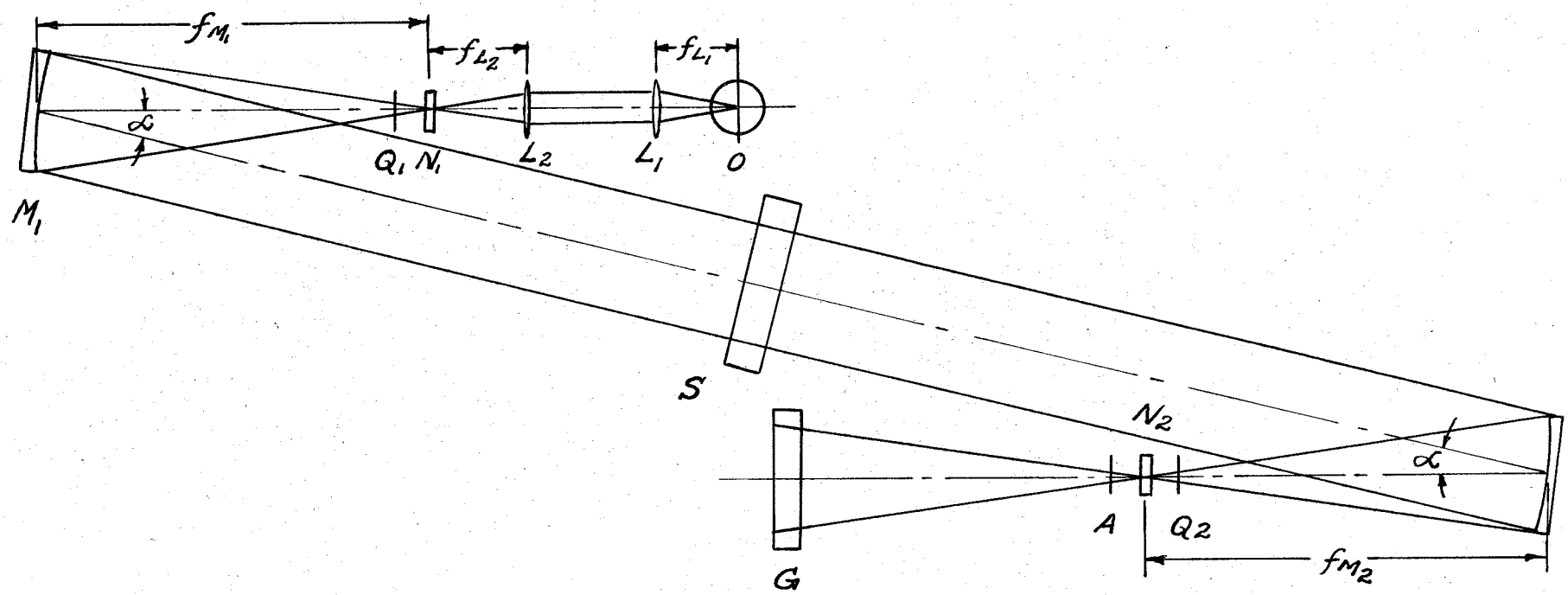

DIAGRAMATIC PLAN VIEW OF PHOTO - ELASTICITY EQUIPMENT

O = SOURCE OF LIGHT (60 WATT SODIUM VAPOR LAMP)
L_1 and L_2 = CONDENSING LENSES
f_{L_1} and f_{L_2} = FOCAL LENGTH OF LENS L_1 AND LENS L_2
N_1 = POLARIZER (LOCATED AT FOCAL POINT OF LENS L_2 AND MIRROR M_1)
N_2 = ANALYSER (LOCATED AT FOCAL POINT OF MIRROR M_2)
Q_1 and Q_2 = QUARTER WAVE PLATES
A = APERTURE
M_1 and M_2 = SPHERICALLY GROUND MIRRORS (RADIUS = 2 METERS)
f_{M_1} and f_{M_2} = FOCAL LENGTH OF MIRRORS ($f_{M_1} = f_{M_2}$ = 1 METER)
S = SPECIMEN OR MODEL IN LOADING FRAME
G = GROUND GLASS OR FILM PLATE

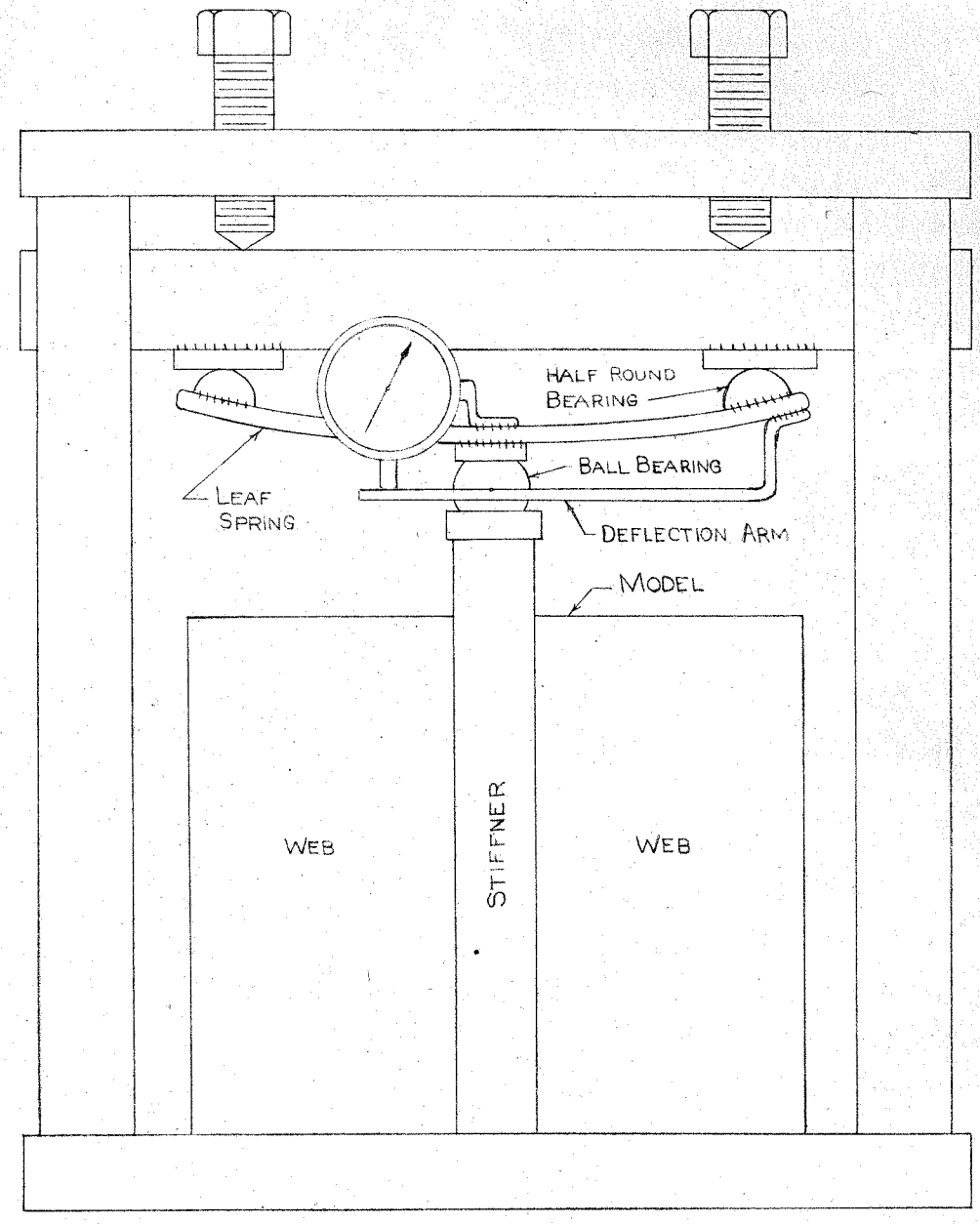

NOT TO SCALE

COMPRESSION
FRAME

FIG. 2

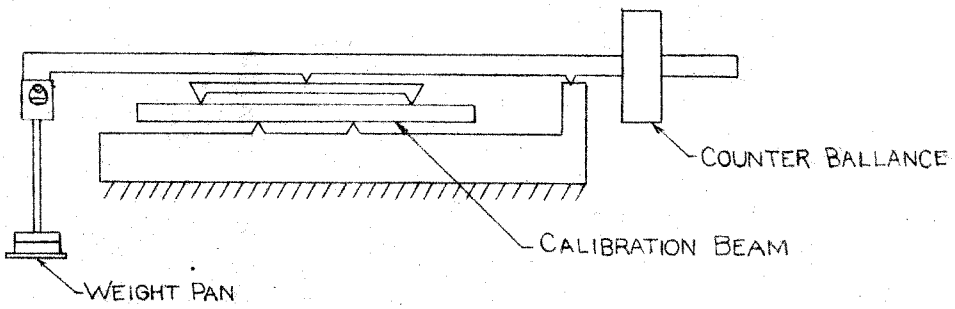

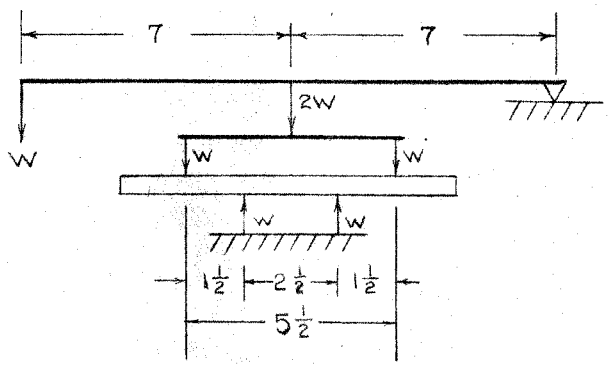

LOADING DEVICE FOR CALIBRATION BEAM

FIG. 3

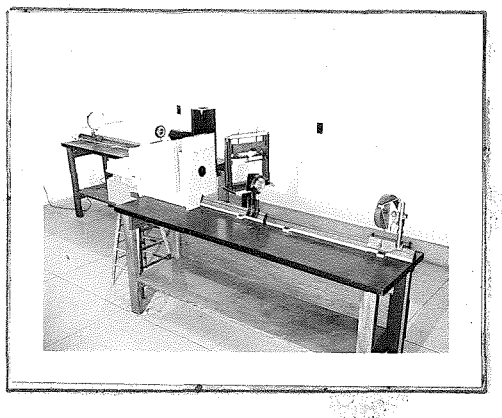

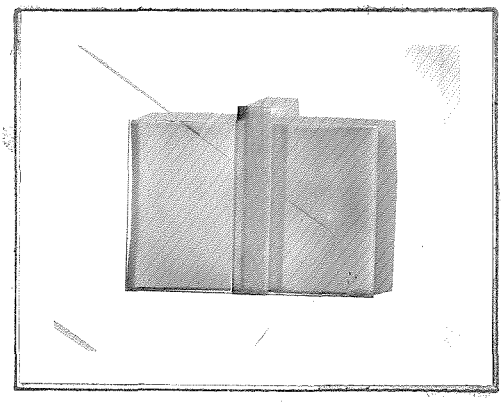

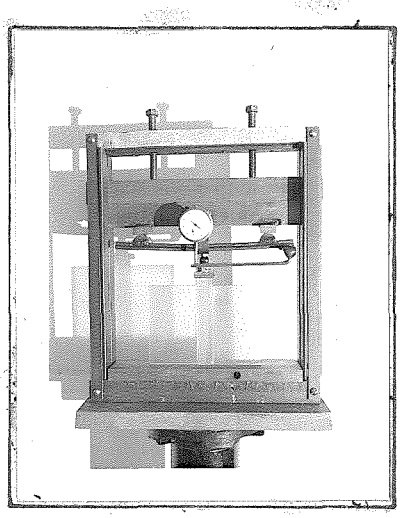

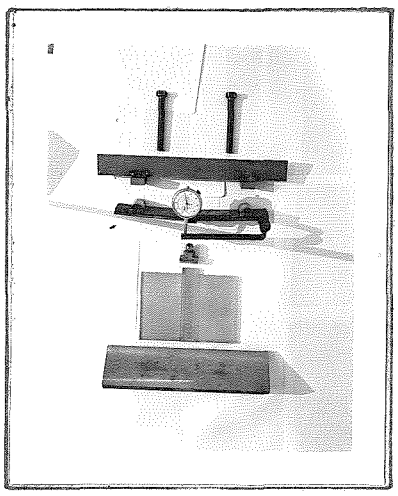

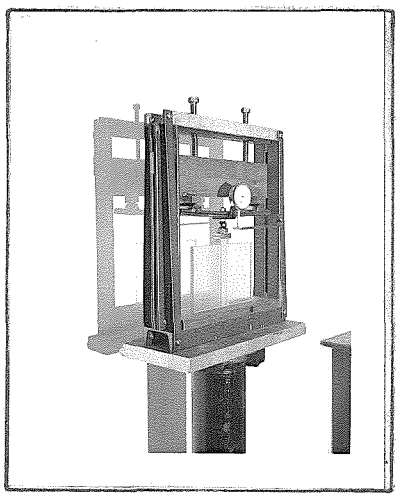

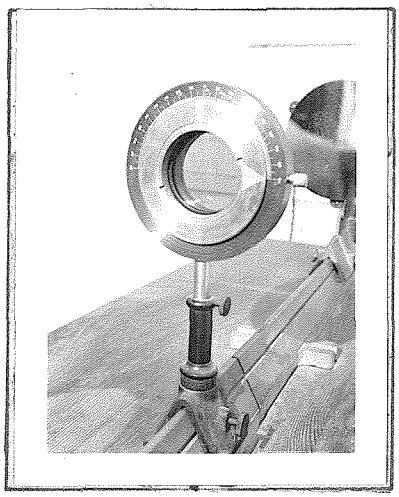

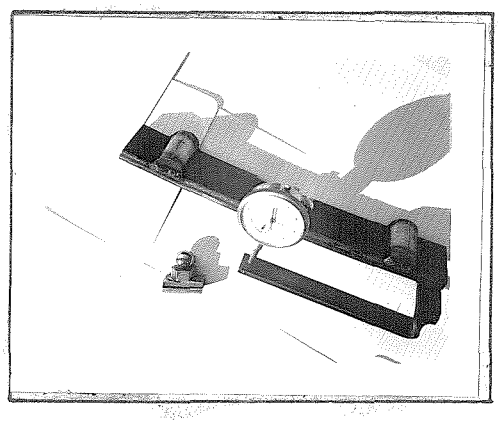

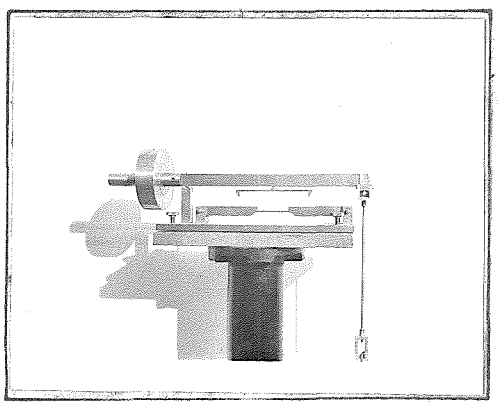

FIG. 4 APPARATUS

PHOTO-ELASTICITY SPECIMENS

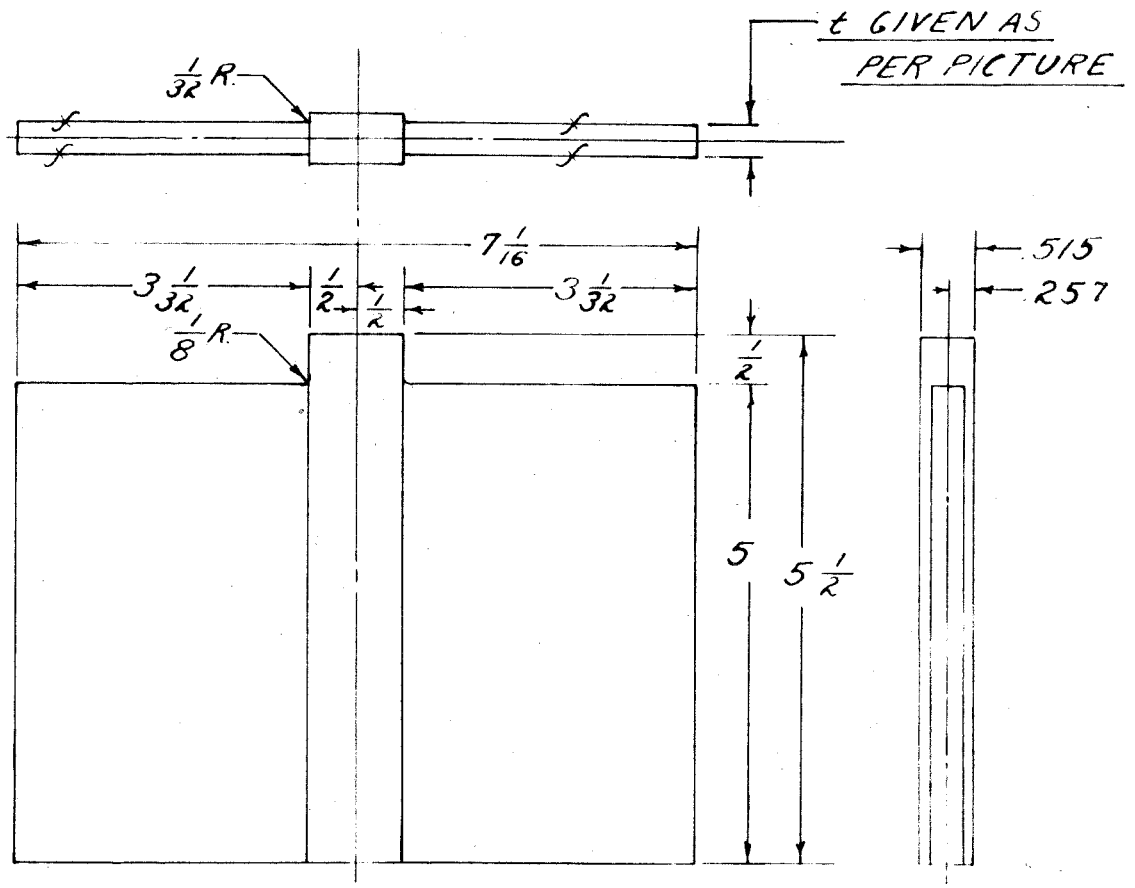

MODEL

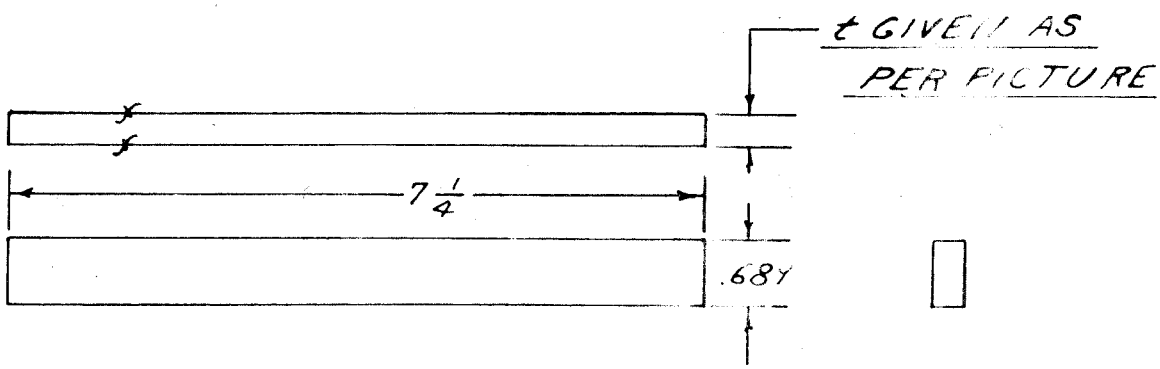

CALIBRATION BEAM

FIG. 5

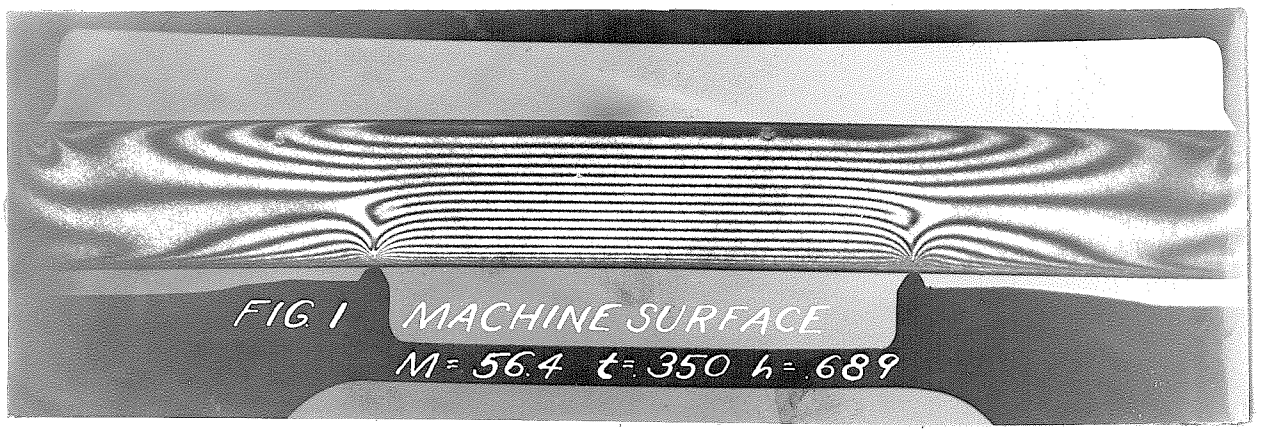

FIG. 1 MACHINE SURFACE
M = 56.4 t = .350 h = .689

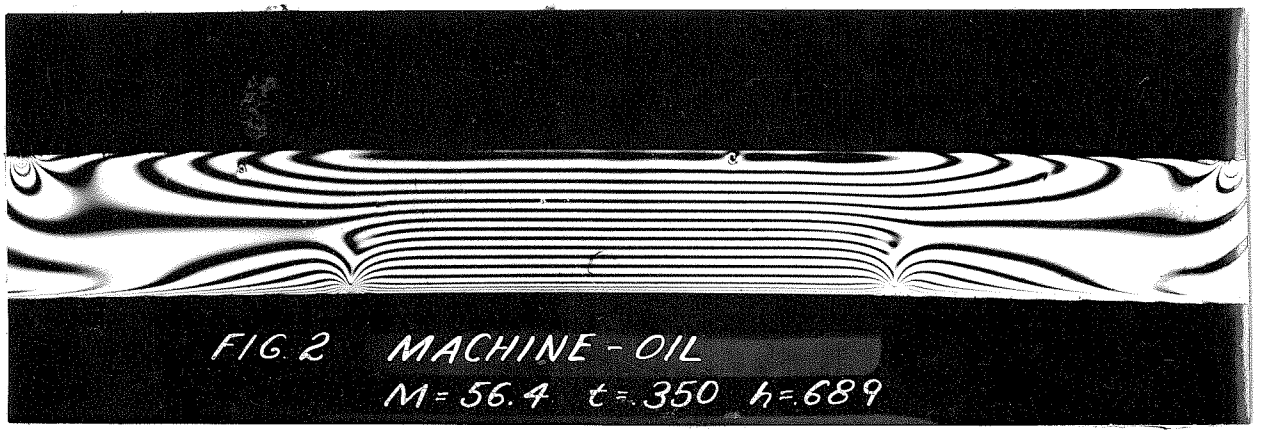

FIG. 2 MACHINE - OIL
M = 56.4 t = .350 h = .689

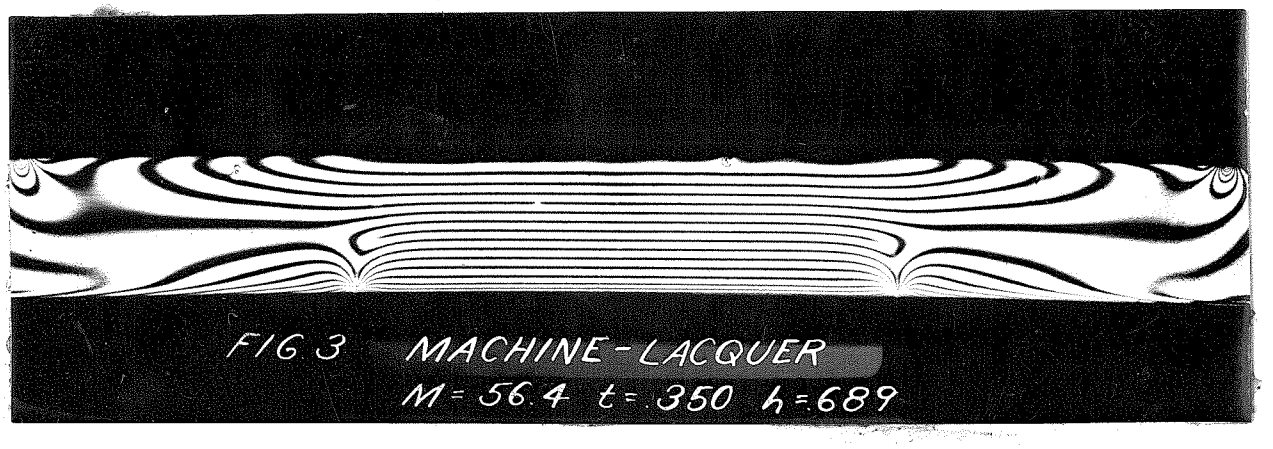

FIG. 3 MACHINE - LACQUER
M = 56.4 t = .350 h = .689

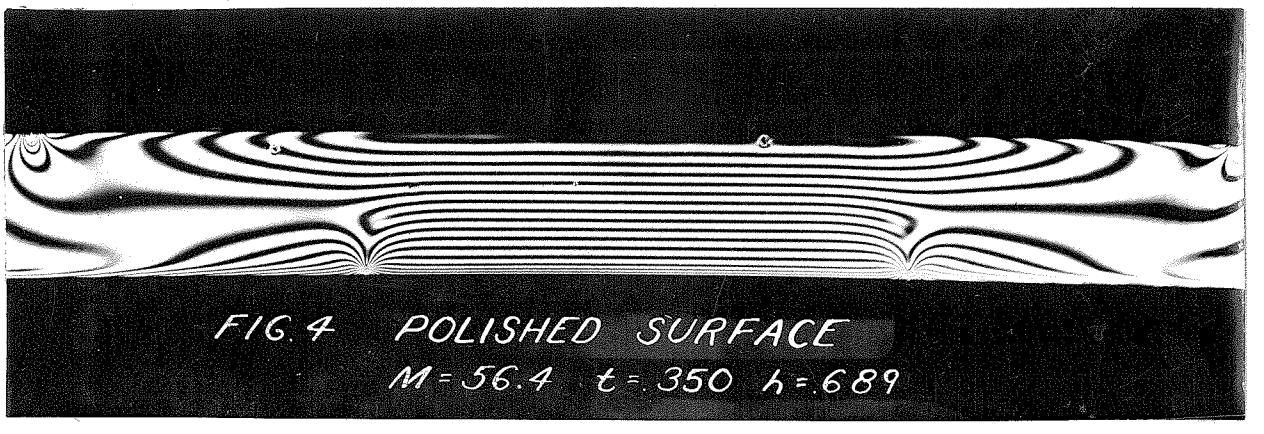

FIG. 4 POLISHED SURFACE
M = 56.4 t = .350 h = .689

FIG. 6

CALIBRATION CURVE

LOADING FRAME BEAM READING

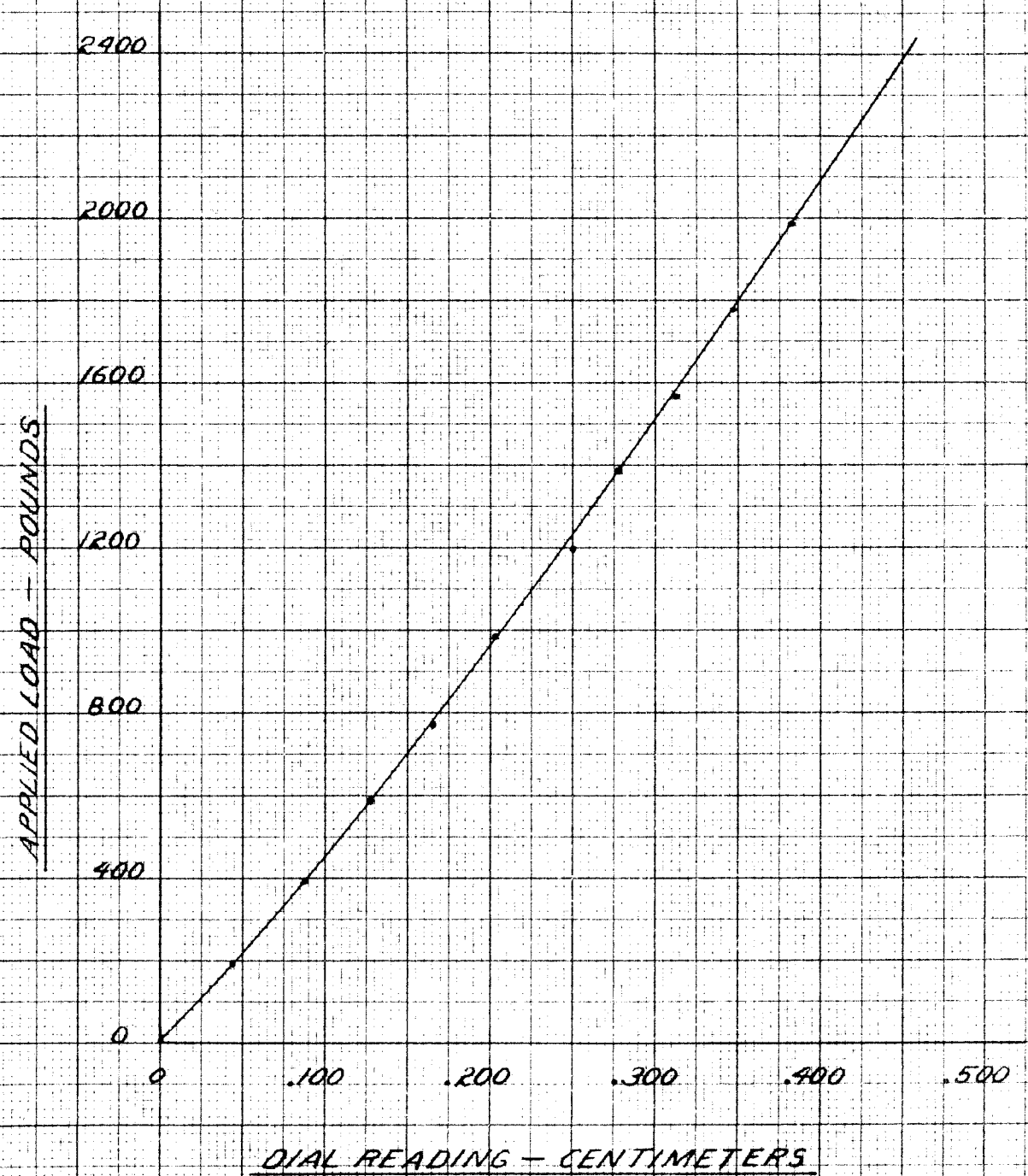

FIG 7

CALIBRATION BEAM

t = 350 INCHES h = 689 INCHES

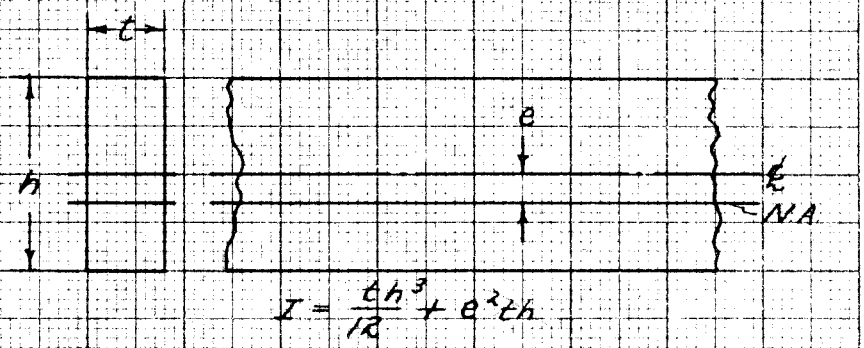

$$I = \frac{th^3}{12} + e^2th$$

FIG 8

SERIES C
EVALUATION OF ISOCHROMATIC LINES

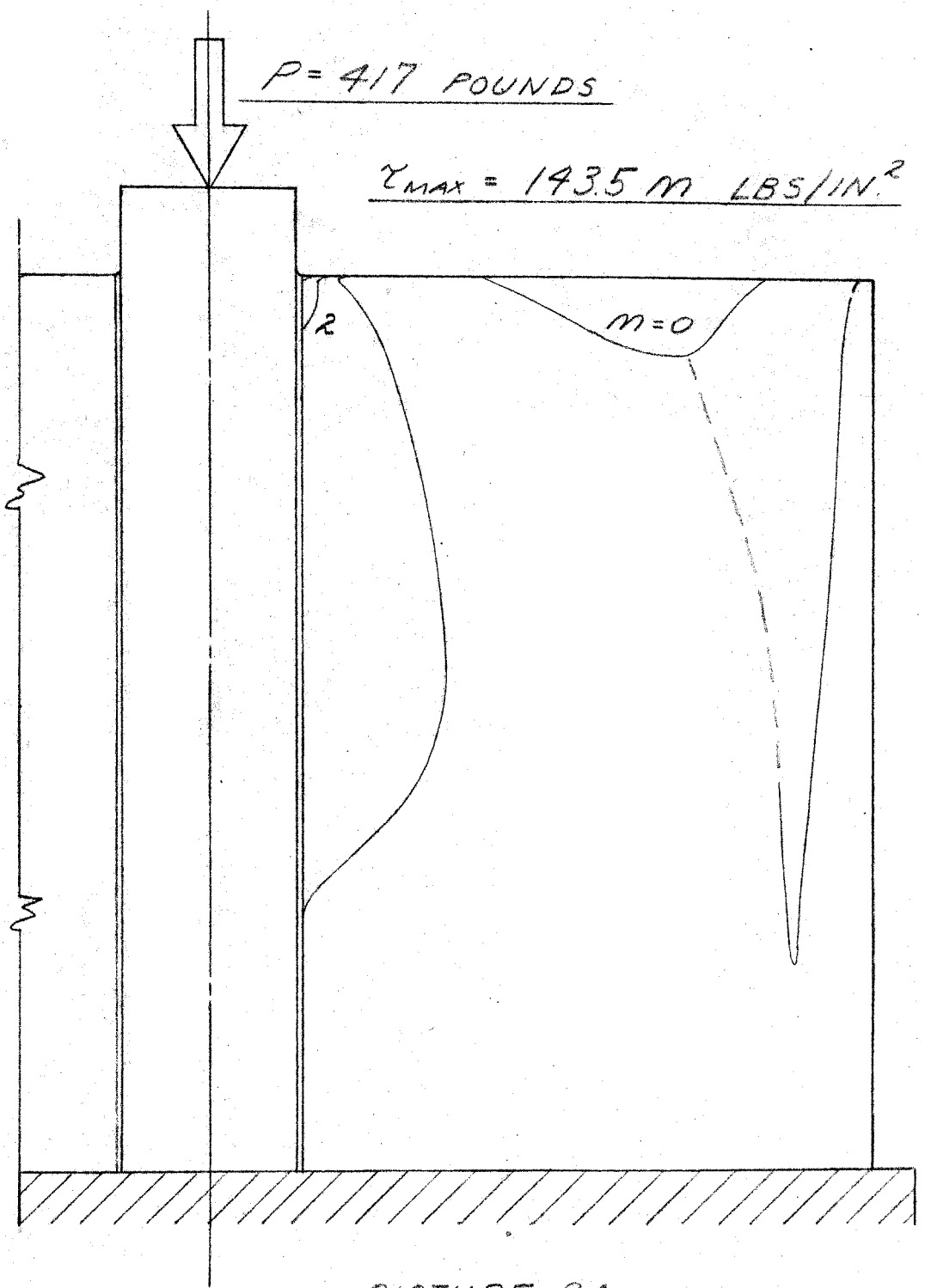

PICTURE 9A
t = .955 INCH
SCALE = 1.080 SIZE

FIG. 9

SERIES C
EVALUATION OF ISOCHROMTIC LINES

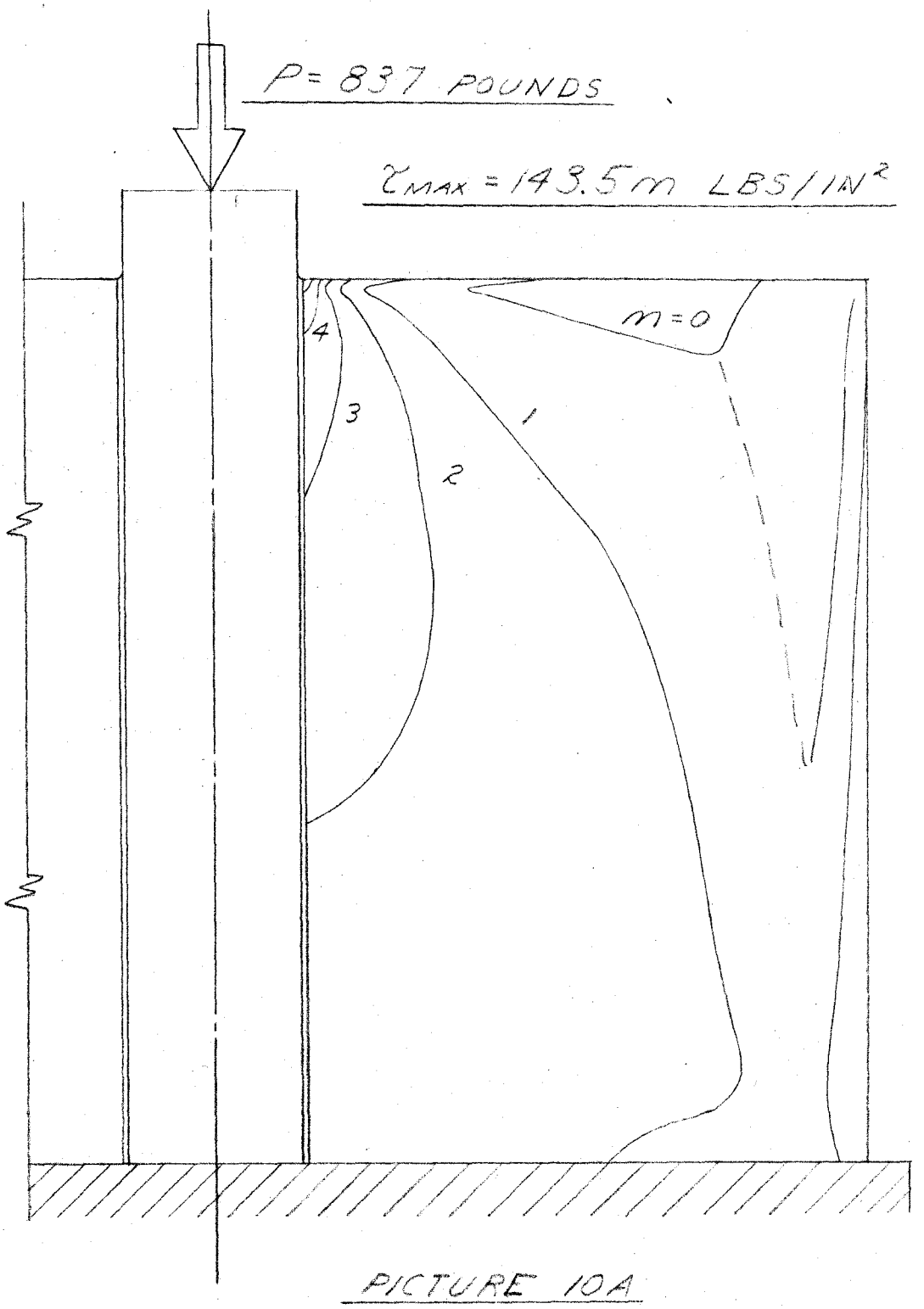

PICTURE 10A
t = .355 INCH
SCALE = 1.080 SIZE

FIG. 10

SERIES C
EVALUATION OF ISOCHROMATIC LINES

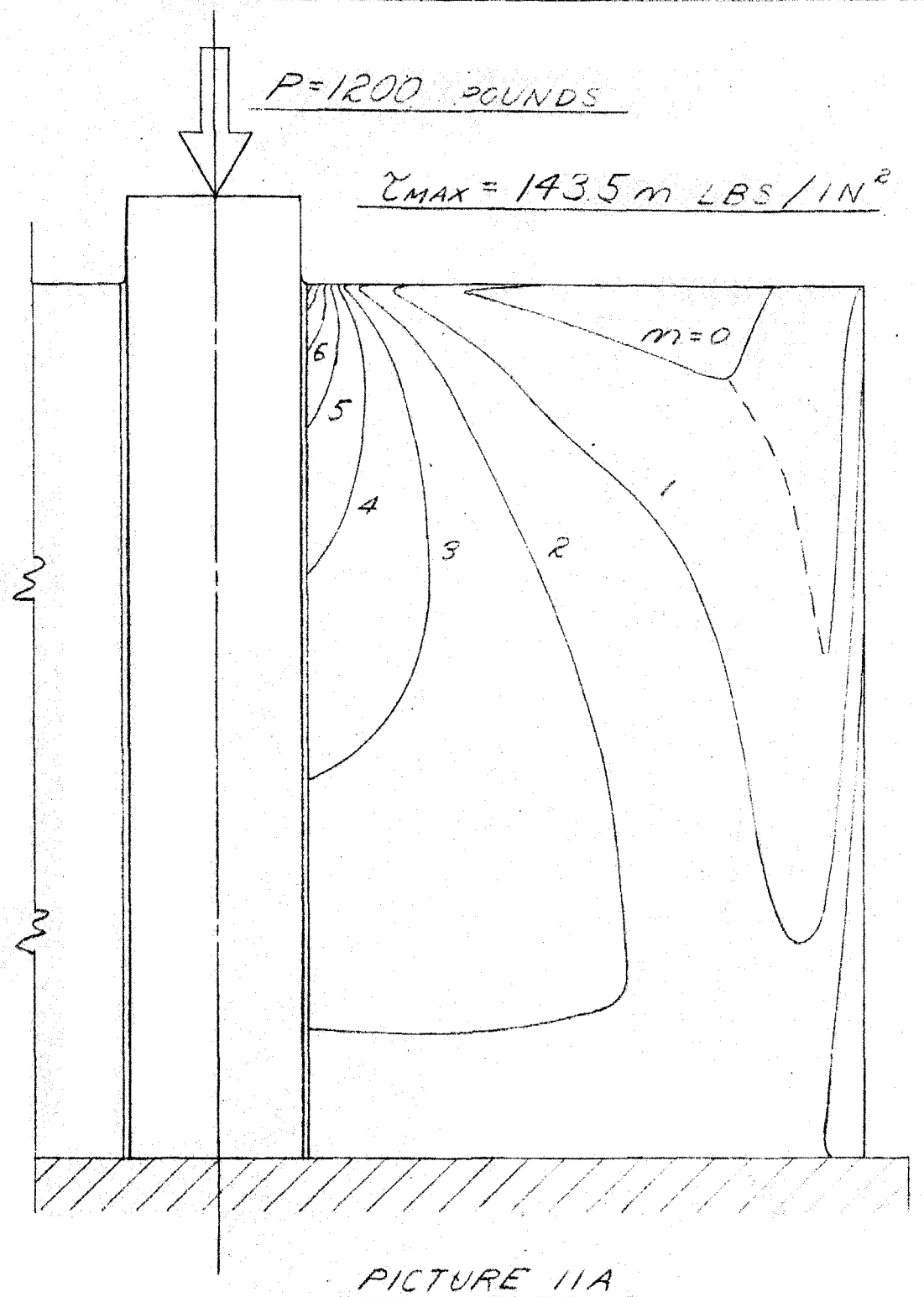

PICTURE 11A
t = .355 INCH
SCALE = 1.080 SIZE

FIG. 11

SERIES C
EVALUATION OF ISOCHROMATIC LINES

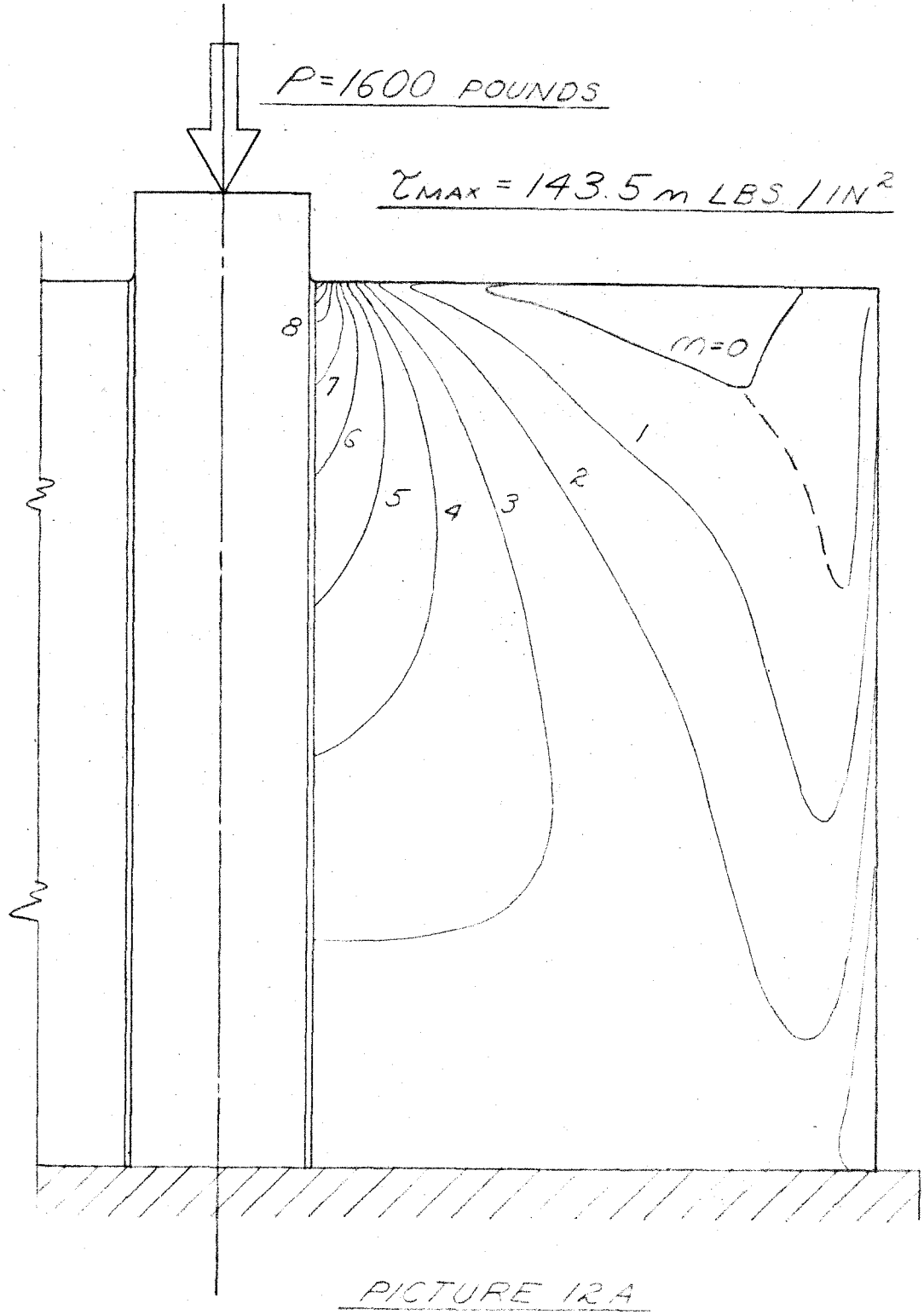

PICTURE 12A
τ = .355 INCH
SCALE = 1.08 SCALE

FIG. 12

SERIES C

EVALUATION OF ISOCHROMATIC LINES

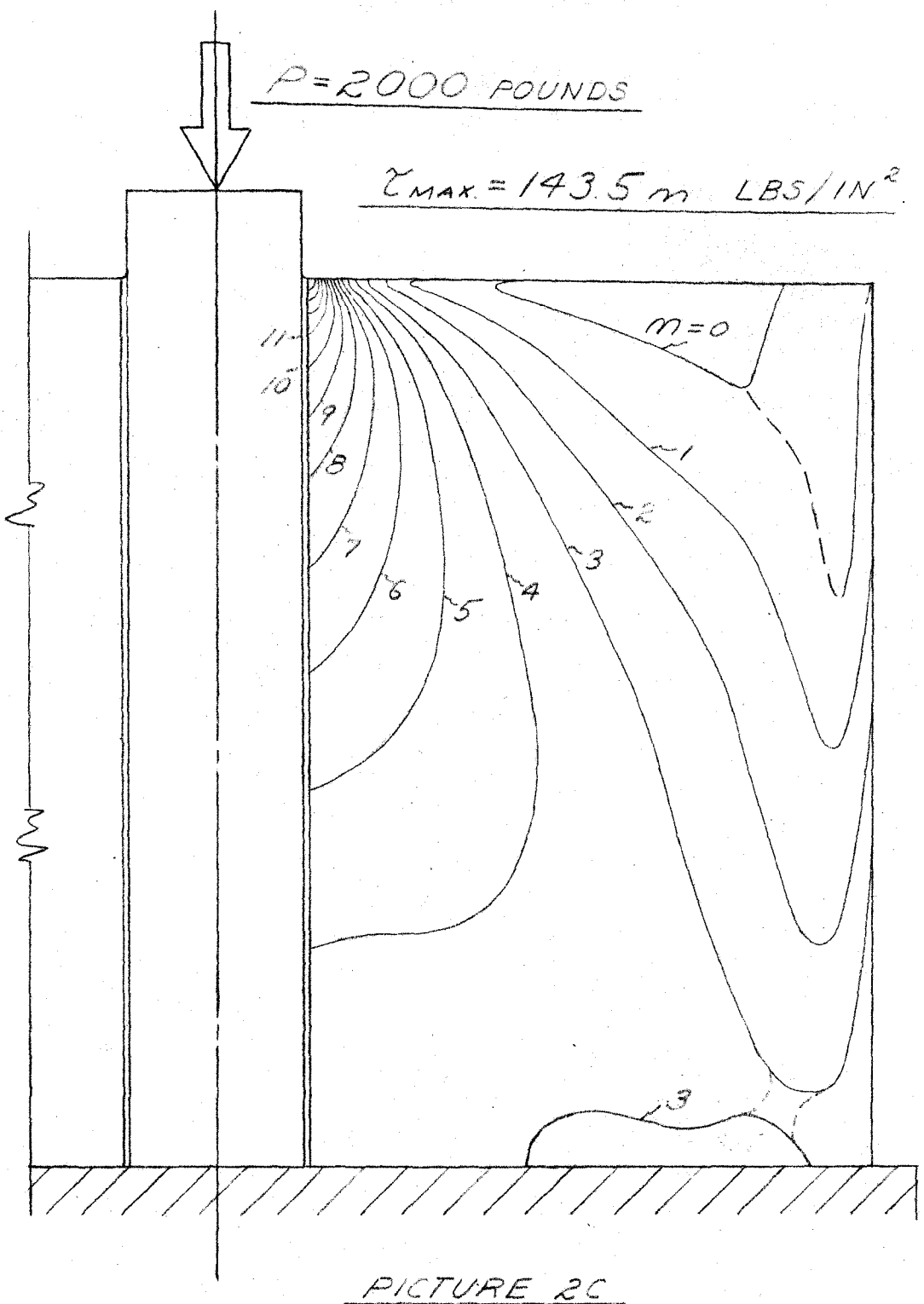

PICTURE 2C

t = .355 INCH

SCALE = 1.080 SIZE

FIG. 13

SERIES C
ISOCLINIC DIAGRAM I

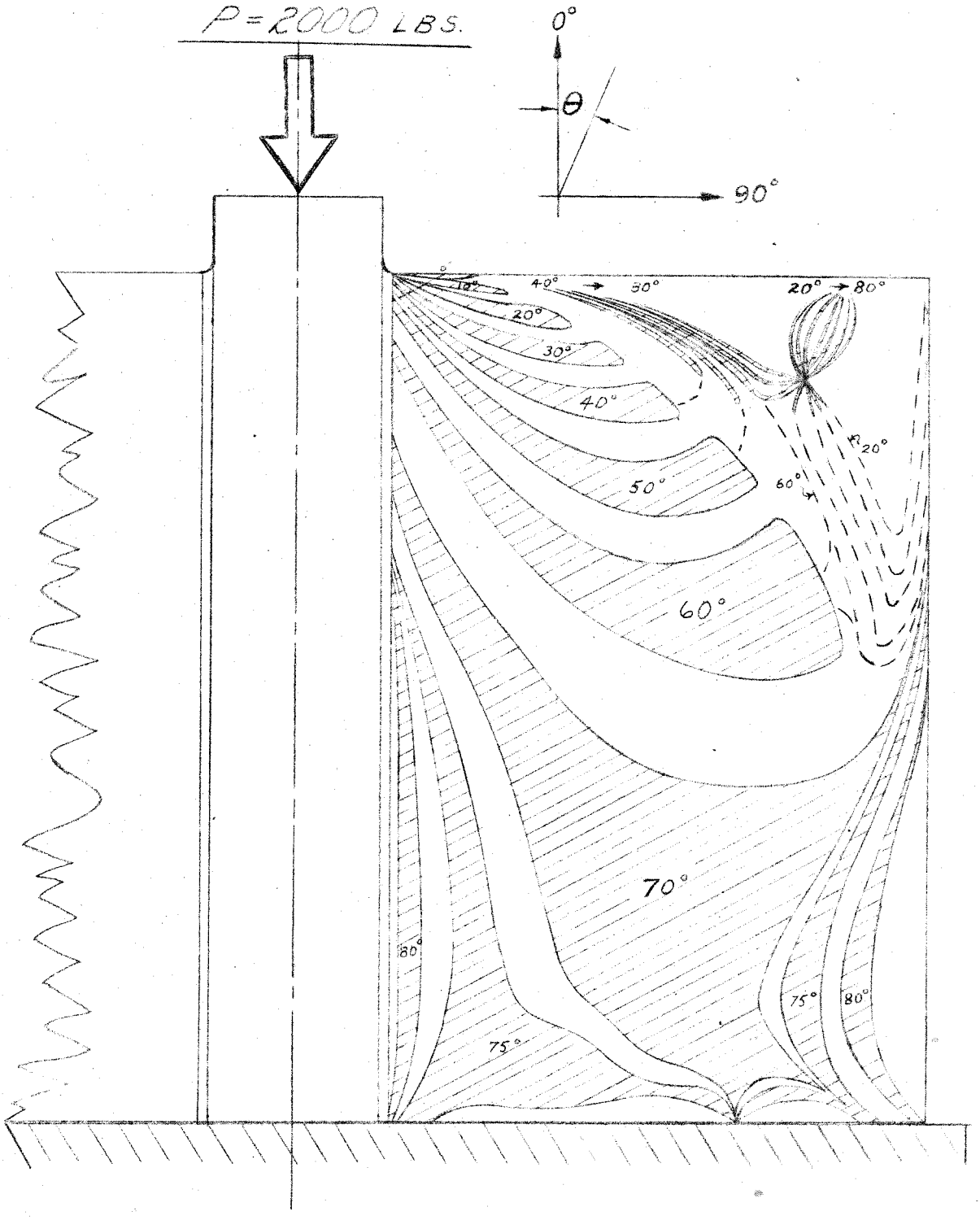

PRINCIPAL STRESS IN DIRECTIONS θ & $\theta + \pi/2$

MAXIMUM SHEAR IN DIRECTIONS $\theta + \pi/4$ & $\theta + 3\pi/4$

FIG. 14

SERIES C
ISOCLINIC DIAGRAM II

P = 2000 LBS.

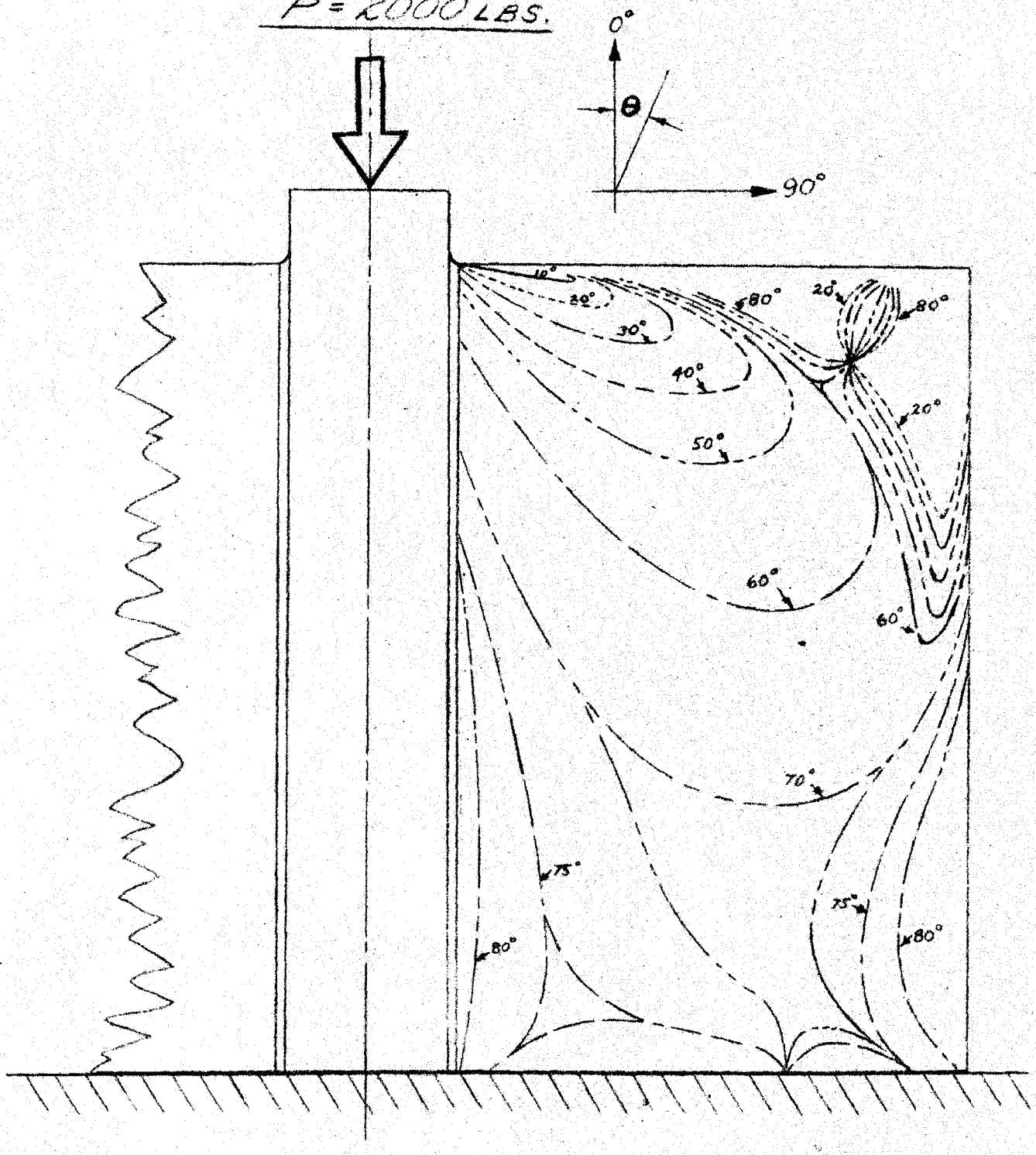

PRINCIPAL STRESS IN DIRECTIONS θ & $\theta + \pi/2$

MAXIMUM SHEAR IN DIRECTIONS $\theta + \pi/4$ & $\theta + 3\pi/4$

FIG. 15

SERIES C - TRAJECTORIES OF THE PRINCIPAL NORMAL STRESSES P & Q

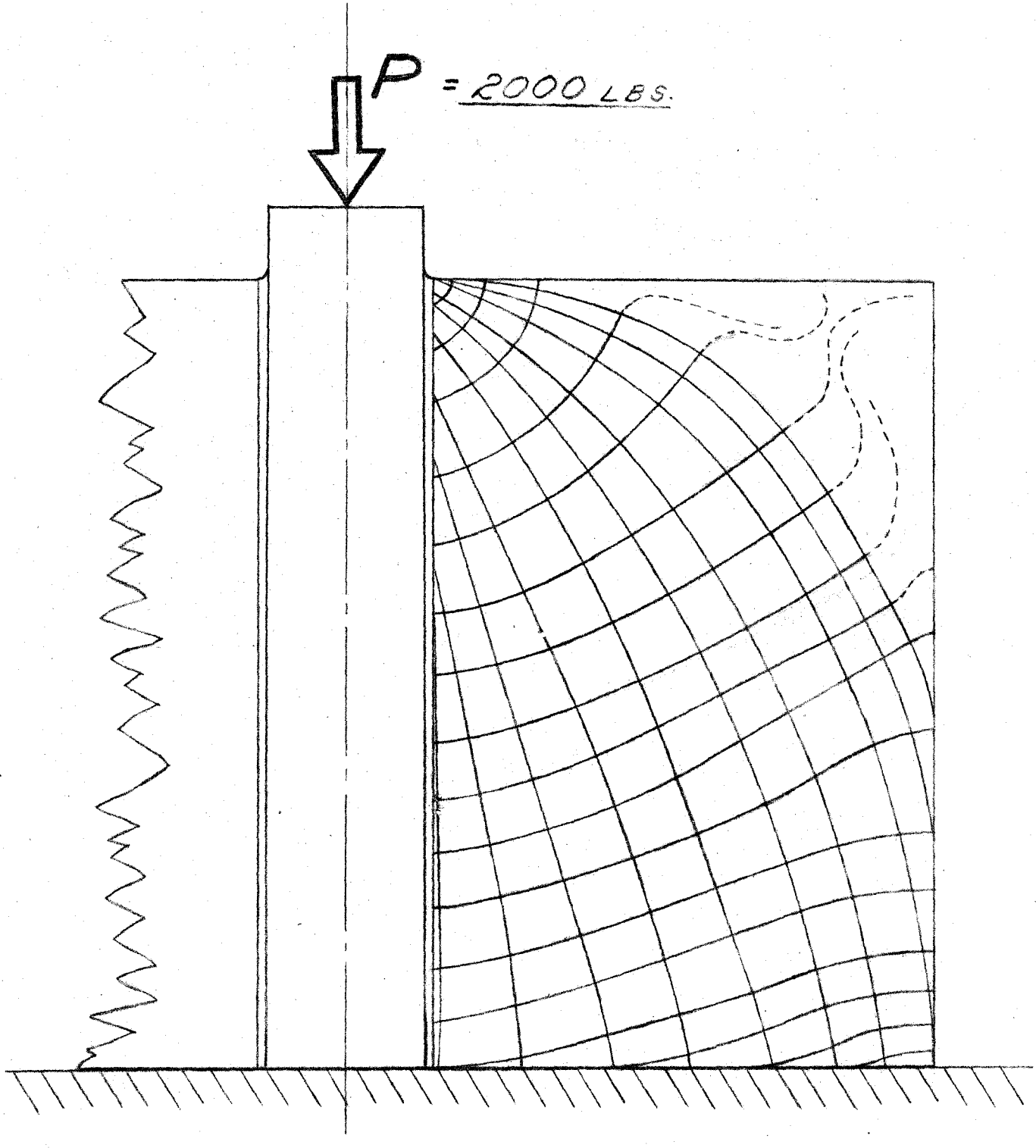

GRAPHICAL CONSTRUCTION FROM ISOCLINIC DIAGRAM

FIG. 16

SERIES C – TRAJECTORIES OF THE MAXIMUM SHEARING STRESSES

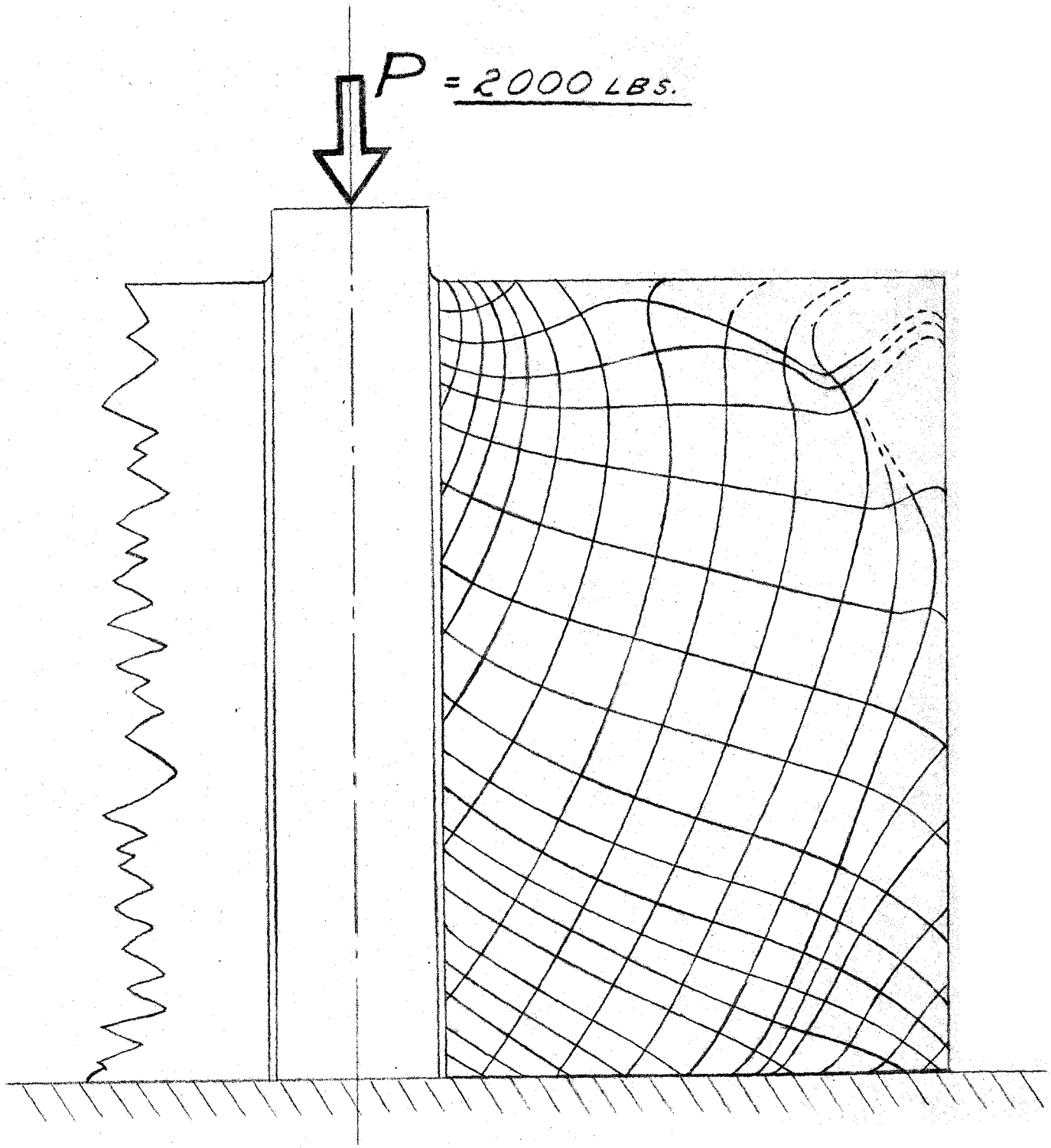

GRAPHICAL CONSTRUCTION FROM ISOCLINIC DIAGRAM

FIG. 17

SERIES B
EVALUATION OF ISOCHROMATIC LINES

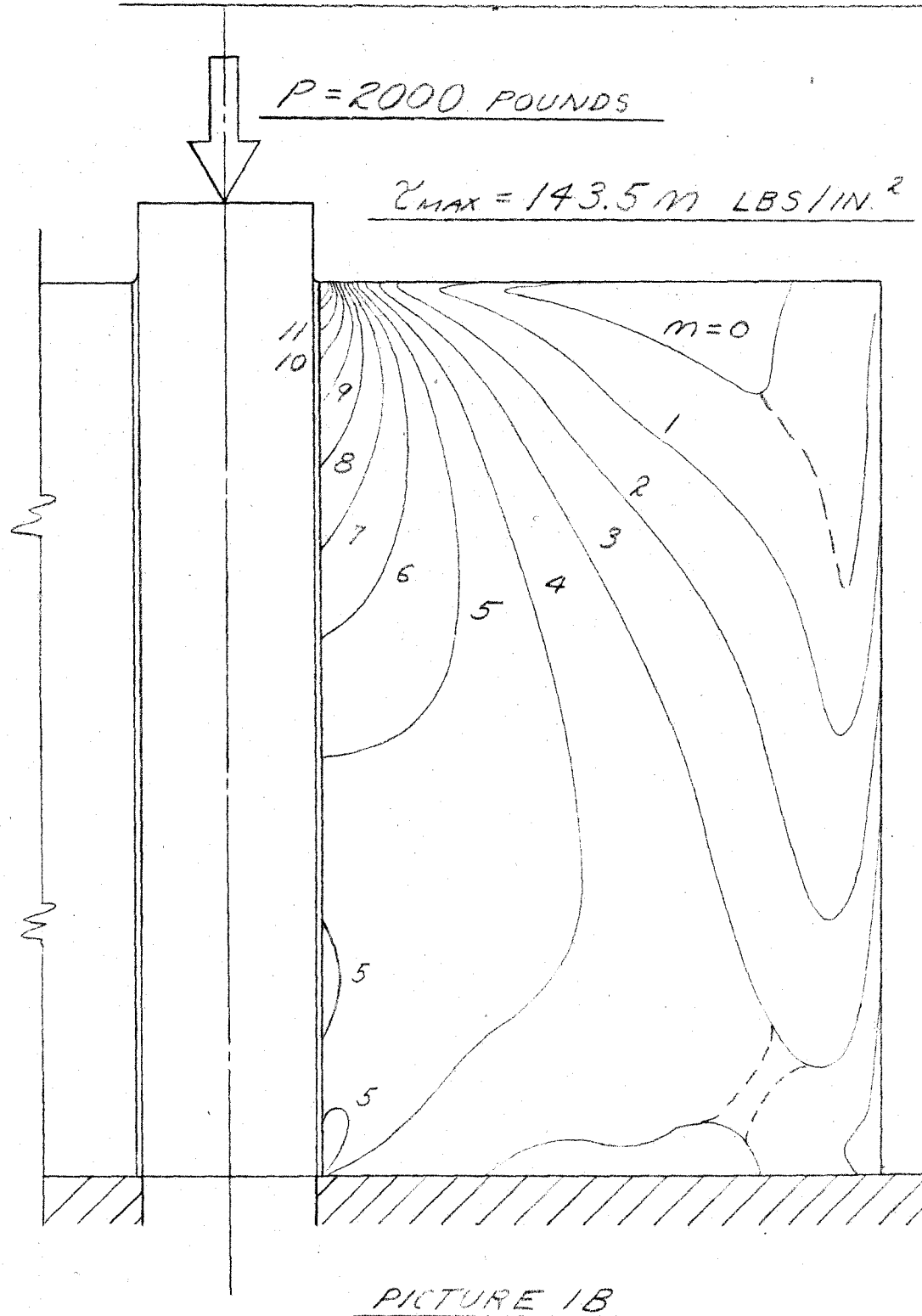

PICTURE 1B
t = .355 INCH
SCALE = 1.050 SIZE

FIG. 18

SERIES B
ISOCLINIC DIAGRAM I

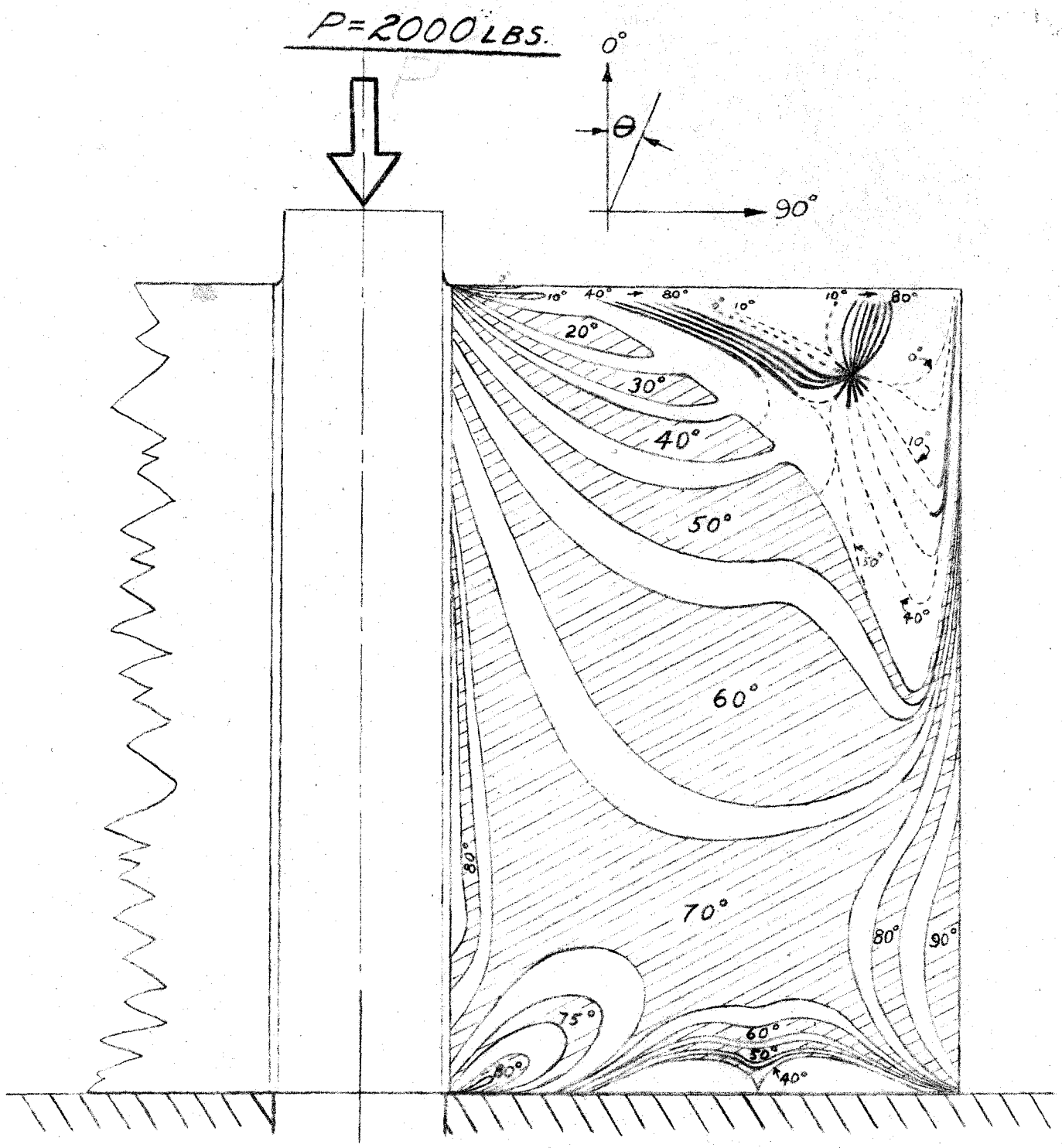

PRINCIPAL STRESS IN DIRECTION θ & $\theta + \pi/2$
MAXIMUM SHEAR IN DIRECTION $\theta + \pi/4$ & $\theta + 3\pi/4$

FIG. 19

SERIES B
ISOCLINIC DIAGRAM II

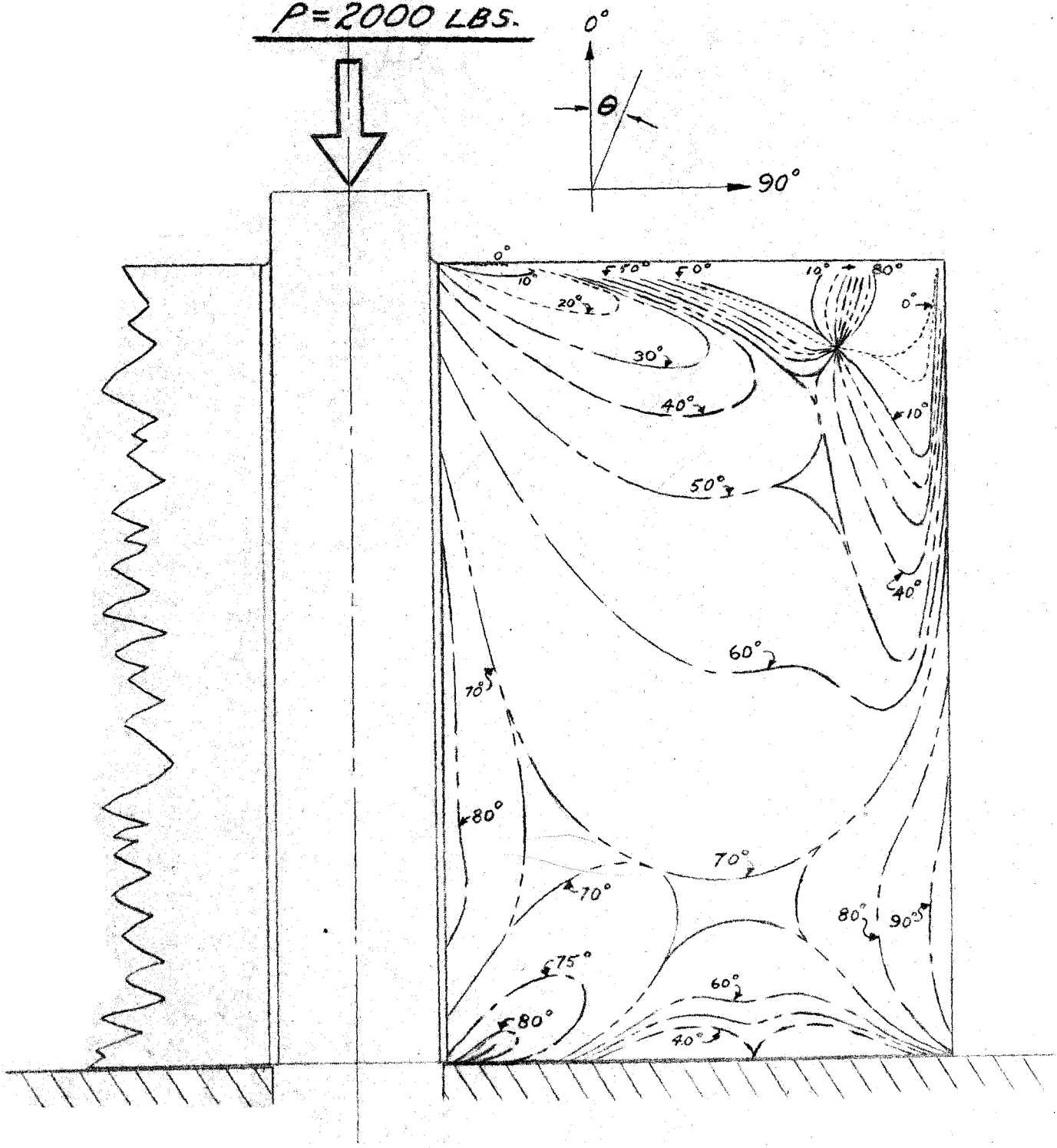

PRINCIPAL STRESS IN DIRECTION θ & $\theta + \pi/2$
MAXIMUM SHEAR IN DIRECTION $\theta + \pi/4$ & $\theta + 3\pi/4$

FIG. 20

SERIES E
EVALUATION OF ISOCYLINTIC LINES

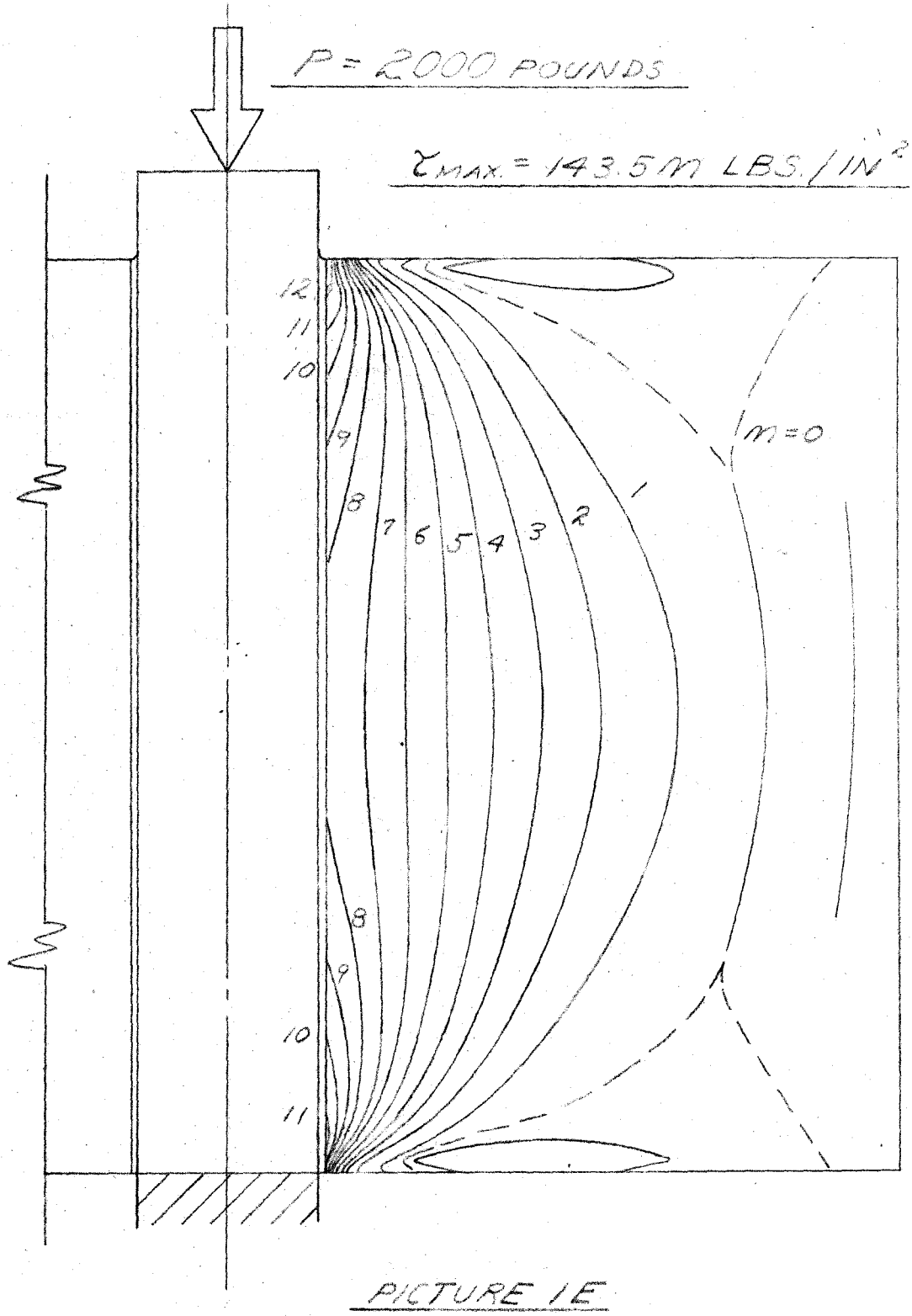

PICTURE 1E
t = .355 INCH
SCALE = 1.125 SIZE

FIG. 21

CALIBRATION BEAM

$t = .230$ INCH $h = .689$ INCH

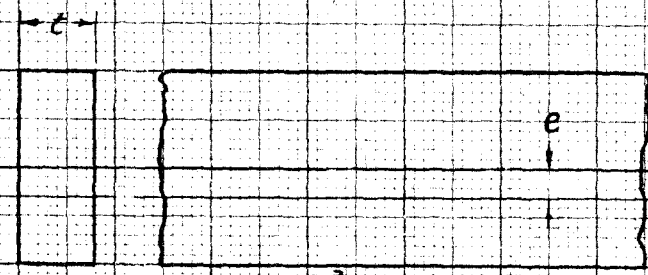

$$I = \frac{th^3}{12} + e^2 th$$

$\Delta\gamma_{max} = 206.6$ PSI/FRINGE

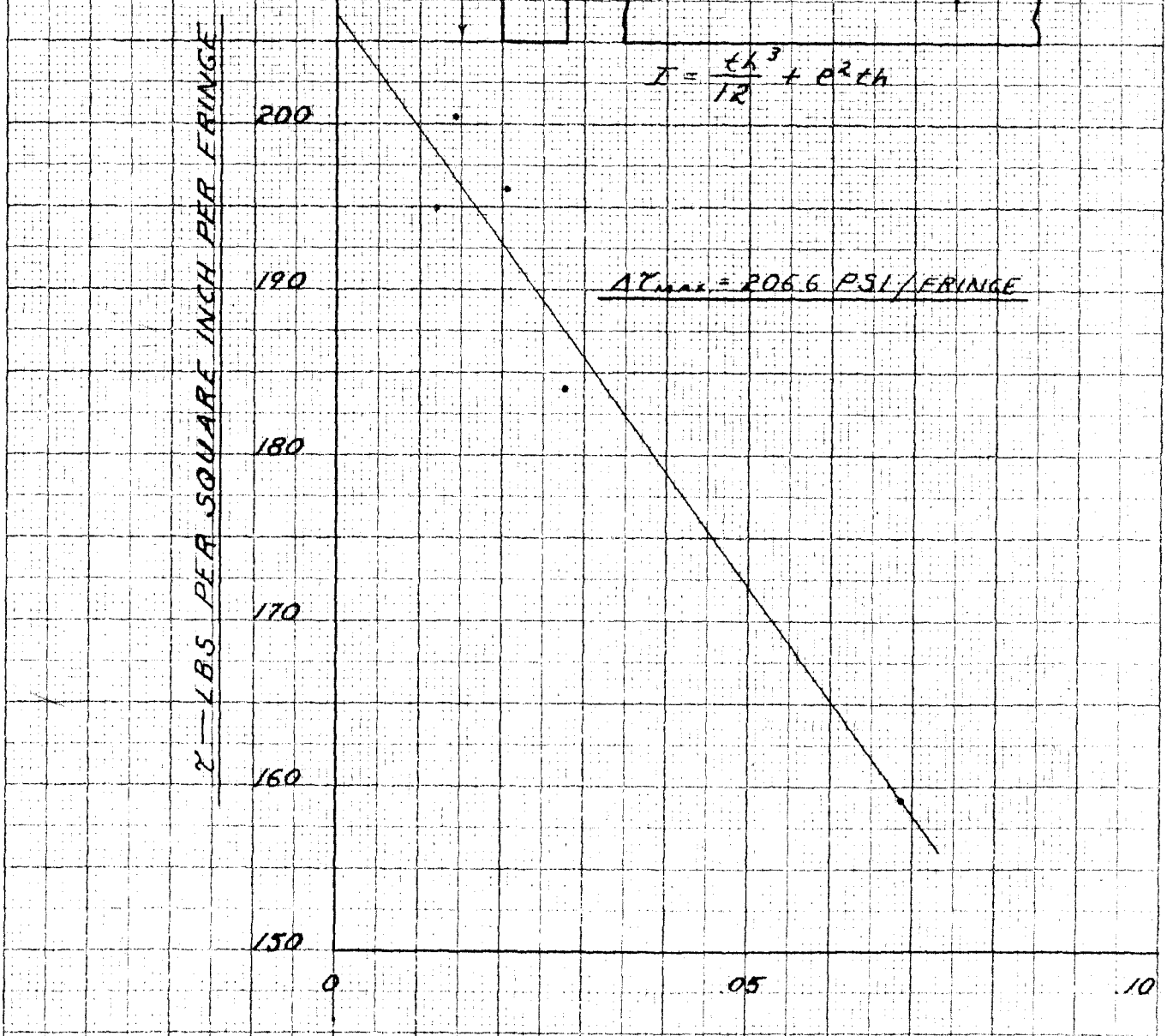

FIG. 22